A comparison of vertical land motion observed by GPS and Space Gravity

Guadalupe Alvarez Rodriguez

A thesis submitted for the degree of Master of Philosophy of The Australian National University

June 2024

Declaration

This is an account of research undertaken between March 2020 and June 2024 at The Research School of Earth Sciences, College of Science, at The Australian National University, Canberra, Australia.

To the best of my knowledge, except where acknowledged, the material presented in this thesis is original and has not been submitted in whole or part for a degree in any university.

Guadalupe Alvarez Rodriguez
June 2024

Acknowledgements

I am grateful to the Australian National University for accepting me into the program and to the Research School of Earth Sciences (RSES) for welcoming me into their cohort.

I would like to express my gratitude to my supervisor, Dr. Paul Tregoning, for his invaluable guidance and support throughout my degree and the writing of this thesis. His expertise was instrumental in the completion of this work. I am deeply grateful for your patience as I completed my degree.

Thanks to my supervisory panel, Dr. Sebastian Allgeyer, Dr. Simon McClusky, and Dr. Matt King, for their valuable insights during my thesis proposal review.

To my Geodesy Group friends: Dr. Rebecca McGirr, thank you for your friendly guidance and help when I first arrived at RSES, I was very lucky to get to share my office with you. Dr. Mahdiyeh Razeghi, thank you for fostering a friendly group dynamic; it was wonderful to come to work every day with your company. Dr. Herb McQueen, thank you for being a supportive listener and for all the late nights spent helping me decode and navigate various issues with my work. Special thanks to Dr. Siyuan Zhao, for your company during late nights, and Dr. Romain Beucher, our unofficial geodesy group member.

Virginia Riddle, thank you for offering me one of the best opportunities within the admin team at RSES and for creating a welcoming environment that brightened my time here. Jos, your guidance and friendship were invaluable. Sia, Adam, Kevin, Honor, Elmira, and Eric, simply thank you; it was a joy working with you daily.

To my RSES friends: Yamila, thank you for being my first friend in Canberra and for introducing me to the RSES student groups. Carlos, thank you for working with me over the weekends. Christina, thanks for joining me in all the "Shut Up and Write" sessions. Cat, thank you for encouraging me to participate in the Thesis Boot Camp, that one really pushed me over the finishing line. Nova and Hendro, thank you for being my late-night companions at OHB, sharing dinners, and cycling home together through the harsh Canberra winter. Adi and Thomas, thank you for visiting and having those midday impromptu chats to clear my head. I deeply appreciate all my RSES friends through this journey, including Ziyi, Corinne, Emily, Tha, Alana, Leo, Buse, Monika, Thuany, Ale, Sebas, Javi, Miguel, Galia, Lennart, Jordan, Sima, Ping, Bei, Shub, Yajie and many others. Even though the academic path is utterly lonely, thanks to you guys I was never alone.

Whether you were there for impromptu calls or Zoom chats for help, advice, or simply company during the multiple lockdowns, or joined in on social gatherings like weekend trips, day hikes, or casual drinks, knowing I had such a supportive system was invaluable. I am deeply grateful to all of you. To all my friends outside of science, scattered as you are, thank you for reminding me of the outside world, especially over the last few months. Without my dear friends and support system, I would not have finished this degree.

To my family back home, thank you for all the video chats that helped me when I was homesick, especially my abuelo. And most importantly, to my parents, for supporting my move across the world to pursue my goals. Thank you for answering every call, no matter the time. Your unconditional love and endless support have been my continuous source of strength and safety. Gracias.

Every person mentioned played an instrumental role in my life as I completed my degree. Thank you.

Abstract

The Gravity Recovery and Climate Experiment (GRACE) and GRACE Follow-On (GRACE-FO) missions monitor the Earth's temporal gravity field, allowing to track and study terrestrial water storage changes, groundwater depletion, ice-mass variations, ocean bottom pressure changes, sea level fluctuations, and solid Earth deformation. When possible, succeeding satellite missions become operational prior to decommissioning of the mission they are replacing. Meaning there is an overlap of measurements, which allow one mission to be validated against each other. This was not the case with the GRACE /GRACE-FO missions as there was a ~10-month gap in scientific data between the missions. My thesis investigates the continuity of two gravity missions by comparing its measurements of geophysical processes with ground observations (GPS).

Height changes at the surface of the Earth are caused by multiple processes, including elastic deformation caused by changes in hydrological mass loads and viscoelastic deformation caused by Glacial Isostatic Adjustment (GIA). The geophysical signals observed by the gravity missions are the sum of both deformation signals. I estimated a GIA signal from a least squares inversion using GPS heights data and gravity data. This process enabled me to separate the elastic and viscoelastic components of the gravity measurements. Subsequently, I reconstructed the height time series by calculating the elastic deformation and adding it to the viscoelastic deformation. Finally, I compared the reconstructed time series against the observed GPS height changes to validate the accuracy of my GIA estimate.

This validation approach was found to be a quality assessment tool, not only for evaluating my estimated viscoelastic model, but also for assessing existing GIA models. This allows us to assess the accuracy of models and identify the areas where they require improvement. One of the models assessed included the ICE6G_D model, I found a pattern of under-estimated GIA signal on the south and west coast of Greenland.

Considering that the ICE6G_D model is currently utilized to correct GIA for gravity data, this finding holds significant implications. An under-estimation of GIA by the ICE6G_D model causes an under-estimation of mass balances in Greenland. Given Greenland's accelerated melt rates, accurately assessing mass balance changes requires precise GIA estimation.

This method relies on sufficient GPS observations in areas with detectable hydrology and GIA signals. This method can be applied to validate models in Fennoscandia, Laurentide and Greenland. Antarctica, however, has not been assessed as there are not sufficient GPS available for the approach to work. As it relies on the presence of GPS, this approach cannot estimate a regional GIA model unless the spacing between GPS is 200 km; however, it can accurately estimate the signal at the location of the GPS.

Table of Contents

List of Figures

List of Tables

1. Introduction

On March 17, 2002, the Gravity Recovery and Climate Experiment (GRACE) satellites were launched into orbit around 480 km above the surface of the Earth. For 15 years, the mission monitored the Earth's temporal gravity field with a level of precision down to a few centimetres of equivalent water thickness. The GRACE mission provided scientists with continuous global observations that helped them observe and understand terrestrial water storage changes, groundwater depletion, ice-mass variations, ocean bottom pressure changes, sea level fluctuations, and solid Earth deformation (Tapley et al., 2019). The success and novelty of the contributions the mission made to science and the community raised the strong need for similar space gravity observations to be continued upon its decommissioning in October 2017. The subsequent mission, GRACE Follow-On (GRACE-FO) was launched in May 2018 and has been recording information ever since.

It is essential to validate any satellite mission to ensure the accuracy of its measurements, however the process of validation can encompass certain challenges. In the case of GRACE and GRACE-FO, the biggest challenge is validating the measurements with other measurements of a compatible spatial scale. Unfortunately, there are no in-situ observations with the same spatial footprint as GRACE/GRACE-FO against which they can be validated. Ideally, a satellite mission would be validated against its predecessor(s) while the missions are orbiting simultaneously. This was not possible with GRACE/GRACE-FO because of the 10-month gap in science data in between the missions.

Despite not being able to directly validate the missions, there are alternative ways that have been used to partially validate the GRACE missions without having the same spatial footprint, such as in situ-observations, against remote sensing measurements or through modelling. In this thesis, I will assess the consistency of the measurements from one mission to another against observed changes in vertical height estimates at permanent GPS installations. Using Global Positioning System (GPS) height estimates that have data during the GRACE/GRACE-FO period gives the opportunity to validate each mission in the same way since, even without overlapping orbits, the missions still have the same spatial footprint.

The GRACE/GRACE-FO observations measure the gravitational effect caused by the changes in load on Earth and have allowed us to monitor the redistribution of mass on the surface of the Earth over the last 21 years. GRACE/GRACE-FO observations sense different hydrological and geophysical processes, including elastic and viscoelastic deformation caused by changes in load. Elastic deformation is the instantaneous (or nearly so if anelastic) response of the solid Earth to changes of the load, including the ice-mass variations caused by present-day mass changes (being the ice variations due to accelerated melt rates). Viscoelastic deformation is caused by changes in the load on the surface of the Earth over timescales of years to decades to thousands of years ago. Also known as Glacial Isostatic Adjustment (GIA), it is the continuing adjustment of the viscoelastic Earth mantle in response to significant ice mass load change since the Last Glacial Maximum, and ongoing changes in polar ice (Han & Wahr, 1995; Wahr et al., 1998). There are few areas where both types of deformation occur, meaning that the gravity change observed by GRACE/GRACE-FO is the sum of both processes. This study focuses on three areas: Fennoscandia (1), Laurentide (2) and Greenland (3), figure 1.1.

Figure 1.1 Fennoscandia (1), Laurentide (2), and Greenland (3).

In these areas the hydrological, and GIA signals have been measured by independent geodetic technologies, GPS, GRACE, and GRACE-FO. Today, each area has a different magnitude and extent of snow cover and GPS coverage. Fennoscandia today has an extensive GPS network, Laurentide has a sparse GPS network, and Greenland only has GPS sites along the coastline. Each area is later explained in more detail in the background section. These areas have been chosen for this study as they have observations of both elastic and viscoelastic deformations with different techniques.

A change in mass can alter the Earth's temporal gravity field and vertical land deformation in the form of elastic and/or viscoelastic deformation (Wahr et al., 1995). Cases where the measurement of GRACE senses both elastic and viscoelastic deformation can be problematic to interpret and distinguish between the two parts to the signal. For instance, an increase in the temporal gravity field detected by GRACE alone could be caused by either a positive hydrological gain or GIA uplift. However, a positive GRACE signal interpreted along with GPS height measurements can differentiate between a hydrological or a GIA signal. A positive hydrological gain would mean that GPS site would have subsided elastically, while a GPS site showing uplift would suggest a positive GIA change. Conversely, a negative gravity signal can be interpreted as a hydrological loss or GIA subsidence. A reduction in hydrology would cause an upwelling of the lithosphere and an increase in height measured by GPS. A negative GIA signal, losing mantle material, would cause a subsidence of the surface (Segall & Davis, 1997). It has been shown that elastic deformation caused by mass redistributions measured by GRACE compares well with Global Positioning System (GPS) observations (Davis et al., 2004; Tregoning et al., 2009), while it has been argued that there must be several decades of observation to separate the short-term elastic and long-term viscoelastic deformation (Velicogna et al., 2014). The work presented here uses GRACE, GRACE-FO, and GPS height time series across 2002 to 2023, at least two decades of almost continuous measurements.

Even though the GRACE and GRACE-FO missions do not have overlapping observations, the launch of GRACE-FO presents an opportunity to validate the missions and to assure continuity between them. The measurement of the changes in height on a network of ground stations using GPS provides a continuous record that can be compared against comparable height changes estimated from data of the two gravity missions. Although GPS height time series do not have the same spatial footprint as the GRACE observations, providing information only at discrete locations, the fact that there are GPS height measurements that have continuous observations spanning the GRACE period, the gap between the gravity missions, and the GRACE-FO mission, means that it can be used to assess the continuity of the two missions. This presents an opportunity to validate vertical movement computed by GRACE against that measured by GPS by assessing whether the vertical movement of the surface of the Earth as measured by GPS match both the GRACE and GRACE-FO estimates of vertical land movement.

Furthermore, as is shown in this thesis, it is possible to separate the elastic and viscoelastic signals in the GRACE/GRACE-FO estimates of mass change through a joint inversion by least squares of GRACE, GRACE-FO and GPS heights, one can validate each gravity mission with strategic GPS sites that measure elastic and viscoelastic deformation to separate the hydrological and geophysical signals. There are an unlimited number of combinations of elastic and viscoelastic signals that can match the observed GPS or the observed GRACE/GRACE-FO. However, there is only one set of elastic and viscoelastic combinations that will match both GRACE/GRACE-FO and GPS. If the inversion solving for the viscoelastic component is correct, the addition of the estimated elastic and viscoelastic values would be consistent with the GPS height time series, and vice versa.

This thesis outlines my work validating the GRACE and GRACE Follow-On mission against vertical land deformation measured by GPS height changes. It will show whether the vertical deformation estimated from each gravity mission agrees with the observed vertical land movement at key GPS sites, resulting in the validation of both GRACE and GRACE-FO missions. If the modelled deformation from each mission matches the GPS height estimates, then the missions are validated. A by-product of the method is a tool that can assess any GIA model at discrete points where there are GPS height estimates.

This thesis creates a GIA model through the inversion by least squares of GPS and GRACE/GRACE-FO observations to solve for coefficients of a spherical harmonic model that represents the GIA signal. I discuss how I selected and processed the GPS and gravity observations, and the parameters involved in building the GIA model. I assess the accuracy of the GIA model, by comparing my estimate of vertical land movement at key sites in Fennoscandia, Laurentide and Greenland, against GPS height time series. I also assessed other external models.

1.1. Objectives

The objectives of this thesis are:

- To validate the accuracy of GRACE-FO and GRACE.

- To accurately separate the elastic and viscoelastic deformation signals through a joint inversion using GRACE/GRACE-FO and GPS.

- To show whether the vertical deformation estimated from each gravity mission agrees with the vertical land movement measured at key GPS sites.

- To assess the quality and accuracy of GIA models in Fennoscandia, Laurentide and Greenland.

2. Background

Even though there are multiple missions monitoring Earth's processes, the GRACE mission was unique in detecting mass redistribution on and within the Earth. The GRACE mission detected any mass changes from the centre of the Earth to the satellites, providing the complete "profile" of the global mass redistribution. It is up to the analyst to assign the gravitational signal to the relevant geophysical process and to isolate the GRACE observation into the component that they are interested in interpreting.

The launch of the GRACE Follow-On mission provided the first opportunity to validate GRACE against measurements of comparable size. A similar approach has been used with altimetry missions, such as Topography Experiment (TOPEX)/ Poseidon (1992-2005), which was followed by Jason-1 (2001-2013), then Jason-2 (2008-2019), and Jason-3 (2016-present),(Young et al., 2017). The new altimetry missions were placed in tandem orbits, following the same ground tracks, enabling the new mission to validate the previous mission, assuring continuity. Unfortunately, this was not possible with the GRACE and GRACE-FO missions because of the ~10 months gap in scientific observations between the decommissioning of the GRACE mission and the launch of the GRACE-FO mission.

One of the challenges in validating the GRACE observations is that there are no measurements with a compatible spatial footprint. When the GRACE mission first launched it could only be validated through the compilation of information from various data sources (hydrology models), or measurements at discrete points (GPS, in situ measurements of groundwater levels, soil moisture, etc..), or against remote sensing measurements with different spatial coverage such as satellite altimetry. The direct validation of GRACE gravity field solutions is essential for accurately forecasting trustworthy mass balance trends (Wahr et al., 1995). Depending on the GRACE solution, the spatial footprint can be around 2-3 degrees. At the equator that is around $(220\text{-}330)^2$ km^2 and there are no in situ measurements of a comparable scale. Depending on whether the type of area being measured by GRACE is ice, land, or ocean, scientists have sought alternative ways of validating the GRACE mission. These methods include comparing GRACE estimates with the combination of in-situ measurements and models; comparing the estimates with satellite altimetry with different spatial and temporal resolutions and comparing estimates against proxy data using “null tests” (Niu et al., 2007). Each of these approaches has its own limitations. For example, groundwater variations derived from GRACE can be compared against in-situ groundwater observation well networks (Bhanja et al., 2016), while ocean bottom pressure estimates can be compared against in-situ pressure sensor measurements (Böning et al., 2008). However, because of the large spatial scale of GRACE, mass change estimate results cannot be directly validated with ground measurements without the incorporation of models (Landerer et al., 2020). In some cases, in-situ anomalies may be merely local anomalies that cannot be recorded at the satellite level. Regardless of the best efforts to validate the mission and its data, it could only be done partially comparing against independent models.

Even though GRACE has contributed to better understanding processes occurring on Earth, it has been done in tandem with other techniques, to corroborate observations. For instance, GRACE observations contributed to a closure of the sea level budget estimations or net mass changes; being the combination of ocean mass changes (eustatic) and thermal and saline changes (steric) which affect sea level (Willis et al., 2008).

Before the GRACE/GRACE-FO missions, changes in global sea level could be measured through satellite altimetry or by measuring the sea surface using drifting buoys, such as eXpendable Bathy Thermographs (*eXpendable BathyThermographs (XBTs) - Frequently Asked Questions*, n.d.) and Argo floats. These floats measured the steric sea level changes in the top 2000 to 6000 metres of the ocean, by taking salinity and temperature profiles of the ocean. The buoys sink and drift, then rise and capture the measured profiles (*Argo*, n.d.). Satellite altimetry can measure changes in ocean surface, being the combination of manometric and steric sea level (Willis et al., 2008). Manometric sea level changes are caused by the increase of volume, due to ice sheet melting. Steric sea level is caused by density changes in the water caused by ocean salinity (halosteric) or thermal expansion of water. Together, satellite altimetry and Argo floats allowed the understanding of what contributed to sea level rise, separating the steric and eustatic contributions (Lyman et al., 2006).

The GRACE mission provided the missing part, the mass change contribution to sea level rise, and provided a new measurement which allowed for the closure of the sea level budget, in a way that was not possible before. This led to the detection of an error in the Argo measurements. Lombard et al., (2007) combined observations from Topex/Poseidon and Jason-1 altimetry and GRACE gravity observations to estimate steric sea level variations. Subtracting the gravity observations from altimetry recordings should equal the thermosteric sea level variations. They discussed the sampling error in the Argo cooling recordings commencing in 2003, with an unexpecting decreasing rate of –2.8 ± 0.2 mm/yr for thermal expansion. If that was correct it would suggest a sudden significant increase in ocean mass, that did not agree with altimetry or gravity observations.

The arrival of GRACE invalidated the sea level budget, which lead to the detection of an error in the ARGO processing. Thanks to the work of Lombard et al., (2007), corrections were implemented on the ARGO instruments (Willis et al., 2008). Because of the GRACE observations, the closure of the sea level budget was enabled and therefore provided validation for the GRACE mission. This was an indirect validation of the GRACE mission. To date, validating GRACE hydrology signals can only be done partially because of the spatial scale difference and model uncertainties. Nevertheless, GRACE measurements have been a significant tool for validating and calibrating such techniques (Lombard et al., 2007; Niu et al., 2007).

2.1. Glacial Isostatic Adjustment – GIA

The discussion to better understand the deformation of the Earth caused by surface loads has taken place since the 70’s (Farrell, 1972). Glacial Isostatic Adjustment (GIA) is a time varying signal caused by a solid Earth process; being the postglacial adjustment changing over timescales of decades to centuries. GIA is the consequence of deglaciation observed in the vertical rebound of previously ice-covered regions, and it is reflected in raised shorelines in such areas. It is the ongoing rebound and readjustment of the Earth’s lithosphere and mantle in response to ice mass loss since the Last Glacial Maximum and ongoing changes in polar ice, glaciers and ice sheets (Simon et al., 2010). The Last Glacial Maximum (LGM) was the time with the greatest ice advances, it occurred in the last 29 to 19 thousand years ago. During this time the continental ice sheets reached their largest /maximum total ice mass cover. It is also known as the Pleistocene glaciation cycle (Mitrovica & Peltier, 1989).

The Earth responds to geophysical processes on its surface, caused by mass loads that have a geophysical impact on the elastic Earth, altering its shape and gravity field. Farrell, (1972) explained the theory (for computing and estimating) and methodological foundation of the effects that changes in load have on continental and oceanic crust. Present day elastic deformation caused by mass changes are caused by a change in surface load, that can be observed in lakes, rivers, aquifers, glaciers, snow cover, or anthropogenic disruptions, like dams and well pumping. Present day viscoelastic deformation is the effect of the mantle response to past and current surface load changes. The present-day deformation is the sum of the viscous signal caused by past ice changes and the instantaneous elastic signal due to mass changes today (Simpson et al., 2009). Mass loss in ice sheets has an initial elastic response and a subsequent viscoelastic response.

The Earth's crust and mantle have been deformed due to the water-mass fluctuations between ice sheets and oceans, caused by the changing load of ice sheets on land and water load in the oceans. Figure 2.1 illustrates the impact of glacial rebound, where an increase in hydrological load applies pressure on the Earth's surface causing an initial subsidence of the crust. During the LGM the ice weight on land caused an enormous subsidence in the crust of several hundreds of metres into the mantle (Steffen & Wu, 2011). The mantle material is pushed, relocating beyond the hydrological load and causes a crustal uplift, known as a peripheral bulge. The peripheral bulge is finite in width: as it gets further away from the load the redistribution of the mantle is negligible. During the glaciation period the sea level fell, removing the weight over the ocean floors and causing the crust and mantle over oceans to rise.

With the deglaciation, the hydrological load diminishes, forcing a rebound of the crust uplifting beneath the load, and the bulge collapses as the mantle flows back underneath where the load was (Wahr et al., 1995). The current glacial deglaciation is seen on the present-day sea level rise, increasing the water loads in the ocean basins, pushing a subsidence in the crust and mantle (W. R. Peltier, 1974). It is important to understand that the ongoing changes in load are not just load removals but load redistributions, altering the shape of the Earth. The mass redistributions of ice sheets comes with a rise and fall in mass of water in the ocean, therefore the total load has contributions from both ice sheets and water loads, and the variations in load are also reflected on the crust (Mitrovica & Peltier, 1989).

The longer a load is in place, the more the Earth deforms viscoelastically (Wahr et al., 1995). GIA is not synchronous with the Earth's glacial history, the viscous properties of the Earth's mantle cause a delay on the glacial rebound of thousands of years; therefore, the effects of deglaciation can be observed today (King et al., 2010). It is complicated to model the glacial rebound because there is not a homogeneous, single temporal and spatial deglaciation history (W. R. Peltier, 1974). There are many factors that can affect the way in which the mantle can be deformed, how much stress is applied, the temperature and pressure conditions, the material being impacted, the time scales of glaciation and deglaciation, the ice distribution and ice volume (King et al., 2010; Lambeck et al., 2000). Understanding the response of the Earth's shape to surface loads brings insights on the rheological properties of the Earth. For detailed work of the Earth's viscosity profile, refer to Han & Wahr, (1995) and W. R. Peltier, (1974).

The modelled GIA signals depend upon the value of viscosity used for the Earth. A low value of viscosity causes the signals to dissipate faster and have a spatially smaller signal. High viscosity means that the load penetrates over a bigger spatial area, and it takes longer for it to respond. It is difficult to do the GIA modelling accurately, because the viscosity is not well known. The viscosity and density of the mantle varies throughout the Earth and changes with depth, the heterogeneous characteristics of the mantle make it difficult to understand and model the Glacial Isostatic Adjustment signal.

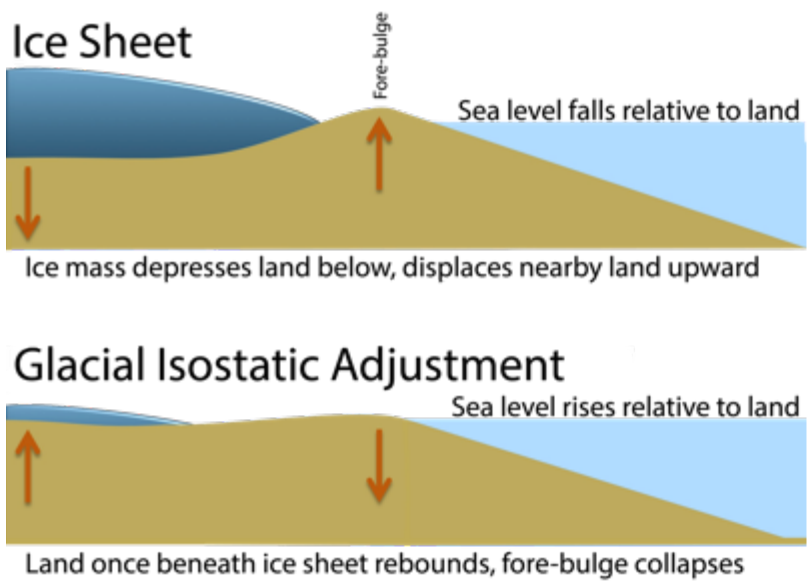

Figure 2.1 Diagram representing the GIA dynamics. From *U.S. East Coast Sea Level | Virginia Institute of Marine Science*, (2022).

During the Last Glacial Maximum (LGM), 80% of the total ice mass on Earth covered continental land masses in the Laurentide, Innuitian, Fennoscandia, Greenland, and Antarctic ice sheets. The remaining ice sheets in the Barents Sea, the Cordillera, East and West Siberia deglaciated much faster. During these major glacial episodes, sea levels were lower than today, with the largest changes in ice cover observed in North

America and North-western Eurasia, where ice sheets fully developed. Today, Fennoscandia, Laurentide, Greenland and Antarctica are the main regions where a GIA signal can still be detected, along with hydrology signals (Mitrovica & Peltier, 1989).

The LGM occurred recently enough for reliable and quantifiable evidence of the climate to be preserved in sediment and ice records. Today, there are various indicators of GIA, including raised shorelines, paleo climate signatures (indicating past sea level shorelines), radiocarbon signatures, and vertical land movement. The effects of GIA can be observed through ancient sea level history, present–day sea level changes, from tide gauge records, gravity anomalies, and in vertical land movement measured by GPS. To adequately build a GIA model there must be sufficient information on the ice-load history and Earth's rheology in the area of interest. Today there are large GPS networks in the Northern Hemisphere that have contributed to building a record of continental observations to model the GIA signal (Denton & Hughes, 2002). The development of space-geodetic techniques has improved the ability to analyse GIA with a high degree of accuracy. Remote sensing tools used to monitor mass balances estimates include laser altimeter and satellite radar imaging observations (Sasgen et al., 2012; Simpson et al., 2009; Velicogna & Wahr, 2006).

Glacial rebound has been known to be reflected in gravity anomalies (W. R. Peltier, 1974) and the presence of space gravity missions, such as GRACE, allow for continent-wide assessments. Estimates of present-day ice mass balance from GRACE data are derived by subtracting a GIA model from the predicted gravity rates, applying a GIA-correction (Caron & Ivins, 2020). To correctly estimate and understand surface mass trends from GRACE observations, there needs to be an accurate GIA correction applied from a model, to enable the present day melting in ice sheets to be separated from the ongoing GIA signal. Surface mass trends can be extracted from GRACE observations only by first removing the GIA signal (King et al., 2010). GIA modelling uncertainties presently dominate the GRACE mass balance error budget (Velicogna & Wahr, 2006). Only accurate GIA modelling allows proper estimation of the magnitude of the GIA contribution to changes in the Earth's gravitational field. Therefore, it is important to have an accurate understanding of present-day GIA to determine current ice mass balances and the rate at which they could affect sea levels.

There are various ways of constructing GIA models and Sasgen et al., (2017) discusses two approaches. First, is a forward modelling GIA, forcing the viscoelastic Earth model with an ice-loading history, based on reconstructed geomorphological observations of ice thickness or numerical ice-sheet modelling (Ivins & James, 2005; W. R. Peltier, 2004; Whitehouse et al., 2012). Second, through an inversion estimate, as presented in this thesis, using multiple geodetic measurements affected by GIA and present-day mass changes.

To this day there is no universally accepted GIA model. GIA models are derived by sampling a range of maximum and minimum parameters for upper mantle and lower mantle viscosity, and lithospheric thickness using a set of parameters that allows the model to match the observed relative sea level curves. The models are affected by the correlations between the Earth's rheological properties, glacial history and sea level history. The broad variety of possible parameters and constraints in models has led to large uncertainties on the models (Gunter et al., 2009). Existing GIA models must deal with the presence of errors due to uncertainties caused by insufficient constraints in the ice timing of deglaciation and in the Earth's viscoelastic profile (Caron et al., 2018; King et al., 2010; Wahr et al., 1998). The uncertainties in GIA models propagate through errors in the viscoelastic deformation estimates, thereby affecting the validation of the models (Purcell et al., 2011).

Wahr et al., (1995) stated that, with gravity observations alone, it is not possible to separate the gravity perturbations caused by vertical displacement and gravity anomalies caused by elastic and viscoelastic signals. They discussed a method implementing gravimeters and GPS receivers to constrain mass balance estimates to determine the changes in ice thickness in Antarctica and Greenland. The mass balance changes observed are the difference between the mass gained by accumulation and the mass lost through coastal outflow and evaporation. They showed that the use of GPS uplift rates of bedrock caused by present-day ice variations around the edges of glaciers can help constrain estimates in coastal mass changes.

GPS can contribute to estimating and understanding ice mass changes in the present day, since vertical deformations of the Earth surface measured by GPS are significantly affected by GIA (Caron & Ivins, 2020; Thomas et al., 2011). Regional GIA models are often estimated, separating GIA from alternative geophysical signals measured by techniques such as altimetry, gravimetry or GPS data. Particularly since local models are mainly controlled by specific ice distribution, upper mantle viscosity and lithosphere thickness, the addition of GPS data can improve the accuracy existing regional models (King et al., 2010).

In summary, GIA has a gravitational signal that affects space gravity observations. The crustal motion caused by GIA can be (in certain areas) large enough to be seen in ground observations such as GPS heights used to monitor changes in vertical land motion. Separating hydrological changes from present-day GIA is an ongoing challenge, and it is not possible to separate the two signals with just one measurement (Purcell et al., 2011; Wahr et al., 1995; Wu et al., 2010). Often the GIA signal is removed from the gravity signal to identify hydrological signals rather than the solid Earth deformation signal contribution (Purcell et al., 2011). But, since ice deglaciation is not perfectly known, there is a range of GIA models used in this way, and the resulting hydrology (including ice mass change) that is derived by this process can have a range of values.

In the following sections I will explain the regional GIA work for the areas of interest in this thesis. I will present some background of the area and some available GIA models.

2.1.1. Fennoscandia

Fennoscandia and Europe have been a key area for GIA work, due to its long settlement infrastructure, and well-identified uplift and subsidence patterns (Steffen & Wu, 2011). During the LGM the Weichselian Ice Sheet covered Fennoscandia, the ice sheet maximum was located in the Gulf of Bothnia and central Sweden. The European ice models include the Barents Sea Ice sheet and the Scandinavian Ice sheet, and later as it split it included the Kara Sea Ice Sheet (Lambeck et al., 2000).

Figure 2.2 Map of Fennoscandia.

The postglacial rebound in Fennoscandia has been documented in various ways: using sea level data, vertical land movement observations and in situ gravity data, recorded with gravimeters, tide-gauges, and levelling across Fennoscandia (Ekman, 1996). Ekman & Mäkinen, (1996) recompiled sea level, lake-levels and levelling records, to map out the uplift rates across Fennoscandia. They incorporated data from tide-gauges in Russia, Finland, Sweden, Norway, Denmark, Germany, Poland, and Baltic countries, dating up to 1811. GIA signals were detectable in variations of lake water levels from records spanning up to 80 years and vertical land movement observations beginning in 1886.

Over the years there have been new approaches to documenting the crustal response through GPS (BIFROST project), absolute and relative gravity measurements, and nowadays satellite missions. These different observations provide insights of past and ongoing deformation and ice thickness variations. These data have allowed scientists to build detailed models of sea level change caused by the mass redistribution between ice sheets and the ocean in Fennoscandia (Steffen & Wu, 2011).

The collapse of the peripheral bulge in Fennoscandia, even though is smaller in amplitude than the areas undergoing the rebound of the crust due to GIA, has a significant impact. It has formed a band of subsidence through the coast of the North Sea and along the southern Baltic coast, extending through Germany, Poland and Russia. In Fennoscandia, it is possible to identify the transition zone between the peripheral subsidence and the GIA uplift (Steffen & Wu, 2011). For a detailed description of the evolution of the ice sheet across Fennoscandia, please refer to Kaufmann & Wu, (2002); Lambeck et al., (2006); Schmidt et al., (2013).

2.1.2. Laurentide

During the LGM the Laurentide Ice Sheet, excluding the Cordilleran and Inuuitian contributions, held enough ice to raise global sea levels by approximately 40 to 110 metres (Lambeck et al., 2000). Today, Hudson Bay is an ideal place to observe the geophysical evidence of the present-day deglaciation. In this area the coastlines record sea level changes following deglaciation, which can be correlated with the exposed topography of the now vanished Laurentide Ice Sheet (Denton & Hughes, 2002; Mitrovica & Peltier, 1989).

Figure 2.3 Map of Laurentide.

During the LGM, the Laurentide Ice Sheet maximum was thought to be a single-dome located in the eastern and northern parts of Laurentide (Lambeck et al., 2000). Later, Lambeck et al., (2017) introduced a multi-dome ice sheet across Laurentide, with domes south of Hudson Bay (Quebec, Ontario, Manitoba), known as Keewatin Dome, and the Labrador Dome north of Hudson Bay (Baffin Island and Ellesmere Island). They use geological evidence of paleo-lake shorelines, relative sea level change and present-day crustal displacement. For a detailed history of the Laurentide ice sheet and the associated Late Wisconsin ice models please refer to Lambeck et al., (2017).

Peltier and colleagues have presented various versions of the ICEnG model, later discussed in global models section. Each version with updated data, for instance the ICE-4G was predominantly constrained with relative sea level histories for North America (W. R. Peltier, 2004). In the ice history of North America they consider a multi dome structure for the Laurentide ice sheet being: the Keewatin Dome (near Yellowknife), the Hudson Bay dome and in the Baffin Dome (near the Foxe Basin). For the ICE-5G model W. R. Peltier et al., (2014) included GPS to constrain for land motion, very long baseline radio interferometric (VLBI) measurements, Satellite Laser Ranging (SLR) measurements, and measurements derived from Doppler Orbitography and Integrated Radio-positioning by

Satellite (DORIS) observations. They constrain the ice history with deglaciation isochrones obtained from radiocarbon dating. For a detailed description of the mantle rheology modelling for the ICEnG models please refer to Roy & Peltier, (2015).

2.1.3. Greenland

The Antarctic and Greenland ice sheets hold 99% of the Earth's freshwater ice found on land (Otosaka et al., 2023). Global climate models predict that annual temperatures in the Arctic are expected to increase approximately 2.5 times faster than in the tropics. The Greenland Ice Sheet has the potential to raise mean global sea level by 7.4 m (The IMBIE Team et al., 2019). In Greenland, heavy snowfall accumulation mainly occurs in the interior of the ice sheet, where it compacts, and then flows outwards. Currently about one-third of Greenland's ice loss is attributed to an increase of iceberg calving, with the remaining due to an increase in surface melting (Sasgen et al., 2012; Simpson et al., 2009).

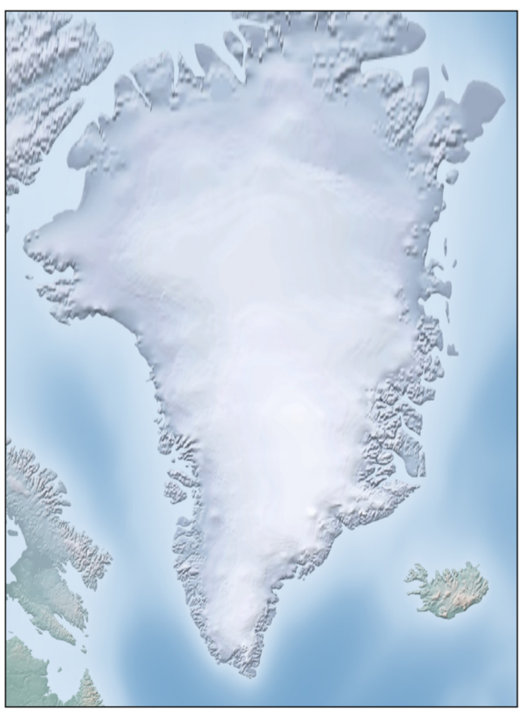

Figure 2.4 Map of Greenland.

In Fennoscandia and Laurentide the glacial rebound signal is dominant where the largest ice-load was located during the LGM. In the case of Fennoscandia and Laurentide dating remnant marginal moraines or weathering profiles located in mountain peaks, previously covered by ice during the LGM, have allowed to quantify the changes of ice thickness (Lambeck et al., 2000). However, in Greenland and Antarctica the record is limited, as they are still predominately covered in ice (King et al., 2010). GIA models are problematic in polar regions, as models are generally data poor in both Greenland and Antarctica, where the largest uncertainty values are over the interiors of the ice sheets (Wu et al., 2010).

Unlike present day deformation in Fennoscandia and Laurentide that is predominately governed by the ongoing response to the glacial rebound, in Greenland the accelerated ice loss contributes to the high elastic uplift rates along with the GIA signal (Simpson et al., 2009). Variations in snow accumulation, meltwater runoff, ocean-driven melting and iceberg calving drive the variation of mass in Greenland (The IMBIE Team et al., 2019). Currently increasing air temperatures and decreasing cloud cover, reductions in surface albedo, and the snow line moving to higher altitudes have increased surface melting and runoff, while outlet glaciers are retreating due to warming ocean temperatures (Otosaka et al., 2023; Sasgen et al., 2020). The atmospheric blocking and reduction of snowfall during the summer has been speeding up meltwater runoff since 2019 (Otosaka et al., 2023).

The Greenland ice sheet has a significant vertical land movement signal, that can be observed in the exposed bedrock surrounding the ice sheet. Berg et al., (2024) argued that the GPS stations located in bedrock along the coast of Greenland are closer to the peripheral glaciers than the margins of the ice sheet itself. Peripheral glaciers in Greenland are not connected to the Greenland ice sheet, predominately in the north and eastern parts. It is important to know if the height velocities recorded are recording signals related to peripheral glaciers or the ice sheet to properly constrain GIA models because, even though peripheral glaciers cover 4% of the area covered in ice in Greenland, they contribute more than 10% to the total ice loss of Greenland.

Recent studies have provided significant knowledge to better understand the changes occurring in the Greenland Ice Sheet, due to the accelerated mass loss and associated variations in glacial rebound. Berg et al., (2024) identified a negative GIA uplift rate in southwest Greenland, potentially due to subsidence caused by the forebulge collapse. Their highest rates were observed at the QUAK and MIK2 GPS sites near the receiding Kangerlussuaq glacier (which has retreated over 10 km since 1900), revealed that Greenland's ice loss is currently estimated at 262.3 ± 39 Gt/year. However, when comparing their estimates with those from other GIA models such as, Peltier et al., (2017), Caron et al., (2018), and Steffen et al., (2021), significant discrepancies were found at specific GPS locations. Berg et al.(2024) discuss how these discrepancies arise because the models have not been calibrated to the GIA rates observed at the GPS stations. Overall, each GIA model has particular strengths depending on the different drainage basins in Greenland.

To further understand the broader glacial history and its effects on GIA, Bennike & Björck, (2002) used radiocarbon dating remains of plants and animals in sediment cores in basins in the south of Greenland. Their work presented a history of sea-level changes caused by GIA, relying on assumptions about glacial history and seismological models to characterise properties in the lithosphere, such as thickness and elasticity.

Simultaneously, the accelerated mass loss of the Greenland Ice Sheet has been the focus of several studies using satellite and geophysical data. Velicogna & Wahr, (2006) presented numerous studies monitoring the development of the Greenland Ice Sheet and the mass loss acceleration rates. They discovered that, between April 2002 to April 2004 and May 2004 to April 2006 the ice loss in Greenland increased 250 percent, equivalent to a global sea level rise of 0.5 ± 0.1 mm/yr. In an updated analysis Velicogna, (2009) showed that the Greenland mass loss doubled between April 2002 to February 2009. Extending their work through 2012, Velicogna & Wahr, (2013) found a mass change of –258 ± 41 Gt/yr, with an acceleration of –31 ± 6 Gt/yr across Greenland. They found that this accelerated ice loss was concentrated in the south of Greenland, while the mass loss in north Greenland remained constant.

Building on these findings, Wu et al., (2010) presented a comparative estimate for Greenland's mass loss between 2002 and 2008, which they calculated at 104 ± 23 Gt/year, while Alaska/Yukon saw losses of 101 ± 23 Gt/year. Using GRACE and GPS data they found that the interior of Greenland showed a positive mass balance, while negative signals were observed along the coastline, particularly in the west, and in the southeast near the Kangerdlugssuaq and Helheim glaciers. Their GIA estimates, which agreed well in Fennoscandia and Laurentide with ICE-5G/IJ05/VM2 model, showed large discrepancies in Greenland, suggesting that the ICE-5G/IJ05/VM2 models may be under-estimating the GIA signal in Greenland.

The IMBIE Team et al., (2019) presented a study incorporating satellite altimetry, gravimetry and ice velocity measurements to assess the mass balance fluctuations in Greenland over a longer time scale. They found that the Greenland ice sheet had lost 3,902 ± 342 billion tons of ice between 1992 and 2018, contributing 10.8 ± 0.9 mm to global mean sea level rise. However, their results also revealed disagreement among GIA models, particularly between ICE-5 and ICE-6G models, in northern Greenland. Similarly, Schrama et al., (2014), using GRACE data, estimated Greenland's mass loss at −278 ± 19 Gt/yr between February 2003 and June 2013.

Additionally, Sasgen et al., (2020) showed that between 1992 to 2018, the Greenland ice sheet lost an average of −148 ± 13 Gt/year of ice, with total losses exceeding the total gains from snowfall by more than one third. Interestingly, their data also showed a brief slowdown in mass loss from 2017 to 2018, likely due to two unusually cold summers in western Greenland and with the snow-rich autumn and winter. However, by 2019, the mass loss rates rebounded, increasing −223 ± 12 Gt/ month.

These are some of the studies that have investigated the accelerating ice loss in Greenland and the complexities in modelling its mass changes. While there has been significant contributions to better understand the glacial rebound occurring in Greenland, discrepancies among different models highlight the need for further refinement in both observational data and modelling techniques.

2.1.4. Antarctica

Understanding GIA in Antarctica is significantly more challenging, primarily because the entire continent has remained covered by ice over most of its surface. Due to the hostile environment, there are not as many observations to constrain a GIA model to estimate accurately the parameters and the sea level histories that are available are confined to sites along the limited coastlines, challenging modelling the ice dynamics. The lack of in-situ observations along the coastlines is a clear problem in Antarctica, unlike in Fennoscandia and Laurentide where there is exposed bedrock to place GPS, as well as inland seas in Hudson Bay and Gulf of Bothnia whose coastlines record sea level changes following deglaciation (Clark & Mix, 2002). A challenge in accurately assessing the mass balance of the Antarctic ice sheet using satellite gravimetry and altimetry, is the poor understanding for the corrections needed for the Earth's ongoing crustal rebound (Sasgen et al., 2017).

Even though Antarctic GIA models are beyond the scope of this work, there are models available, that discuss the different approaches and challenges involved, including A et al., (2012); Budd & Jenssen, (1989); Denton & Hughes, (2002); Ivins et al., (2013); Ivins & James, (2005); James & Ivins, (1995); Otosaka et al., (2023); Sasgen et al., (2017); Thomas et al., (2011); Whitehouse et al., (2012).

2.1.5. Global Models

I have briefly described some regional GIA models, alternatively there are global GIA models available. I am going to discuss two well-known ones, the ICEnG models by Peltier and colleagues and the Australian National University (ANU) models. Caron &

Ivins, (2020) discussed that a disadvantage of global GIA models is that, to accommodate relative sea level constraints in Fennoscandia and Laurentide, models tend to compromise the ice history and viscosity in Antarctica and Greenland. The global models predominantly differ on the ice-loads over continental shelves or shallow basins (Lambeck et al., 2017).

Mitrovica & Peltier, (1989) introduced an early global GIA model, using gravity field observations to constrain mantle rheology. There have been many updates of the model throughout the years. Tushingham & Peltier, (1991) presented an updated version of the model, the ICE_3G model, the ICE-4G (W. Richard Peltier, 1996), the ICE-5G (W. R. Peltier, 2004), the ICE6G_C (W. R. Peltier et al., 2015) and the latest one, used later in this thesis, the ICE6G_D (R. W. Peltier et al., 2017). Each version has been updated due to new available data to improve constraints and improve modelling. Therefore, as a consequence of different patterns of rebound between each version of the ICEnG models, there are uncertainties in the ice-load model, deglaciation history and the mantle viscosity assigned (Steffen & Wu, 2011).

Lambeck et al., (2000) global ice model comprises late Pleistocene ice sheets over north America, north Europe, the Barents Sea, Greenland, the British Isles, parts of Siberia, northern Russia, the Alps, and Antarctica. Lambeck et al., (2017) presented a global ice model (LW-6) with an updated ice history of Laurentide, where they discuss the role of proglacial lakes, update relative sea level history, ice thickness, geoid change and paleo topography. They include ice domes across Laurentide.

2.2. Global Positioning System- GPS

The Global Positioning System (GPS) was designed by the United States Department of Defence (DoD) for military and civilian navigation and positioning, for all time and all-weather conditions. In the 1970’s the first GPS satellites were launched and by, the 1980s, it was possible to calculate the positioning of a receiver with an accuracy up to several metres (McClusky, 1993). Today GPS provides three-dimensional (vertical and horizontal) relative positions to the centre of the Earth being latitude, longitude, and height with a precision of a few millimetres to tens of centimetres. One of the most significant contributions of GPS has been insights into geophysical processes on Earth. From the analysis of GPS data, it has been possible to estimate or quantify precisely estimates of the Earth's active processes; continental tectonics, earthquakes, active faults, tsunamis, volcanoes, aquifers, sea level changes, glaciers, ice sheets, mantle flow, terrestrial water storage, anthropogenic influence (i.e. oil extractions, water pumping), improving the accuracy of reference frames and many more applications (Blewitt et al., 2018).

There are three segments of the GPS system: the space segment, the control segment and the user segment. The space segment consists of the satellite constellation and the transmission of signals; the control segment is the analysis and processing of information; and the user segment includes anyone that makes use of the signals transmitted by the satellites (mobile phones, transportation systems, financial system, kinematic positioning, high precision positioning, etc...).

2.2.1. Space Segment

2.2.1.1. Constellation

By 1993 there was a complete Global Positioning System constellation consisting of 24 satellites, with that number increasing up to 31 satellites today. The satellite constellation has six near-circular orbit planes with an inclination of 55-60 degrees and an orbital radius of ~26,000 km, with at least 4 satellites (often more) in each orbit plane. This configuration can provide a continuous global coverage (Grimes, 2007).

2.2.1.2. Satellites

Each satellite has a 12-hour sidereal repeat track over the surface of the Earth. On each satellite there are radio frequency transmitters, atomic clocks, computers, ancillary equipment, solar panels, and a propulsion system for orbit adjustments and stability control (Hofmann-Wellenhof et al., 1992). Each satellite emits a signal with the estimated positions of the satellites to the receivers. The positions of the satellites are estimated by the control and user segment which are uploaded to the satellite.

The atomic clocks onboard the GPS satellites are aligned to GPS time, and the ground receivers are offset from GPS time. To overcome the offset the receiver measures distances to at least four satellites simultaneously, known as pseudoranges. The pseudorange is derived from demodulating the signal sent by the satellite, identifying the clock error between the satellite transmission and receiver time (Hofmann-Wellenhof et al., 1992).

The satellites produce continuous L-band frequencies, L1 and L2 carrier waves transmit coded information of timing and position (McClusky, 1993).The L-band carrier frequencies are modulated by lower-coded frequency signals. The GPS satellites broadcast two types of carrier signals, Coarse/Aquisition (C/A-code) and Precision (P-code). As originally set up, the P-code signals had a high precision modulation measured by the inphase component and the C/A-code have a lower frequency (Hofmann-Wellenhof et al., 1992). The information the C/A-code transmitted was intended to be decoded by civilian, commercial and scientific receivers and the P-code could be encrypted to become Y-code by the military solely for authorised use (Grimes 2007).

Most commercial and civilian GPS receivers (in navigation mode) have a C/A-code single L1 frequency, for instantaneous timing and positioning. Precise geodetic work uses dual frequency (L1 and L2) C/A-phase and P-code to track satellites on both broadcast frequencies. There are various sources of error that make the difference between the millimetre to centimetre level for high accuracy geodetic GPS measurements. The GPS signal transits through the dispersive ionosphere and the non-dispersive troposphere, both which affect the signal with velocity delays and bending ray signals. The combination of two frequencies reduces and eliminates the ionospheric delay. During the analysis of the GPS data there are various linear combinations of the L1 and L2 carrier phases to address these issues.(McClusky, 1993).

2.2.1.3. Modes

There are two different ways GPS is used, either navigation mode or geodetic mode. The navigational mode is done by cross correlating the satellite signals modulated by codes. In navigation mode the receiver tracks the frequencies with modulated signals on the carrier waves and records the time of arrival of the signal to the receiver. The user decodes the information on the carrier waves (satellite ID, coordinates, and time), and by differencing the satellite time and the receiver time, the travel time is estimated. Multiplying by the speed of light, converts time into distance, or the “range”. Since there is an offset between the satellite and receiver clocks and GPS time, it is referred to as the “pseudorange”. Through a least squares inversion where the coordinates of the satellites are known and the pseudoranges are the observations, the user can solve for the position of the receiver and the clock errors. Navigation mode is accurate at the 1–5 metre level, its accuracy is dependent on the atomic clocks (GPS time) and ignores the atmospheric delay, for instantaneous positioning (Tregoning, 1996).

Geodetic work required higher accuracy than the navigation mode. In geodetic mode the satellite clock offsets, orbits and atmospheric delays can be estimated from the carrier phase to avoid using the modulated signals. In the geodetic mode the receiver is tracking the change in phase with the satellite. The geodetic mode uses the phase information, being the initial ambiguity, the Doppler shift, and the fractional phase of a wavelength. The GPS phase measurement is biased in an unknown way, known as phase ambiguity. It is the initial range expressed in terms of number of wavelengths from receiver to satellite. It is the largest part of the signal, and is unknown integer number of wavelengths at the time of the start tracking and is estimated along with other parameters in the least squares process. The Doppler shift is counted perfectly by the receiver, it is the change in number of full wavelengths of the carrier frequencies. Due to the impact of atmospheric refraction, cycle slips (wave discontinuities, abrupt loss of signal) can occur. The phase slips and loss of signal can be caused by high electromagnetic interference, unexpected atmospheric conditions, multipathing, or physical obstructions and require the estimation as a new ambiguity. The fractional part of a wavelength is measured to a 1 mm accuracy. The ambiguity is estimated through least squares, the Doppler is counted, and the fractional part is measured. Altogether is possible to know the range with millimetric accuracy (Tregoning, 1996).

There are different ways of processing GPS data in geodetic mode: a network approach and precise point positioning (PPP). Through a network solution, with multiple sites and multiple satellites, the phases are used to calculate the position for each site. This can be done as a zero-difference approach (from one satellite to one site), single difference, or double difference (two sites and two satellites, the difference of four signals). PPP uses a constellation of satellites and a single receiver, only solving for the position of one site at a time (Hofmann-Wellenhof et al., 1992). Geodetic mode has a higher accuracy than navigation mode as the carrier phase has shorter wavelength in comparison to the lower frequency code modulations used for the navigation mode (Tregoning, 1996). Geodetic mode analysis produces sub centimetre accurate positions, hence the GPS data used in this thesis was processed in the geodetic mode.

2.2.2. Control Segment

The Operational Control System is the Master Control Station (MCS), the Backup Master Control Station (BMCS), ground antennas and worldwide monitoring ground control stations. The MCS is the main control station for the GPS satellite constellation, the BMCS is used only when there are issues with the MCS. The ground antennas are the main interface between the satellites and MCS (Grimes 2007). The control segment computes the space coordinates of each satellite relative to the centre of the Earth; with a GPS ground receiver the user can determine the distance between the satellite and the receiver, by recording the time required for the satellite signal to reach the receiver (Hofmann-Wellenhof et al., 1992). The main purpose of this segment is to track the satellites for prediction modelling and clock and orbit determination, synchronizing the satellites' time, and managing data adjustment in satellites control and operation. The control segment uploads the predictions to the satellites, then satellites transmit that as part of the modulated signal. Monitoring stations receive the modulated signals and measure the P-code pseudoranges, the satellite ephemerides and clock information of all satellites. The ground control stations are the antennae that communicate to the satellites through a S-band correction.

The estimation process in the control segment has an impact on the resulting accuracy of the GPS. Clock bias in satellite and receiver are sources of error that affect the precision positioning of the GPS. For millimetre precise geodetic applications, it is essential to know the precise position of the satellites at the time of observation. There are six orbit parameters essential for its understanding, the eccentricity, the size and shape of the orbit, the inclination, the perigee (point in the orbit), the position and orientation of the orbital plane. The GPS orbits are estimated through a process that integrates the motion of the satellites, taking into account the Earth's gravity field, gravitational effects of Sun and Moon, and empirical models for the atmospheric drag and solar radiation pressure and albedo. The orbit positions of the satellites are computed in an inertial reference frame (Space fixed), and the location of the ground stations in a terrestrial reference frame (Earth fixed), they must be measured and estimated to correct for them.

Initially the GPS was set up with the ability to degrade the satellite signal through Selective Availability (SA) and anti-spoofing (A-S). From the control segment through SA, the U.S. Department of Defence degraded the modulated signals, the broadcast orbit information, the satellite clock offset, and the oscillator frequency signal to prevent instantaneous accurate positioning (navigation mode). It was possible to later estimate the satellites' orbits and the satellite clock offsets from phase measurements for millimetre precision estimates (geodetic mode). Selective Availability was used intermittently and discontinued in 2001 (Grimes, 2007). Anti-spoofing is the encryption of the P-code, polluting most of the L2 wavelength.

2.2.3. User Segment

Initially the primary use of GPS was intended for military use, and it was later adapted for civilian use. The GPS receivers were a relatively low-cost technique for geodetic observations, compared to other/alternative satellite missions such as Very Long Baseline Interferometry (VLBI). GPS antennas and receivers are portable and can operate under essentially all atmospheric conditions. The transition to GPS for civilian/geodetic measurements not only resulted in cost efficient and durable equipment, but it was also affordable to keep running, obtaining good temporal coverage of site displacements. The low cost permitted more organizations to become involved (like academic, research and private institutions installing receivers), growing the global GPS infrastructure and, as a result, the positioning time series lengthened, the accuracy of the satellite orbit determinations improved, and velocity uncertainties decreased (Kreemer et al., 2018; Segall & Davis, 1997). GPS has become an essential tool for Earth scientists monitoring natural hazards and geophysical features.

Estimated GPS products include GPS orbits, Earth rotation parameters, satellite and receiver clock information, and atmospheric (ionospheric and tropospheric) information. Coded observations are processed through least squares or Kalman filter solution to estimate clock parameters for receivers; P-code information is used along with phase data for precise relative positioning. The pseudorange data is used with phase data to improve orbit estimation and solve cycle ambiguities of phase measurements (Segall & Davis, 1997).

There are campaign and permanent GPS networks, with the former being more susceptible to bias. The location of the receiver can also affect the quality of the recorded signals. The receiver antennas can receive signals from all directions from multiple satellites simultaneously. There are cases where the signal can be reflected from nearby objects (such as buildings or vehicles) and the antenna receives multiple arrivals. The signal multipath can alter the phase and code data. Also, the satellite geometry in relation with the receiver can affect the quality of the signals, the receiver must receive at least four satellite signals to estimate its positioning (latitude, longitude, and height) and estimate the clock error (McClusky, 1993).

2.2.4. GPS noise

GPS time series are a combination of signal and noise (Blewitt et al., 2018). It is important to know the magnitude and the type of noise to understand the GPS uncertainties, as it affects the interpretation of the GPS data. Even though there are vertical and horizontal noise assessments (Dmitrieva et al., 2015), in my work I am only using vertical height time series, therefore for the purposes of my work I only consider vertical noise.

The noise in GPS height estimates signals can be uncorrelated in time or temporally correlated, described as a power law process (Williams et al., 2004). White noise is not time correlated and it is reduced through repetition (Dmitrieva et al., 2015). On the other hand, time dependent noise increases as the time series extends. The different types of noise are classified with a spectral index (k), white noise is k = 0, flicker noise is k = -1 and random walk noise k = - 2. Numerous studies have investigated optimal noise models, with the majority indicating that the best characterisation of noise involves a combination of noise signals. This combination can be white noise and flicker noise, white noise plus flicker and random walk, or white noise and random walk noise (Dmitrieva et al., 2015; He et al., 2019; Wang et al., 2022; Williams et al., 2004).

Wang et al., (2022) investigated an optimal noise model combining different noise models. They tested their method with 500 simulated GPS stations, spanning 10 years and later examined the approach with 15 real GPS stations. Their findings concluded that the largest noise amplitude in the vertical component is white noise and ranges between 5 and 9 mm. Dmitrieva et al., (2015) assessed the noise and uncertainty levels of GPS stations with 10 to 20 years of data across the United States. Their findings conclude that the predicted vertical white noise is 2.34 mm. Williams et al., (2004) presented a noise assessment using 954 continuous GPS time series from 414 stations across the world and found that there is a latitude dependence in the noise, which is higher at the equator. They found that the global white noise in the vertical component can range from 1.9 to 7.7 mm, depending on the processing strategies employed.

2.2.5. GPS and GIA

Present-day GIA has been observed as a change in vertical elevations, where land masses rise due to reduced weight of melting glaciers. GPS has been used to monitor loading and unloading on the surface of the Earth. From GPS data we can measure the vertical motion associated with GIA and elastic deformation due to the changing hydrological loads, and crustal deformation (Johansson et al., 2002; Segall & Davis, 1997). Kreemer et al., (2018) presented work using GPS height time series to observe the deformation caused by GIA across North America. Their results showed that the velocities estimated were higher than the those predicted by the ICE6G_C(VM5a) model.

In 1993 the Baseline Inferences for Fennoscandian Rebound Observations Sea Level and Tectonics (BIFROST) project launched. It consisted of GPS stations installed across Sweden and Finland to monitor ongoing crustal deformation associated with GIA, and the observations have helped constrain models of GIA processes. Milne et al., (2001) used GPS height time series to map 3D crustal deformation caused by GIA in Fennoscandia. They presented a map of the radial and horizontal velocity across Fennoscandia due to GIA, consistent with BIFROST observations.

Johansson et al., (2002); published an adjoint paper to Milne et al., (2001) work discussing the geodetic results of the estimated postglacial adjustment in Fennoscandia, including GPS height time series in Norway provided by the Norwegian Mapping authority. They had a dense GPS network in Fennoscandia, with ~100 km spacing. They concluded that overall, the maximum observed uplift rate was ~10 mm/yr. The GPS time series show temporal variations seasonally, and a high correlation amongst regional sites. Nevertheless, it was common for there to be misleading readings in GPS height estimates caused by snow accumulation on the receiver antennas. Even though the vertical motions observed by GPS are associated with GIA, there were significant differences between the model and observed GIA.

2.2.6. UNR GPS Processing

All GPS results used in this project were retrieved from the Nevada Geodetic Laboratory (NGL) at the University of Nevada Reno (UNR) open source, that processes over 17,000 stations globally. All GPS are processed in geodetic mode using PPP zero-difference approach.

There are various mapping functions available to model the atmospheric delay in height estimates, in particular the choice of Mapping Function (the mapping of the tropospheric delay in the vertical direction to any elevation angle) and the choice of reference frame. Blewitt et al. (2018) used the Vienna Mapping Function (VMF1) and all sites are in a centre of mass (CM) reference frame aligned with the terrestrial reference frame of GRACE observations. Hence, the degree 1 spherical harmonics coefficients are effectively zero. For detailed description of mapping functions and atmospheric effects on GPS refer to Tregoning and Watson (2009).

Blewitt et al., (2018) use Jet Propulsion Laboratory (JPL) obit model products, estimates of satellite positions, velocities, satellite clocks, Earth orientations parameter estimates. They did not apply atmospheric pressure loading corrections. They use all observations recorded above 7 degrees elevation angle. NGL process the carrier phase and pseudorange observations. They resolve ambiguities using wide lane phase bias (WLPB) products from JPL.

2.3. Gravity missions

There have been multiple gravity monitoring missions that have helped scientists to better understand mass redistribution over time and its effects on the Earth’s rotation and geoid shape. The knowledge gained from each mission has paved the way for subsequent gravity monitoring missions. I will briefly explain some of them.

The Challenging Minisatellite Payload (CHAMP) was a specialized gravity satellite mission, a German single satellite mission, part of the now German Aerospace Centre (DLR). It was in orbit from July 2000 to September 2010, started at ~454 km altitude decreasing to ~260 km by the end of the mission, collecting information on the variations of the Earths gravitational potential, its magnetic geopotential, and atmospheric properties (Reigber et al., 2002). CHAMP was essentially a single GRACE satellite, it was a pilot mission to test that the equipment, the orbit, and field parameter determination methods worked correctly. CHAMP encouraged possible accurate inter-satellite measurements (GPS – CHAMP) and Star accelerometer measurements from low near-polar orbits, techniques employed in succeeding gravity missions. CHAMP provided significant data that contributed to the improvement of Earth's static gravity fields models, figure 2.2 shows one of CHAMP derived gravity fields (Flechtner et al., 2021).

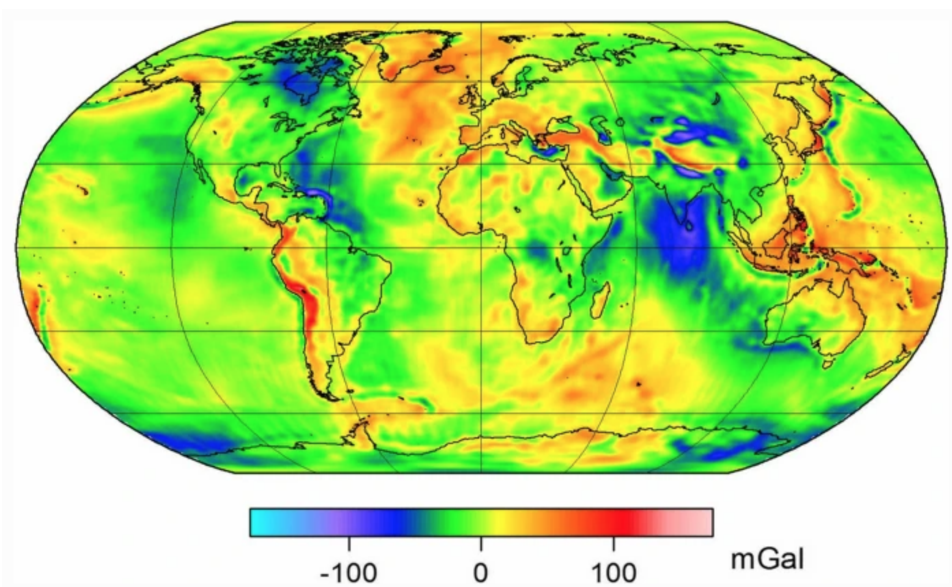

Figure 2.5 Gravity field model from 860 days of CHAMP data. From Flechtner et al., (2021).

The Gravity field and steady-state Ocean Circulation Explorer (GOCE) was a single satellite gravitational gradiometry mission launched by the European Space Agency (ESA); it was in orbit from March 2009 to 2013. The purpose of the mission was to measure gradients of the three components of the gravitational vector, map the Earth's static gravity field and geoid heights with unprecedented high accuracy and detail. GOCE distinguishing features in comparison with the CHAMP and GRACE mission, was the satellites low orbit (~250 km) and drag free mode that provided a high-resolution estimates of the Earth's static gravity field, with a resolution of 100 km (Drinkwater et al., 2007; Flechtner et al., 2021). The framework of GOCE is now being used to set up the fundamentals of Mass Change and Geophysics International Constellation (MAGIC) mission, a collaboration between the European Space Agency (ESA) and the National Aeronautics and Space Administration (NASA). The purpose is to set up two pairs of gravity tracking satellites, Next Generation Gravity Mission (NGGM) and GRACE-FO mission with the purpose of improving water management and understanding water distribution (Massotti et al., 2021).

Satellite Laser Ranging (SLR) satellites has been used to improve gravity field solutions. Some of the SLR satellites in orbit include, the Laser Geodynamics Satellite (LAGEOS) launched by NASA in 1976, LAGEOS-2 designed by NASA and the Italian Space Agency (ASI) launched in 1992, the Laser Relativity Satellite (LARES) launched in 2012 and LARES-2 launched in 2022 as part of the ASI and ESA, all monitoring the changes in the Earth's gravity field, while improving satellite ephemeris estimation and determination of Earth's reference frame. Each satellite is a supplementary orbit with respect to each other (Paolozzi et al., 2011; Tucker et al., 2022). Their main purpose is to measure the dragging of the Earth's inertial frame, or gravitomagnetism, coupling the orbital data of all the missions for better understanding of fundamental physics. From their estimates they could provide insights into the Earth's shape, rotation, and gravity field, essential for geoid models fundamental for Earth sciences (Ciufolini et al., 2016).

Other passive geodetic satellites primarily used to maintain a stable geodetic reference system include Starlette (1975), AJISAI (1986), ETALON-1 and 2(1989), STELLA (1993), and GFZ-1 (1995) (Flechtner et al., 2021). SLR measurements have been shown to have a higher long wavelength accuracy than GRACE. SLR low degree $C_{2,0}$ and $C_{3,0}$ coefficients are substituted in the GRACE monthly temporal gravity field solution to improve GRACE solutions (Allgeyer et al., 2022; Save et al., 2016; Tucker et al., 2022; Watkins et al., 2015).

Together CHAMP, GRACE, GOCE, GRACE-FO gravity satellite missions, LAGEOS, LAGEOS-2, LARES, LARES-2 SLR missions, along with altimetry and terrestrial measurements have been instrumental for the ongoing development and improvement of global gravity field models.

2.3.1. GRACE

In 2002, the National Aeronautics and Space Administration (NASA) and German Space Agency (DLR), under the NASA Earth System Science Pathfinder Program, launched the Gravity Recovery and Climate Experiment (GRACE). GRACE was the first tandem satellite to satellite mission, initially intended to be in orbit for five years, but it operated until October 2017, providing 15 years of observations.

The mission consisted of a pair of identical satellites orbiting the Earth, which are affected by the total gravity field, being the sum of the mean gravity field and the temporal gravity field. The static or mean gravity field of the Earth accounts for known bathymetric and topography features, such as mountain ranges and ocean trenches, along with the internal density structure of the Earth. The variations of the temporal gravity field occur at a smaller magnitude, changing periodically, reflecting variations in mass across the globe. These are mostly related to hydrological changes, in the form of atmospheric water vapor, glacial water, groundwater, surface water, freshwater, and ocean changes. The temporal changes in the gravity field also reflect the solid Earth changes after major plate movements and with Glacial Isostatic Adjustment.

2.3.2. GRACE analysis

The GRACE mission had a unique satellite-to-satellite tracking design, the twin satellites maintained a separation of about ~220 ± 50 km along-track; one satellite followed another in a near-polar orbit around the Earth, with the principal measurement being the change in distance between them. In the following section I will explain the instrumentation onboard of the satellites, what they measure and how the measurements are used.

GRACE twin satellites follow each other in a near-polar orbit, at a low altitude starting at ~490 km and descending to about ~320 km by the end of the mission. The near-polar orbit allowed for a better ground track coverage at the poles, covering high-latitude regions up to 89° north and south. The satellites orbit ~15 times per day with enough sampling to permit monthly estimates of the temporal gravity field (R. McGirr, 2022).

On board each satellite there is a Microwave Interferometer (MWI) that can measure the changes in inter-satellite distance with sub-micrometre precision. The MWI consists of an Ultra-Stable Oscillator and a K/Ka-band ranging system. The Ultra-Stable Oscillator generated the microwave signals exchanged between the satellites, which were transmitted and received by the K/Ka-band system. Onboard each satellite there is also an Instrument Processing Unit, two Star Cameras, and a SuperSTAR accelerometer. The Instrument Processing Unit processed the timing and the signal for the Microwave Instrument and GPS (Save et al., 2016).

There are two tracking systems onboard both GRACE satellites, a K-band, and a GPS. The K-band inter-satellite measures the change in distance between the satellites and is the primary observation used to estimate monthly gravity fields (Dahle et al., 2019; Tapley et al., 2004). The GPS receivers and attitude sensors tracked the position of satellites (Luthcke et al., 2006; Save et al., 2016). The GPS receivers measure the incoming phase of the signals as transmitted by the GPS satellites, used for orbit determination. The measurements are used to calculate the Earth-fixed position and velocity of each satellite.

The inter-satellite changes in distance, recorded the range-rate (Luthcke et al., 2006; Watkins et al., 2015) or range acceleration (Allgeyer et al., 2022; Tregoning et al., 2022). The change in distance varies according to the mean gravity field and the gravitationally induced accelerations acting on the satellites due to the mass variations below. These may be caused by ocean mass fluctuations, changes in glaciated regions, variations in continental hydrology, or significant movement in the solid Earth (Landerer et al., 2020). Range-rate is the rate of change of distance between the satellites and range-acceleration is the time derivative of the range-rate. This is further explained in the processing centres section.

The two Star cameras determined the attitude/orientation of the satellites using celestial images captured by the camera, with respect to the inertial frame, the International Celestial Reference Frame. When the cameras face the light of the Sun and Moon, light enters the cameras and caused “blinding” or poor data quality, this can cause the observations to have gaps, however usually there is data available from at least one camera (Dahle et al., 2019). The star camera data is required to process the accelerometer and K-band data. Attitude data is essential for in-orbit manoeuvres, such as inter-satellite pointing, keeping the K-band antennas directed towards each other. The star camera data is used to rotate the accelerometer data, from sensor frame to inertial frame (Bandikova & Flury, 2014).

Various measures were implemented to extend the lifespan of the GRACE mission. From 2011 the batteries on both GRACE satellites started to degrade, whenever they were deep cycled when the satellites where in eclipse orbits. To mitigate this, instrumentation had to be turned off, when the satellites where in the shadows of the Earth and turned on to charge when the satellites were facing the sun (Flechtner et al., 2021). Some included turning off the accelerometers and the microwave instruments at times, the accelerometers were no longer thermally regulated, resulting in bias along the cross-track axis measurements. From November 2016 to June 2017 the accelerometers on GRACE-B were turned off due to battery issues (Bandikova et al., 2019). When one satellite relies on transplanted accelerometer data from the other satellite, the estimate of low degree gravity field component become less accurate, therefore they had to be replaced by the estimates of SLR (Loomis et al., 2019; Tucker et al., 2022). GRACE-A accelerometer data was used with attitude and time corrections to create transplanted observations for GRACE-B during this period (Bandikova et al., 2019; Dahle et al., 2019). Because of these shortcomings, there are some months where gravity field estimates could not be provided. Toward the end of the mission there was a trade-off between the fuel used for orientation thrust to keep the satellites oriented towards each other or fuel to stay in orbit, hence by the end of the mission the spacecraft altitude had decreased to ~320 km from ~490 km. By October 2017 due to instrumentation failure, battery drainage and fuel outage, GRACE-B was decommissioned, followed by GRACE-A.

The mean gravity field and the temporal gravity field cause accelerations acting on the GRACE satellites. As the leading satellite approaches a mass anomaly, it will accelerate towards the mass and decelerate once it passes over the anomaly. The same would occur to the following satellite. By measuring the change in range, the magnitude of the anomaly on Earth can be derived. The main contributor to such changes are hydrological changes, including ice sheets (Tapley et al., 2004).

The International Centre for Global Earth Models (ICGEM) website provides a directory of static and temporal gravity field models available (http://icgem.gfz-potsdam.de/vis3d/longtime). Static gravity field models are the resulting product of GOCE, GRACE, radar altimetry, and topographic observations (Ince et al., 2019). For reference to the magnitude of static gravity field refer to figure 2.3, the magnitude of the geoid undulation combined with the gravity field can vary from –106.5 to 86.3 metres. Figure 2.3 shows the European Improved Gravity model of the Earth by New techniques: EIGEN-6C4 GFZ (Förste et al., 2014) model with a resolution of ~9 km.

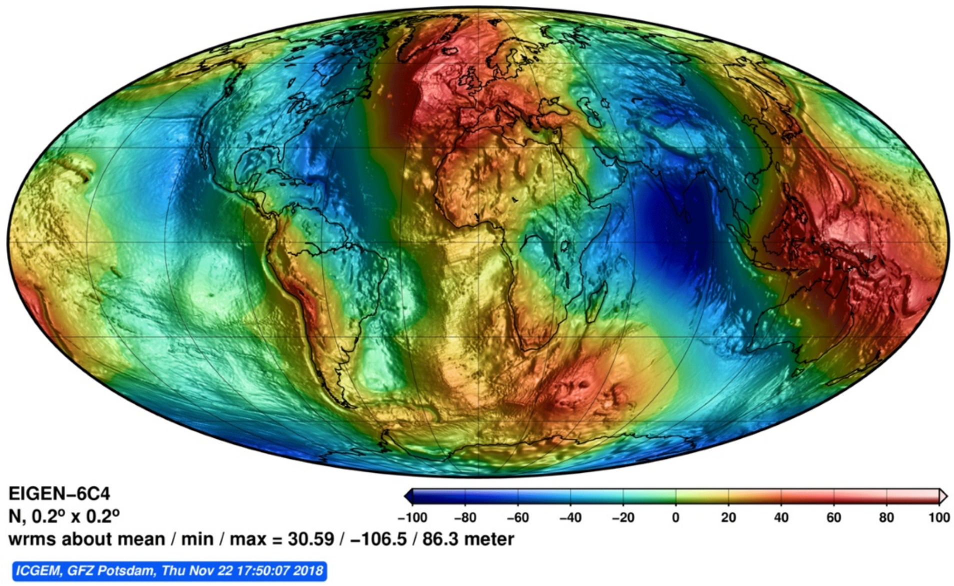

Figure 2.6 ICGEM EIGEN-6C4 GFZ Static gravity field. From Förste et al., (2014).

There are various forces that affect the GRACE/GRACE-FO satellites that must be considered for the orbit integration modelling. There are gravitational forces acting on the satellites from, the Earth and celestial bodies, such as the Sun, Moon and planets. Then there are non-gravitational forces that in essence encompass the interaction between the satellites and the Earth's atmosphere, including atmospheric drag, solar radiation pressure and Earth's albedo effect. The effects of non-gravitational forces acting on the spacecraft are accounted for using precise accelerometers that measure the surface force accelerations in the along-track, cross track, and radial axes (Allgeyer et al., 2022; Bandikova et al., 2019).

The SuperStar three-axis electrostatic accelerometer was mounted at the centre of mass of each satellite, was thermally controlled, and measured the non-gravitational accelerations acting on the satellite. Thermal variations in the satellite were found to affect the accelerometer observations. The along-track non-gravitational accelerations are mainly caused by atmospheric drag and solar radiation pressure. The cross-track axis is mostly affected by solar radiation pressure and atmospheric wind. The radial axis is predominantly affected by Earth's albedo and solar radiation pressure. The impact of forces depends on the orientation, attitude, and physical characteristics of each satellite.

The accelerometer also senses linear acceleration that may sense signals within the satellite caused by thruster firings, twangs, heater switches and magnetic torquer spikes (Allgeyer et al., 2022; Bandikova et al., 2019).

The orbits are integrated taking into account the accelerations from the planets, sun, moon, ocean tides, and atmospheres plus the non-gravitational accelerations measured by the accelerometers. Then the satellite parameters and the temporal gravity field are estimated in a least squares inversion. The orbit is parameterized with the starting position, velocity, and the calibration parameters for the accelerometer. Then the motion of the satellites is integrated taking into account the accelerations of gravitational and non-gravitational accelerations. Adjustment to the parameters is found by minimizing the misfit between the observations and the computed orbit (Allgeyer et al., 2022; Bruinsma et al., 2010).

Background models are applied to account for gravity variations caused by atmosphere and ocean tides, short-term non-tidal atmospheric and oceanic mass variation, solid Earth, or pole tides that do not represent the geophysical signals of interest in the monthly gravity fields (Dahle et al., 2019).

Temporal gravity field either geoid undulations or equivalent water height values tend to range in the centimetre level. Figure 2.4 shows JPL GRACE-FO temporal gravity field for February 2023 where the equivalent water height ranges from ~ –10 to 2 cm.

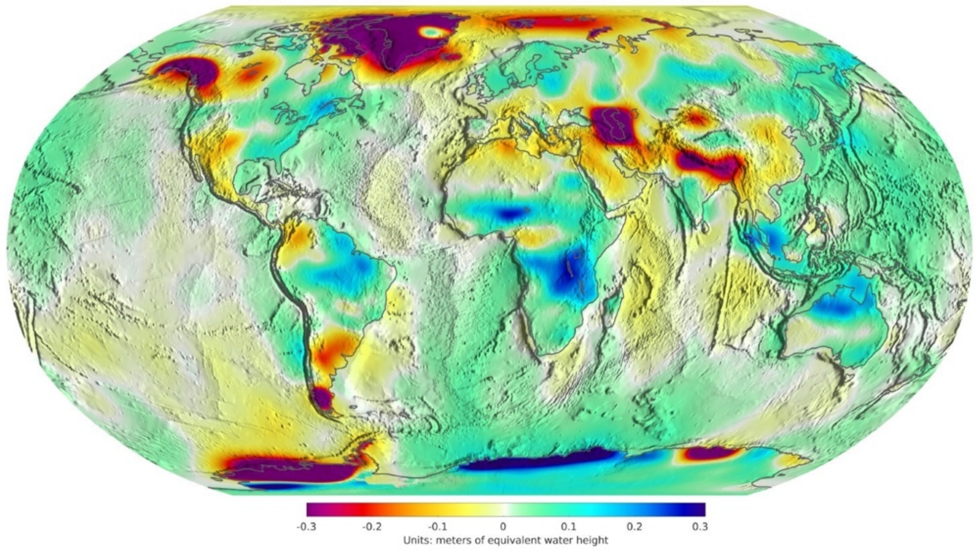

Figure 2.7 Global surface mass anomalies observed by the GRACE-FO satellites. From *GRACE-FO Data | Data – GRACE-FO*, (2020).

GRACE and GRACE-FO monthly gravity field solutions are publicly available in the form of spherical harmonics and/or mass concentration elements, depending on the processing centre. Some centres that produce monthly estimates of the temporal gravity fields include; the German Research Center of Geosciences; GeoForschungZentrum (GFZ) in Potsdam Germany, NASA Jet Propulsion Laboratory (JPL) in Pasadena USA, NASA Goddard Space Flight Center (GSFC) in Maryland, the Center for Space Research (CSR) at University of Texas at Austin, the Centre National d'Etudes Spatiales/Groupe de Recherches de géodésie spatiale (CNES/GRGS), and Research School of Earth Sciences (RSES), Geodesy Group at the Australian National University (ANU).

There are different stages of GRACE data processing, Level-0 are the original raw data, in Level-1A the raw data is converted into engineering units. Level-1B data are the computed ranging measurements from the satellites, the inter satellite microwave, laser ranging observations, star tracking data, GPS orbits, and accelerometer measurements. Level-2 spherical harmonics coefficients are unconstrained representations of the Earth's gravity field, presented as dimensionless Stoke's coefficients. They are estimated through a reduction and inversion process from level-1B data using orbit propagation and estimation systems to solve for the temporal gravity field as spherical harmonics or mass anomalies. Level-2 products are routinely generated by the GRACE Science Data System, consisting of CSR, JPL and GFZ processing centres (Ince et al., 2019). The Earth’s gravity field can also be presented as gridded surface mass concentration anomalies (mascons) in equivalent water height units, derived from Level-1B or Level-2, known as Level-3 (Croteau et al., 2021; Ghobadi-Far et al., 2019). GRACE and GRACE-FO data products are normally delivered either as unconstrained spherical harmonic expansion or as regularized mascon solutions. In the following sections I discuss each one of these.

2.3.2.1. Spherical harmonics

Spherical harmonics are functions defined on the surface of a sphere and are used to represent global gravity field anomalies on the Earth's surface with sine and cosine coefficients. The GRACE Stoke's coefficients can be used to represent the gravity field, in a number of ways, for example, as a geoid, surface load, as equivalent water height, elastic deformation or viscoelastic deformation. They are the most common approach but often require constraints to reduce noise in high-degree solutions. For example, equation 2.1, the geoid shape N is calculated using spherical harmonics (Wahr et al., 1998):

$$N(\theta, \lambda) = R \sum_{n=0}^{\infty} \sum_{m=0}^{n} P_{nm}(cos\theta)(C_{nm}cos(m\lambda) + S_{nm}sin(m\lambda)$$

Equation 2.1

Where θ and λ are the colatitude and longitude of a specific point, R is the radius of the Earth, C_{nm} and S_{nm} are the time variable dimensionless Stoke’s coefficients and P_{nm} are the normalized associated Legendre functions evaluated at the specified colatitude. n and m are the degree and order of the spherical harmonics.

Spherical harmonics solutions are susceptible to errors at higher degrees and orders, which can appear in the form of north/south striping patterns. These amplify the noise and introduce bias into the data (Save et al., 2012). Signal leakage in spherical harmonics occurs when the signals are mixed between land and ocean. This occurs because using spherical harmonics truncated to degree 60 means that there is a very low spatial resolution and that causes the leakage. Croteau et al., (2021) discussed various postprocessing techniques to eliminate correlated noise in spherical harmonics by lowering the maximum expansion of degree and order. There are cases where the leakage occurs in mascon solutions, when the mascon covers both land and ocean (Watkins et al., 2015). This is a very important issue to address particularly in areas of high mass fluctuation, such as most of the mascons along the coast of Greenland, Fennoscandia and Laurentide where the mass redistribution between land and sea can make a significant difference to mass balance estimates.

GRACE unconstrained spherical harmonics solutions have shown north-south striping errors, caused by the poor sensitivity east-west direction, modelling errors, measurement noise, and observability issues in the GRACE processing. They can be mitigated in the postprocessing through empirical smoothing algorithms (Save et al., 2016; Watkins et al., 2015; Wouters & Schrama, 2007) and de-striping methods (Swenson & Wahr, 2006). Smoothing the solution at higher degrees is done to remove the errors in the high degrees coefficients, however the smoothing attenuates the signal. One way of smoothing Stoke’s coefficients is applying a Gaussian filter (Wahr et al., 1998). In essence the filter applies spatial average of the surface mass density to remove noise from the spherical harmonic solutions. Wouters & Schrama, (2007) discussed that applying a Gaussian filter can attenuate signal and cause signal leakage. An alternative smoothing filter is applying an empirical orthogonal analysis function to decompose the Stoke’s coefficients and remove north-south striping. The filter applied on estimated GRACE equivalent water height (EWH) coefficients has shown to retain the expected geophysical signals (Save et al., 2016; Wouters & Schrama, 2007). Nevertheless, any postprocessing method can attenuate geophysical signals. Another approach is through regularization, Save et al., (2012) used Tikhonov regularization and showed a significant reduction in striping errors in the spherical harmonics solutions. Regularization is the introduction of pseudo-information to balance the errors allowed in the solution, it constrains the solution vector.

They used a regularization matrix to add pseudo information, the matrix is designed using the noise information from the GRACE solutions and not the signal properties solutions. Using the error helps constrain the parameters with high error variability. The regularization matrix is used to regularize the monthly gravity fields from GRACE. According to Save et al., (2012), their regularization approach reduces the errors in the GRACE gravity field compared to unconstrained solutions.

GRACE Level-2 spherical harmonics coefficients are determined assuming the Earth has a spherical shape (Wahr et al., 1998). According to Ghobadi-Far et al., (2019) an ellipsoidal reference shape is a better representation of the surface of the Earth, rather than a spherical shape. Because there is higher noise in the high degree coefficients, the filters applied reduce the contribution of those high degree coefficients. The stronger filtering of high degree coefficients attenuates the signal and causes an under-estimation of the mass change at the Earth's surface. They presented a method to transform spherical harmonic coefficients to ellipsoidal harmonic coefficients. The ellipsoidal and spherical coefficients are similar for low degrees up to degree 20 but, as the degree increases, the coefficients diverge, and the ellipsoidal harmonic values showed higher power. Their results showed more realistic mass change estimates, particularly in polar regions. The comparison between signals just in Greenland differed by 14%. Using an ellipsoidal reference frame instead of a sphere for the harmonic coefficients is not only a better representation of the Earth's surface, but it also reflects improvements in the accuracy of mass change estimates.

2.3.2.2. Mascons

Mass concentration elements, also known as mascons, are an alternative method used to represent Earth's temporal gravity fields. A globally distributed mascon field, in essence dividing the surface of the Earth into tiles. This mascon geometry is used to estimate monthly changes in mass with respect to mean. Each mascon has a uniform surface mass at a predetermined location, representing an increase or decrease of surface mass with respect to the mean or static gravity field (Luthcke et al., 2006; Tregoning et al., 2022;

Watkins et al., 2015). It is also possible to convert mascon solutions to spherical harmonics through differentiation (Luthcke et al., 2006).

In mascon solutions, some mascons include both land and ocean regions. In these cases, JPL used a Coastline Resolution Improvement (CRI) filter applied during the gravity inversion to return continental signal that had leaked into the ocean region back to the continental part of the mascon (Wiese et al., 2016). This approach is ideal for mascon solutions as it can be addressed regionally with specific mascons, rather than globally as in spherical harmonics. Separating land and ocean contributions has been shown to have a significant impact in areas with large signals, like outlet glaciers, where the leakage errors were reduced by ~80%.

Mascon solutions also show north-south striping if they are not effectively regularized during the estimation process. Regularized mascon solutions compared to spherical harmonic solutions have shown to contain less noise and do not require post processing smoothing filters to be applied. It has been shown that there is greater flexibility in the way the mascon geometry can be designed, in the form of regular mascons, in spherical caps, in 3°x 3°, 1°x 1°, depending on the processing. Tregoning et al., (2022) presented alternate irregular shaped mascons, the geometry of their mascons could constrain the separation between coastlines, continental borders, and basins, reducing signal leakage. There are three approaches for deriving/estimating mass concentration solutions, that I will briefly explain.

Mass variations are estimated through an analytic expression for the mascon functions using explicit partial derivatives of the mascon formulation and the inter-satellite range-rate. Watkins et al., (2015) used spherical caps and related them to the inter-satellite range-rate measurements. Their processing method prevented the striping in the solutions and were shown to have less leakage errors that their spherical harmonics solutions. Their ocean bottom pressure mascon estimates also showed better correlation with in-situ data than their estimated spherical harmonics solutions.

Mascons can also be directly related to the inter-satellite range-rate or range-acceleration measurements through explicit partial derivatives. Each mascon is represented by a finite spherical harmonic truncated expansion rather than an analytical expression. Each mascon has a signal beyond the mascon boundary (Luthcke et al., 2006). Croteau et al., (2021) work argued that estimating mascon solutions from expanding and truncating spherical harmonics is significantly computationally more efficient than traditional mascon estimation, as it does not require orbit determination.

The third approach is to fit mass elements function parameters to GRACE spherical harmonics coefficients in the postprocessing, this way it can remove striping errors. Jacob et al., (2012) implemented this approach in their work. They derived a set of Stoke's coefficients produced by the mass distributed across each mascon, and they fit the Stoke's coefficients with GRACE Stoke's coefficients to estimate monthly mass values for each mascon.

Velicogna et al., (2014) used the CSR spherical harmonics solutions; they smooth the Stoke's coefficients using a Gaussian filter and they calculate the ice mass grids. They designed 3° mascons spherical caps. For each mascon they calculated their Stoke's coefficients, smoothed and converted into mass estimates. Simultaneously fitting the Stoke's coefficients to the GRACE coefficients to obtain the monthly mass estimates of each mascon.

2.3.3. GRACE Follow-On

The GRACE Follow-On mission was designed to operate the same way as the initial GRACE mission, to continue global mass redistribution observations. After a 10-month gap, GRACE-FO was launched in May 2018 at the same altitude at ~490 km, with a similar orbit design, a low Earth polar orbit with an inclination of 89° and a separation of ~220 ± 50 km along track. The satellites themselves were near replicas of the GRACE satellites, with the addition of instrumentation to improve the quality and accuracy of the measurements and to prevent issues identified in the GRACE mission (Landerer et al., 2020).

A Laser Ranging Interferometer (LRI) was included, a secondary inter-satellite measurement system along with the K/Ka Band to measure changes in the inter-satellite range, for precise ranging capability, allowing for comparison between measurements. LRI laser wavelength has the potential of improving the precision of K/Ka microwave wavelength, by a factor of 10. This could potentially improve the spatial resolution of gravity field solutions (Flechtner et al., 2021). The noise level of the LRI observations has been smaller than the K/Ka Band noise levels, it has been suggested to use the LRI $C_{2,0}$ rather than the ones estimated with the K/Ka Band, since they have higher precision at low degree harmonics (Landerer et al., 2020; Tucker et al., 2022).

A third Star camera was included to improve the quality of the celestial images during Moon and Sun intrusions, the GRACE satellites had two. The addition of the third star camera has shown improvements in the attitude solutions, as it has ensured that there are data from at least two cameras at any time (Bandikova & Flury, 2014; Landerer et al., 2020).

In the initial period of GRACE-FO in orbit, issues with the accelerometers were noticed. In comparison with the measurements recorded during the GRACE mission, the measurements recorded with GRACE-FO accelerometers were contaminated with unrealistic signals, were significantly affected by thruster firings, signal jumps, and other unidentified accelerations. The accelerometer in GRACE-FOB failed with biased and degraded measurements. As a result, since June 2018 only the accelerometer of the leading satellite is being used for measurements and the measurements of the following satellite are inferred based on Bandikova et al., (2019) accelerometer data transplant approach. A consequence of relying solely on one accelerometer is that the quality of low degree components of the gravity field decreases (Landerer et al., 2020).

2.3.4. Processing Centres

There is a large list of GRACE solutions available, in this section I will discuss six of them. Other institutions that have published alternative GRACE gravity solutions from the ones discussed include, the ITSG-Grace2016 (Klinger & Mayer-Gürr, 2016), the AIUB-RL02 (Meyer et al., 2016), the Tongji-Grace2018 (Chen et al., 2019), the ITSG-Grace2018 (Kvas et al., 2019), GOCO06S (Kvas et al., 2020), to mention some. Each processing centre has independent methods for analysis software, parameters used, data editing and weighting. Resulting products vary from each processing centre in gravity field values, temporal and spatial resolution.

1. German Research Center of Geosciences; GeoForschungZentrum (GFZ) in Potsdam Germany.

Dahle et al., (2019) at GFZ described the processing strategy of the routinely processed GRACE gravity fields, particularly GFZ GRACE RL06. It is based on JPL's GRACE Level-1B instrumental data. The GFZ GRACE RL06 solutions are monthly unconstrained spherical harmonics up to degree and order 96 or 60. They do not apply any regularization. Gravity fields available include versions RL01 to RL06. There are multiple versions, improvements in many cases are in the level-1B data.

2. NASA Goddard Space Flight Center (GSFC) in Maryland.

Luthcke et al., (2006) at GSFC presented GRACE monthly gravity field estimates determined from inter-satellite range-rate measurements. Their processing method for the accelerometer calibration and K-band inter-satellite range-rate reduction does not require the estimation of the K-band inter-satellite range-rate empirical parameters. Also, they exclude the GPS data during gravity reductions, they found that it was easier to process the inter-satellite measurements than the GPS data and it improved the efficiency of the computing. The main products retrieved from the GRACE inter-satellite range-rate observations include, highly accurate satellite positions, velocities, orientations, and calibrated accelerometer observations. Their resulting solutions improved the estimates at very low degrees of the spherical harmonic's solutions (degree 2 to 16). They produced both mascon and spherical harmonics solutions.

Croteau et al., (2021) at GSFC discussed an approach of estimating regularized mascon estimates directly from level-2 spherical harmonics rather than level-1B data. The method showed to be more efficient, the resulting solutions had a better signal recovery as there was less noise and leakage.

Currently, the GSFC mascons for GRACE and GRACE-FO are solely processed with the K-band interferometer. Loomis et al., (2021) expands on Croteau et al., (2021) improved regularization, using a diagonal regularization matrix for 1-arc-degree-equal-area mascon solution applied to the level-1B data, instead of spherical harmonics. Their approach showed to improve the signal recovery and the spatial resolution.

3. NASA Jet Propulsion Laboratory (JPL) in Pasadena USA.

Watkins et al., (2015) at JPL provide unconstrained spherical harmonics solution (JPL RL05) and derive from it an alternate mass concentration solution of GRACE gravity field estimates derived from spherical caps (JPL RL05M). The spherical cap mascon model represents in a 3° x 3° the surface mass on a spherical surface. Their solutions are derived through least squares, estimates the geopotential change at each mascon. They processed the inter-satellite range-rate K-band measurements along with GPS phase measurements and pseudoranges. Even though their mascon approach does not cover the entire Earth, as there are gaps between the spherical caps, Watkins et al., (2015) stated that there is no signal lost as it is absorbed/accounted for by the nearest mascon. They regularized the solutions using a combination of geophysical models and altimetry observations.

4. Center for Space Research (CSR) at University of Texas.

Save et al., (2016) at CSR introduced their approach developing a global 1° regularized mascon solution. Their regularization approach only utilises GRACE information to set constraints, they do not incorporate any external models or data. The regularization is time variable, so it will not affect signals based on previous GRACE statistics. Their mascon solutions capture all the GRACE signals, do not have striping errors, and do not require further processing.

5. Research School of Earth Sciences (RSES), Geodesy Group at the Australian National University (ANU).

The inter-satellite observable used at ANU is the range-acceleration, rather than range-rate previously explained. Range acceleration is not commonly used since it tends to amplify short-wavelength signals and reduce long-wavelength signals. Allgeyer et al., (2022) do not employ the level-1B range accelerations, as they contain high-frequency noise. Instead, they differentiated the level-1B range-rate residuals to generate their own range acceleration observations. They argued that using range acceleration over range-rate improved localizing mass anomalies spatially. They estimated monthly gravity solutions using range-acceleration for orbit integration, their solutions showed a reduction in north-south striping. They use irregular shaped mascons, that follow coastlines, continental borders, and basins, reducing signal leakage (Tregoning et al., 2022).

6. The Centre National d'Etudes Spatiales/Groupe de Recherches de géodésie spatiale (CNES/GRGS).

Lemoine et al., (2007) at CNES/GRGS present an alternate geopotential model, EIGEN-GL04S, based on GRACE and LAGEOS 1 and 2 data. They derive the biased K-band ranges, rather than using the level-1B K-band range-rates (because they contain too much noise). They used their orbit determination software GINS for inter-satellite tracking data reduction and generated the normal matrixes to solve for the Stoke's coefficients.

Since GRACE has low sensitivity to low degree harmonics (2-3), they incorporated LAGEOS data to improve the resulting solutions. They provided a spherical harmonic solution up to degree and order 50, with a higher temporal resolution of 10 days, rather than monthly, with a spatial resolution of 666 km.

Bruinsma et al., (2010) presented subsequent work to Lemoine et al., (2007) at CNES/GRGS of 10-day gravity solutions in fully normalized Stoke’s coefficients to degree and order 50, with a resolution of 400 km. The method is mostly the same as Lemoine et al., (2007), but they improved the processing and the constraints, their results showed an improved reduction in north-south striping. Bruinsma et al., (2010) applied a regularization, a set of empirically determined a-priori constraints to the diagonal of the normal matrices. They found that filtering and smoothing the solutions attenuated not only the noise but the signal as well. With the applied regularization they found that more of the signal is retained at higher degrees, reducing the striping. The major improvements between Lemoine et al., (2007) and Bruinsma et al., (2010) CNES/GRGS solutions occurred in the deserts and oceans.

2.3.5. GRACE/GRACE-FO solutions used

The method of my work requires elastic and viscoelastic deformation observations derived from spherical harmonics solutions. For this thesis I have used the ANU monthly mascon estimates of the gravity field, converted to degree 180 spherical harmonic models. Further details on orbit integration, parameterization are described in Allgeyer et al., (2022).

The Geodesy group at ANU introduced irregular shaped mascons solutions (Allgeyer et al., 2022; Tregoning et al., 2022). The approach implemented irregular shaped mascons, that could delineate and separate coastlines and basins, thus mitigated the signal leakage between mascons. Their approach creates initial 'ternary’ mascons of around 18 km x 18 km covering the Earth, separating shorelines. Ternary mascons are grouped to create ‘primary’ mascons of around 200 km x 200 km. Since they are irregular, the area of the mascons varies slightly. A benefit from breaking the Earth in the ternary mascons is that it allows the user to create any shape for the primary mascon, to follow complex coastlines, drainage boundaries of glacier or hydrological basins, to mention some. The Allgeyer et al., (2022) solutions agreed well spatially and temporally with CSR and GSFC solutions in Greenland, one of the areas of interest for this thesis. The ANU Geodesy group provided spherical harmonic solutions derived from their mascons.

As per Allgeyer et al., (2022), the data are monthly solutions produced by stacking the normal equations of daily solutions, produced from the inversion of range acceleration observations. For each 24 hours orbit they estimated the satellite position, velocity, accelerometer calibration scale factor and bias and mascon parameters.

The ANU group continues to improve the temporal gravity field solutions, for my work I am using 200 km x 200 km solutions (McGirr et al., 2024), with changes applied to the regularization from Allgeyer et al., (2022). Estimating the mascons is an iteration process to mitigate the regularization attenuating the estimated signals. After each inversion the a-priori value for the mascons is updated, the orbits reintegrated, and the least squares inversion is repeated until convergence of the mascon estimates. For detailed description of the data analysis refer to McGirr et al., (2024).

The ANU GRACE/GRACE-FO mascon solutions used are available from 2002-08 through to 2023-12 in https://doi.org/10.25911/61dceb9c03396. The ANU gravity solutions are corrected for GIA, I reincorporated the ICE_6G_D into the solutions for my work.

3. Methods

Together GRACE, GRACE-FO and GPS geodetic techniques have contributed to mapping and understanding mass redistribution on Earth. The approach I took in this thesis uses GPS observed vertical land motion to compare against GRACE and GRACE-FO deformation estimates. The combined elastic and viscoelastic signals from GPS and GRACE/GRACE-FO should be the same at any given time, only if the two signals are correct and providing that GPS responds to broad-scale signals that GRACE/GRACE-FO also detect.

Continuous GPS height estimates are available during the GRACE period (2002-2017), through the gap between missions, and during GRACE-FO (2018-present). Even though there are large networks of available GPS sites, for my work it suffices to use a subset of good quality GPS sites in strategic locations that are affected by both hydrology and GIA signals. All sites evaluated are in areas that were covered by ice at the Last Glacial Maximum (Fennoscandia, Laurentia and Greenland) where elastic deformation (hydrology-induced mass loss of ice sheets) and a GIA signal are present today.

From the combination of GPS height estimates and GRACE/GRACE-FO temporal gravity field measurements it is possible to separate the GRACE/GRACE-FO elastic and viscoelastic components, through a joint inversion using GRACE, GRACE-FO, and GPS data through least squares to solve for coefficients of a spherical harmonic model that represents the GIA signal. This is the approach that I have used.

To validate the inversion technique and assure the correct separation of the two signals, I reconstruct the height estimate at discrete GPS locations and compare it to observed height changes. If the GRACE/GRACE-FO deformation signals are separated correctly their sum should match the GPS height estimates. If there is a discrepancy between the GPS height time series and the one derived from GRACE/GRACE-FO, then that could indicate there is a mismatch between the missions.

The verification technique became a tool to assess the reliability and validity of alternative GIA models, at specific locations, an ideal tool for regional assessments of GIA models. The method implemented in this thesis is valid for a range of Earth models, considering various rheological and ice-load history models. If the elastic and viscoelastic signals are not separated correctly there would be a mismatch between the the observed GPS and the reconstructed GPS time series.

3.1. Modelling deformation from Stoke's coefficients

Purcell et al., (2011) inspired by Wahr et al., (1995, 2000), established an empirical expression of the ratio of viscoelastic Love numbers (h^{ve}/k^{ve}) that can be used in a mathematical representation of a GIA signal. h_n^{ve} and k_n^{ve} are the dimensionless viscoelastic Love numbers in the spatial domain, that depend on degree '*n'* and are independent of order '*m*'. The viscoelastic structure of the Earth model determines the Love numbers h^{ve}, l^{ve}, and k^{ve}, (*h*' represents the vertical displacement, and *k*' the gravitational potential and *l*' the horizontal displacement) which are the spherical harmonic amplitudes in the infinite series expansion of the surface load functions (Farrell, 1972; Mitrovica & Peltier, 1989). The load Love numbers are used to transform the mass Stokes coefficients to crustal deformation estimates.

The Purcell et al., (2011) empirical expression is the ratio between changes in the gravitational potential and surface vertical displacement, calculated as a function of position. The method considers and works for various Earth and ice-load models, assuming major deglaciation changes to glaciers finished at least six thousand years ago. The Purcell et al., (2011) method uses the ratio of the coefficients to derive viscoelastic uplift. The method can estimate the GIA spherical harmonics coefficients up to degree 256, from gravity data. Purcell et al., (2011) apply the ratio to express the viscoelastic changes in uplift (ΔU^{ve}):

$$\Delta U^{ve}(\theta,\lambda,t) = R\sum_{n=2}^{N}\sum_{m=0}^{n}\frac{h_n^{ve}}{k_n^{ve}}P_{nm}(cos\theta)[C_{nm}^{ve}(t)cos(m\lambda)+S_{nm}^{ve}(t)sin(m\lambda)]$$

Equation 3.1

Here θ and λ are the colatitude and longitude of a specific point, R is the mean radius of the Earth, C^{ve}_{nm} and S^{ve}_{nm} are the time variable dimensionless Stoke's coefficients representing the viscoelastic change in the Earth's gravity field and P_{nm} are the normalized associated Legendre polynomials evaluated at the specified colatitude of degree n and order m of the spherical harmonics.

Wahr et al., (1995, 2000) have an alternative approximation to estimate the vertical displacement caused by viscoelastic deformation, being $(2n+1)/2$ instead of h^{ve}/k^{ve} :

$$\Delta U^{ve}(\theta,\lambda) = R\sum_{n=2}^{N}\sum_{m=0}^{n}\frac{2n+1}{2}P_{nm}(cos\theta)[\delta C_{nm}^{ve}cos(m\lambda)+\delta S_{nm}^{ve}sin(m\lambda)]$$

Equation 3.2

Purcell et al., (2011) provided a linear approximation that can be used to evaluate the viscoelastic Love number ratios for work up to degree 60, refer to figure 3.1.

$$\frac{h_n^{ve}}{k_n^{ve}} = (1.1677n - 0.5233)$$

Equation 3.3

As seen in figure 3.1 values over degree 60 diverge from linear, as well as low degrees (deg 2-8). Because of this Purcell et al., (2011) provided tabulated values of global averages for h_n^{ve}/k_n^{ve} for work requiring higher values (up to degree 256). These are the values used in this thesis.

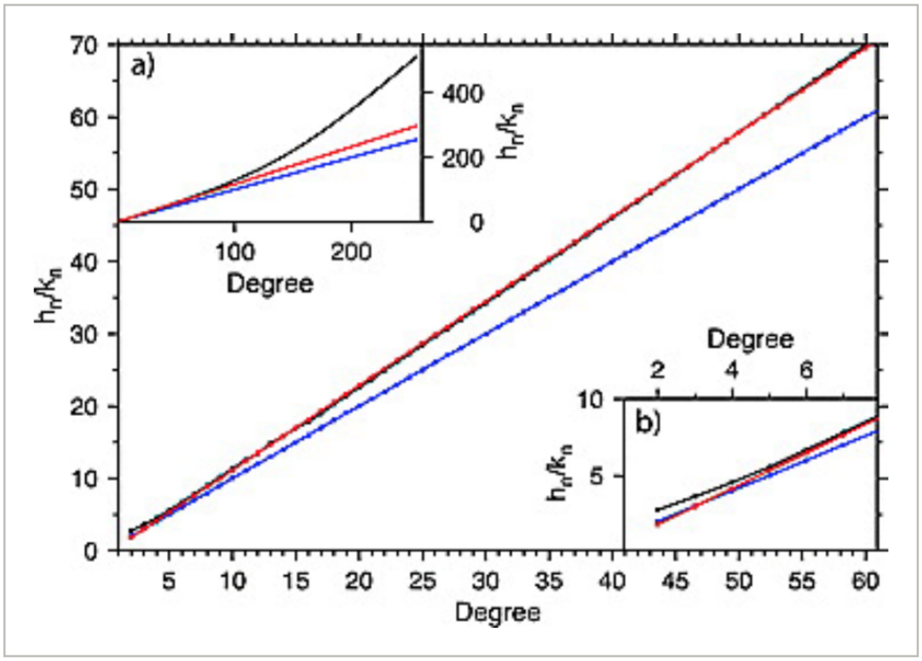

Figure 3.1 From Purcell et al., (2011). The black line is the ratio of h_n^{ve}/k_n^{ve} calculated from the vertical deformation caused by GIA and corresponding changes in gravity over the last ten years for each harmonic degree n. The blue line corresponds to Wahr et al., (1995, 2000) approximation. The red line is the linear approximation from equation 3.3.

The Purcell et al., (2011) method is applicable to a range of Earth models. Lithospheric thickness can vary from 50 to 10 km, and viscosity parameters varying in the upper and lower mantle, and variations in the ice-load by 20% do not influence the answer. They stated that resulting GIA estimates are insensitive to uncertainties in Earth and ice models, as the ratio is the same for any Earth and ice-load model within a ± 20%range. The weak dependence on Earth model parameters and ice-load is valid, providing that major deglaciation changes to glaciers finished at least six thousand years ago.

Davis et al., (2004) introduced the equation to represent changes in elastic load surface displacement (ΔU^e):

$$\Delta U^e(\theta,\lambda) = R\sum_{n=2}^{N}\sum_{m=0}^{n}\frac{h_n^e}{1+k_n^e}P_{nm}(cos\theta)[\delta C_{nm}^e cos(m\lambda) + \delta S_{nm}^e sin(m\lambda)]$$

Equation 3.4

Where h_n^e and k_n^e are the dimensionless elastic Love numbers. Purcell et al. (2011) noted that the "*1*" in the denominator is the ongoing change in the geoid caused by the gravitational attraction of the load. Since major icesheet changes concluded at least six thousand years ago the *"1"* in the denominator is not necessary to express the viscoelastic changes in load (ΔU^{ve}), but it is required for the elastic deformation component.

The use of equations 3.1 and 3.4 allow the separate elastic and viscoelastic deformation to be calculated, if the spherical harmonic GRACE/GRACE-FO coefficients could be separated into their elastic and viscoelastic components.

3.2. Theory: observation equation

The changes in GPS heights at any epoch equal the sum of both elastic and viscoelastic estimations derived from GRACE.

$$\Delta h_{gps} = \Delta h_{GRACE}^{e} + \Delta h_{GRACE}^{ve}$$

Equation 3.5

Substituting the GRACE/GRACE-FO values for their respective elastic and viscoelastic spherical harmonic extension introduced in equation 3.1 and 3.4, the GPS changes in vertical deformation can be expressed as:

$$\Delta h_{gps} = \Delta U^{e} + \Delta U^{ve}$$

Equation 3.6

or,

$$\Delta h_{gps} = R\sum_{n=2}^{N}\sum_{m=0}^{n}\frac{h_n^e}{1+k_n^e}P_{nm}(cos\theta)[\delta C_{nm}^{e}cos(m\lambda) + \delta S_{nm}^{e}sin(m\lambda)]$$

$$+ \mathrm{R}\sum_{n=2}^{N}\sum_{m=0}^{n}\frac{h_n^{ve}}{k_n^{ve}}P_{nm}(cos\theta)[\delta C_{nm}^{ve}cos(m\lambda) + \delta S_{nm}^{ve}sin(m\lambda)]$$

Equation 3.7

I can separate the spherical harmonics coefficients of the GRACE gravity field into the elastic and viscoelastic signals.

$$\delta C_{nm}^{GRACE}(t) = (\Delta t \times C_{nm}^{ve}) + \delta C_{nm}^{e}(t)$$

$$\delta S_{nm}^{GRACE}(t) = (\Delta t \times S_{nm}^{ve}) + \delta S_{nm}^{e}(t)$$

Equation 3.8

Rearranging, the elastic component becomes:

$$\delta C_{nm}^{e}(t) = \delta C_{nm}^{GRACE}(t) - (\Delta t \times C_{nm}^{ve})$$

$$\delta S_{nm}^{e}(t) = \delta S_{nm}^{GRACE}(t) - (\Delta t \times S_{nm}^{ve})$$

Equation 3.9

The elastic component of GRACE spherical harmonics coefficient can be replaced in equation 3.7 as the difference between the total GRACE signal and the GRACE viscoelastic component, leaving only viscoelastic parameters in the equation. The following equation is the observation equation used to solve the GRACE viscoelastic spherical signal.

$$\Delta U^{gps}(\theta,\lambda,t) = R\sum_{n=2}^{N}\sum_{m=0}^{n} P_{nm}(cos\theta)\times[\frac{h'_n}{1+k'_n}[(\delta C_{nm}^{GRACE}cosm\lambda+\delta S_{nm}^{GRACE}sinm\lambda)$$

$$-\Delta t(C_{nm}^{ve}cosm\lambda+\delta S_{nm}^{ve}sinm\lambda)]+(\frac{h_n^{ve}}{k_n^{ve}})\Delta t[C_{nm}^{ve}cosm\lambda+S_{nm}^{ve}sinm\lambda]]$$

Equation 3.10

3.2.1. Pseudo-observations

In areas where there is no GIA signal, it is reasonable to assume that the entire GRACE/GRACE-FO observed gravity changes are related to elastic deformation or ocean bottom pressure change, that is to say it is predominately a hydrological signal. I introduced pseudo-observations on land and ocean, where GPS observations were not present, to help stabilize the estimation of the GIA spherical harmonics and mitigate errors in the inversion. Pseudo sites for the ocean and land are imperative for the inversion to work when there is no coverage of GPS sites.

3.2.1.1. Pseudo land observations

In non-GIA regions over land the change in load is mainly caused by water loading, therefore any vertical movement is caused by elastic deformation U^e. Pseudo-observations were created in land (PSLND) with equation 3.4, assuming all the GRACE/GRACE-FO signal is elastic deformation alone.

I ran inversions including GPS sites in non-GIA areas, this has no effect on the results in GIA regions, therefore I excluded those sites to speed up the computation time.

3.2.1.2. Pseudo ocean observations

Ocean bottom pressure is the combined pressure of sea water and the atmosphere above it. Oceans near regions with GIA signals are also affected as it alters the rate of change in ocean bottom pressure (Hughes et al., 2012). The oceans near regions with GIA signals can also be impacted by the subsidence of the ocean floor due to the peripheral bulge collapsing due to the loss of weight/mass on the surface caused by ice melt and glacial rebound. Ocean loads predominately depend on locally variable properties of the crust and upper mantle responding to ocean circulation and deep-sea tides. The Earth elastic structure beneath ocean basins is susceptible to being affected by the load more than in continents (Farrell, 1972). For pseudo-observation in the ocean (PSOBP), it is assumed that it is solely a change in ocean bottom pressure P (pascals) (Rietbroek et al., 2006). I generate ocean bottom pressure changes caused solely by elastic load at any location in the ocean:

$$\Delta P^e(\theta, \lambda, t) = \frac{Rg\rho_e}{3} \sum_{n=2}^{N} \sum_{m=0}^{n} P_{nm}(cos\theta) \times [\frac{2n+1}{1+k'_n}$$

$$[(\delta C_{nm}^{GRACE} cosm\lambda + \delta S_{nm}^{GRACE} sinm\lambda) - \delta t(C_{nm}^{ve} cosm\lambda + S_{nm}^{ve} sinm\lambda)]]$$

Equation 3.11

Where g is the mean gravity at the surface of the Earth, and p_e is the average density of the Earth. With both observation equations established, it is possible to form a least squares inversion to solve for the Stoke's coefficients of the viscoelastic component that has been detected by both observation systems (GRACE/GRACE-FO and GPS).

To create the design matrix for the least squares inversion, partial derivatives were calculated that differentiate the GPS height, $\Delta U^{gps}(\lambda , \theta , t)$, and ocean bottom pressure, $\Delta P^e(\lambda ,\theta ,t)$, observations with respect to the parameters C^{ve}_{nm} and $S^{ve}{}_{nm}$, to form the Jacobian/A matrix: (partial derivatives matrix = ∂ obs/∂ param).

$$\frac{\partial \Delta U^{gps}(\lambda,\theta,t)}{\partial C^{ve}_{nm}} = R\Delta t P_{nm}(cos\theta)(\frac{h^{ve}_n}{k^{ve}_n} - \frac{h'_n}{1+k'_n})cosm\lambda$$

Equation 3.12

$$\frac{\partial \Delta U^{gps}(\lambda,\theta,t)}{\partial S^{ve}_{nm}} = R\Delta t P_{nm}(cos\theta)(\frac{h^{ve}_n}{k^{ve}_n} - \frac{h'_n}{1+k'_n})sinm\lambda$$

Equation 3.13

$$\frac{\partial \Delta P^{e}(\lambda,\theta,t)}{\partial C^{ve}_{nm}} = \frac{-Rg\rho_e\Delta t}{3}(\frac{2n+1}{1+k'_n})P_{nm}(cos\theta)cosm\lambda$$

Equation 3.14

$$\frac{\partial \Delta P^{e}(\lambda,\theta,t)}{\partial S^{ve}_{nm}} = \frac{-Rg\rho_e\Delta t}{3}(\frac{2n+1}{1+k'_n})P_{nm}(cos\theta)sinm\lambda$$

Equation 3.15

A priori values of zero were used in the inversion to solve for Stoke's viscoelastic coefficients, the GIA parameters, so the $\hat{x}$ values become the estimated values. Because this is a linear least square inversion, there is no need to iterate the solution after the first inversion.

$$\hat{x} = (A^t W A)^{-1}(A^t W B)$$

Equation 3.16

A similar theory has been recently published by Vishwakarma et al., (2022); and Ziegler et al., (2023). They created pseudo-observations sites at 5 degrees spacing which only permitted them to estimate a degree 35 GIA model.

3.3. Areas of Interest

The ice cover in Fennoscandia, Laurentide and Greenland was significantly larger during the Last Glacial Maximum and, along with present day mass loss, has resulted in the large Glacial Isostatic Adjustment signal currently observed (Bennike & Björck, 2002). Fennoscandia, Laurentide and Greenland are ideal areas for this work, as they are all affected by elastic and viscoelastic deformation measured by GPS, GRACE, and GRACE-FO. Having areas with the presence of both signals measured by different geodetic techniques should make it possible to separate the signals through a least squares inversion, solving for a GIA signal. If the reconstructed height time series of vertical deformation follows the observed deformation through the GRACE-FO measurements, the method is successful and would show consistency between the two missions. While the viscoelastic is constant over GRACE/GRACE-FO, the elastic component can be significant and may change in rate. The best way to compare them is to reconstruct the time series as described above.

This methodology is not appropriate for Antarctica, due to the lack and limited GPS height time series to adequately constrain the mathematical framework of this work. This thesis will only discuss the GIA in the Fennoscandia, Laurentide and Greenland. I recognize that it may not work in GIA regions lacking GPS observations (e.g. the centre of Greenland).

All areas of interest have continuous gravity field observations through the GRACE mission and continue on to the GRACE-FO mission after it launched. These areas are tectonically stable with minimal vertical tectonic contributions. The extent of the GPS network varies from place to place. In the following paragraphs I will explain the importance of and difference between each area.

3.3.1. Fennoscandia

The Earth's crust has been rising continuously in Fennoscandia since the Last Glacial Maximum. The active postglacial uplift of Fennoscandia has been observed and monitored for 300 years, which has allowed scientists to document an extensive and continuous network of observations, as far back as 1743 (Ekman, 1996; Ekman & Mäkinen, 1996; Johansson et al., 2002; G. A. Milne et al., 2001; Milne et al., 2004) Fennoscandia is the initial testing area as there is a dense GPS network throughout Fennoscandia and Europe, covering the peripheral bulge signal across Europe. Well-established GPS networks (i.e. BIFROST project, Johansson et al., 2002; G. A. Milne et al., 2001; Milne et al., 2004) have been recording since before the GRACE mission was launched. Because of the extensive observation networks, today there is a good understanding of the GIA signal in Fennoscandia. If the method is accurate, the estimated viscoelastic model should replicate existing GIA models of the area. This would support the hypothesis that with a dense distribution of GPS stations, it is possible to estimate a high-resolution GIA model, with spatial accuracy, from an inversion of GRACE/GRACE-FO and GPS height data.

3.3.2. Laurentide

The Laurentide ice sheet is believed to have been the largest of the ancient ice masses, as its maximum extent covered all of Canada and the north-eastern part of the United States (Mitrovica & Peltier, 1989). GIA models are relatively well known in this area. Laurentide is the second testing site, encompassing Canada, the Canadian Arctic, and the northern part of the United States. There is a good distribution of GPS stations that adequately span most of the area of interest. However, unlike Fennoscandia, spacing between the GPS stations across Laurentide is not as dense, which prevents the estimation of a high-resolution spatial GIA model. Nevertheless, with a working method in Fennoscandia, the approach still provides useful information in Laurentide. The primary objective in Laurentide, as the second area of interest, is to assess the accuracy of estimating a GIA signal at discrete locations where real observations are available, under the mathematical constraints of the inversion. That is, while the GPS distribution may not allow for an accurate spatial estimation of GIA across Laurentide, it is still possible to obtain accurate GIA estimates at the precise locations of the GPS.

3.3.3. Greenland

As Greenland is one of the largest freshwater reservoirs on Earth and a major contributor to sea level change, it is essential to better understand its GIA signal because it has to be removed from GRACE/GRACE-FO estimates to quantify Greenland's contribution to sea level rise. Between 2002 and 2006 the rate of ice loss in Greenland had increased by 250% from previously estimated rates (Velicogna & Wahr, 2006). The GPS network in Greenland is quite sparse with GPS height time series only on rock outcrops along the coastline, inhibiting properly constraining the GIA signal of the interior. No other observations exist in the interior to help constrain the GIA models. A working method (tested in Fennoscandia), reliable at discrete points (tested in Laurentide), can be expected to work with a limited GPS network such as Greenland; and contribute to a better understanding of the GIA signal in Greenland.

Greenland is the last and the main area of interest to validate my method. In Fennoscandia and Laurentide, vertical deformations are predominantly linear, with seasonality, over the years. In contrast, the rapid non-linear melting rates in parts of the Greenland ice sheet, together with seasonal hydrology and GIA signal, cause non-linear time series of vertical deformations, refer to figure 3.2. The Kangia North GPS station

(KAGA), located on the west coast of Greenland, is an example where non-linear height changes throughout the years can be observed.

Through the inversion proposed, I solve for the spherical harmonics coefficients that represent the GIA signal. With an estimated GIA model, it is possible to separate the GRACE/GRACE-FO spherical harmonic coefficients into the elastic and viscoelastic. Once separated, the two components can be used to calculate the elastic and viscoelastic heights which, when summed, form the reconstructed time series. The separation into elastic and viscoelastic is successful if the reconstructed time series matches the GPS observations.

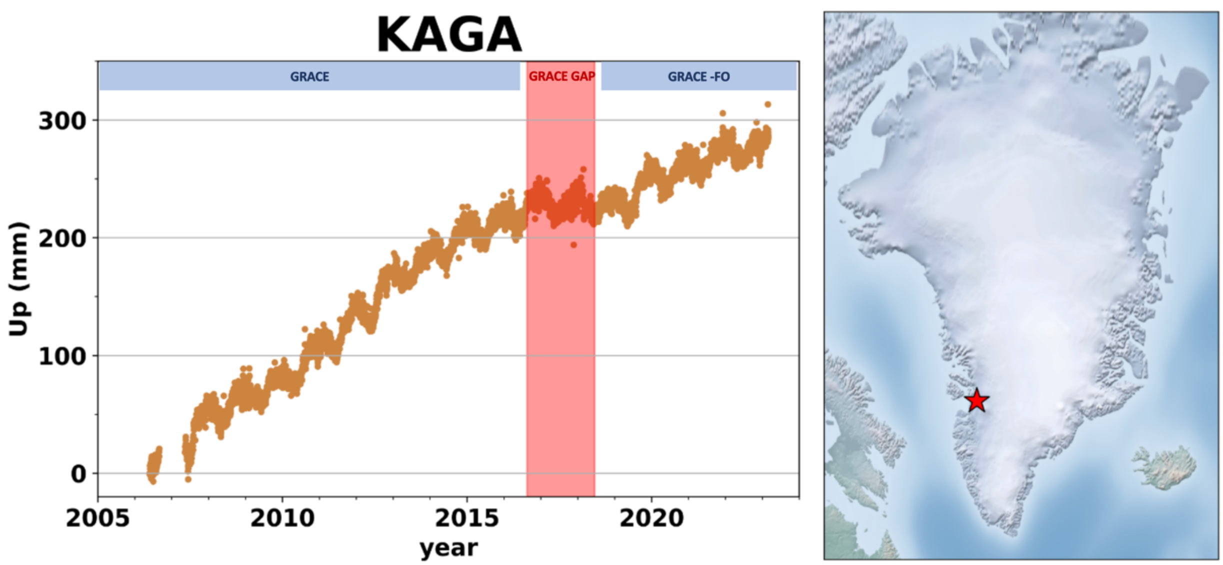

Figure 3.2 GPS time series in KAGA site, located on the west coast of Greenland.

3.4. Data input into the inversion

All GPS height time series used are publicly available from the Nevada Geodetic Laboratory at the University of Nevada Reno (Blewitt et al., 2018). Even though there are GPS sites available across the world, for the purpose of the study I require a comprehensive network predominantly in Fennoscandia, Laurentide and Greenland, and their surroundings; including Europe and the northern part of the United States as they can reflect a signal of a peripheral bulge. Altogether they can show how the GIA signal attenuates away from the ice-covered areas with a strong GIA signal.

The primary interest is to have “true/*real*” good quality GPS height observations in locations where both elastic and viscoelastic deformation is occurring. The presence of both signals helps the inversion distinguish between present-day elastic loading and GIA. I undertook a thorough GPS site selection process where I included as many high-quality GPS height time series as possible in the areas of interest. In section 3.5.1 I describe in detail the selection criteria for the GPS sites. It is essential to have good quality GPS height observations in areas with GIA for the inversion to work, as the extent of the GPS network can determine the maximum degree of the spherical harmonic model of the inversion. To calculate a spherical harmonics model for a high-resolution GIA model, the spatial resolution to which the model can be estimated accurately is determined by how closely spaced the GPS observation points are.

To invert for the spherical harmonic field, the spacing between the measurements must be 180/n times the kilometre spacing required. For the inversion to work, there must be GPS measurement covering the entire surface of the Earth with a particular spacing, to solve for the GIA at any spatial resolution. Even if I incorporated all the GPS sites available around the world, it is not possible to cover the entire Earth, so I introduced pseudo-observations to overcome this issue.

3.5. Preparation of data

3.5.1. GPS analysis

I visually assessed the quality of each GPS height time series, as part of the GPS data selection process. Suitable GPS height time series had to have good quality data and could not be near tectonically active boundaries, as that can represent other physical processes other than elastic and viscoelastic signals. Ideally, uncorrupted GPS sites would have near continuous information from 2002 to 2023, without offsets, or outliers. The rates of vertical land motion depend on several factors, such as time series length and gaps in data. By elongating GPS time series, vertical land movement rates are less sensitive to interannual variations. However, common issues associated with GPS recording include gaps in the data when there is a change in the antenna, or in colder regions when there are rapid changes in snow accumulation (Segall & Davis, 1997). Therefore, only using uncorrupted GPS sites would limit the amount of GPS height time series suitable, so the criteria for suitable GPS to be included in the work was to have mostly continuous data. “Mostly continuous data” means that I could include sites with gaps of a couple of months, sometime years in the time series, as long as there is sufficient data in the GPS height time series, contributing information when there are no GRACE/GRACE-FO observations.

In the quality control process, there were cases with offsets in the GPS readings, that could have been caused by instrumental changes or defective equipment and, if corrected, the GPS time series could contribute to the observations of the thesis. The presence of significant offsets and outliers can corrupt the analysis of data as they can contribute to misleading interpretations in the inversion. In the following section I explain how I corrected for offsets and major outliers corrupting GPS time series, to help expand GPS network.

3.5.1.1. Offset and outlier correction

The offset correction program is inspired by the Median Interannual Difference Adjusted for Skewness (MIDAS) method of Blewitt et al., (2016). MIDAS is a trend estimator that, using data pairs separated by one year, can detect and avoid discontinuities, outliers, seasonality, skewness, and heteroscedasticity. In essence, the purpose of the MIDAS method is estimating velocities, uncontaminated by offsets. An unacknowledged by-product of the method is that it can identify and quantify the size of offsets that may be present in the time series. To mitigate the impact of seasonality and step discontinuities, MIDAS compares data pair separated by 1 year, equation 3.18.

$$vel = height_{t+365} - height_t$$

Equation 3.17

Inspired by the approach of using data pairs separated by one year. I adapted the theory of MIDAS into a program accounting for discontinuities and offsets that identifies the timing and the magnitude of the offsets. In the following paragraphs I explain how it works:

1- Figure 3.3- Shows the original GPS time series at the Aberporth site (ABEP) in the UK, and it shows a notable offset around 2009, marked with the orange line.

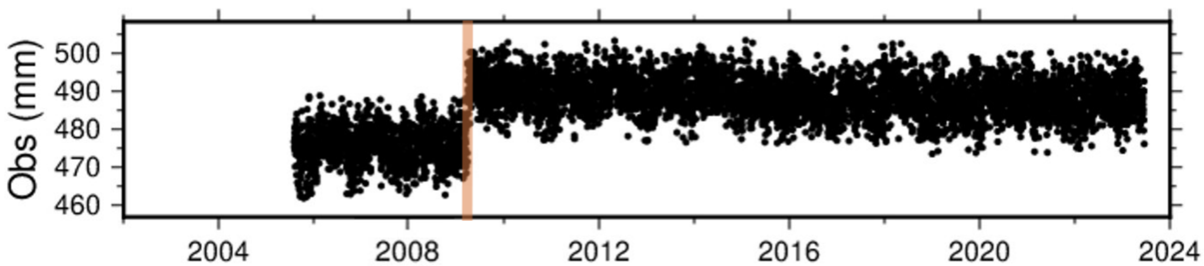

Figure 3.3 Offset correction step 1.

2- The velocities at each point are calculated using equation 3.18, a 12-month sliding window, resulting in figure 3.4. The orange line is the epoch of the offset, and the green line is the epoch where the Midas velocities first identify the change in velocities, because of the offset.

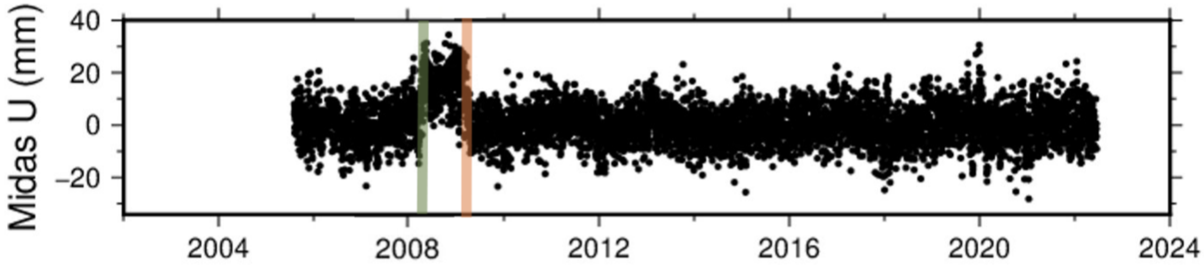

Figure 3.4 Offset correction step 2.

3- The program calculates the correlations of the running mean with a 2-year function of expected change in the presence of an offset. I smoothed the MIDAS velocity for each year; if there is an offset it causes the smoothed values to jump up and down, for one year, by the size of the offset in a triangular shape (red line in figure 3.5), with the peak exactly one year before the offset.

4- I compute the correlation between the MIDAS velocity time series and a synthetic, 2 year wide triangular shape (blue line in figure 3.5). Correlations exceeding ± 0.97 tend to indicate the presence of an offset, this threshold was arbitrarily determined by trial and error and it worked for all cases (except when there were multiple offsets within 2 years, in such case the site was removed from the study). The peak of the blue line indicates the exact epoch of the offset.

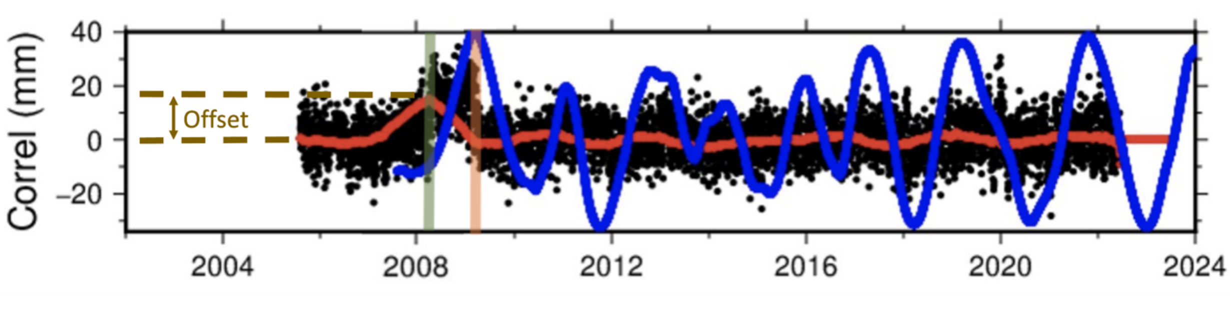

Figure 3.5 Offset correction step 3 and 4.

5- From this it is possible to identify the date when the correlation or anti-correlation occurs. The magnitude of the offset is computed as the difference between the peak of the correlation with the MIDAS median velocity. I adjust the date by moving the date of the red peak forward one year to pinpoint the exact date the offset occurs. I then apply the estimated offset to that and all subsequent epochs. In the case of the ABEP site, the offset was on March 23, 2009, and had a magnitude of 14.6 mm. The corrected time series (blue line) over the original GPS time series (black line) is shown in figure 3.6.

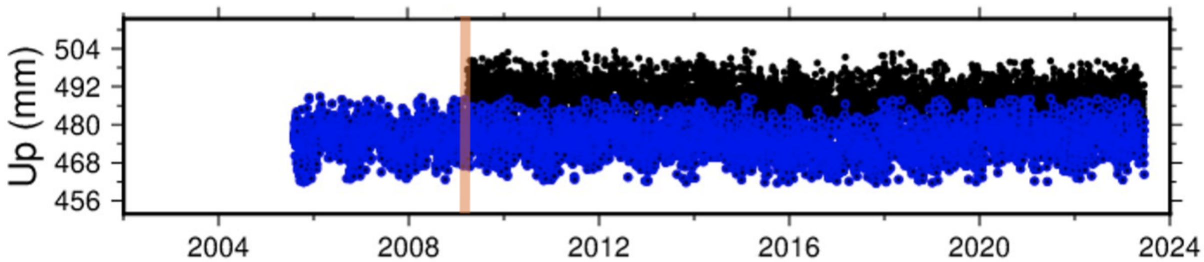

Figure 3.6 Offset correction step 5.

A limitation of the program is that, since it relies on the correlation of data separated by a year, it cannot identify 2 offsets within 12 months. Therefore, I visually assessed each time series and removed from the analysis any sites with time series that were not repaired using this approach.

In the cases where there were significant outliers that could corrupt the solution, as in the case of the Vilhelmina GPS station (VIL6) in Sweden figure 3.7, I applied an outlier correction process. To identify the presence of outliers I applied a box plot calculation to the height observations, which depends on the variability of the data. This method examines the distribution and concentration of data, identifying the outliers. It starts by identifying the median, the first quartile (Q1) and the third quartile (Q3). The range of values between the Q1 and Q3, known as the interquartile range (IQR), should account for ~50% of where the measurements concentrate. Having ~50 % of the measurement's constrains the sample population too much. Thus, I extend the range to each extreme by setting a maximum range to Q3 + 1.5 * IQR and a minimum range to Q1 - 1.5 * IQR. Since the GPS sites used in the work have decades worth of data available, there is no need to risk corrupting the solution with outliers, so any values outside the established range were flagged as outliers and removed for all the GPS sites used in the thesis.

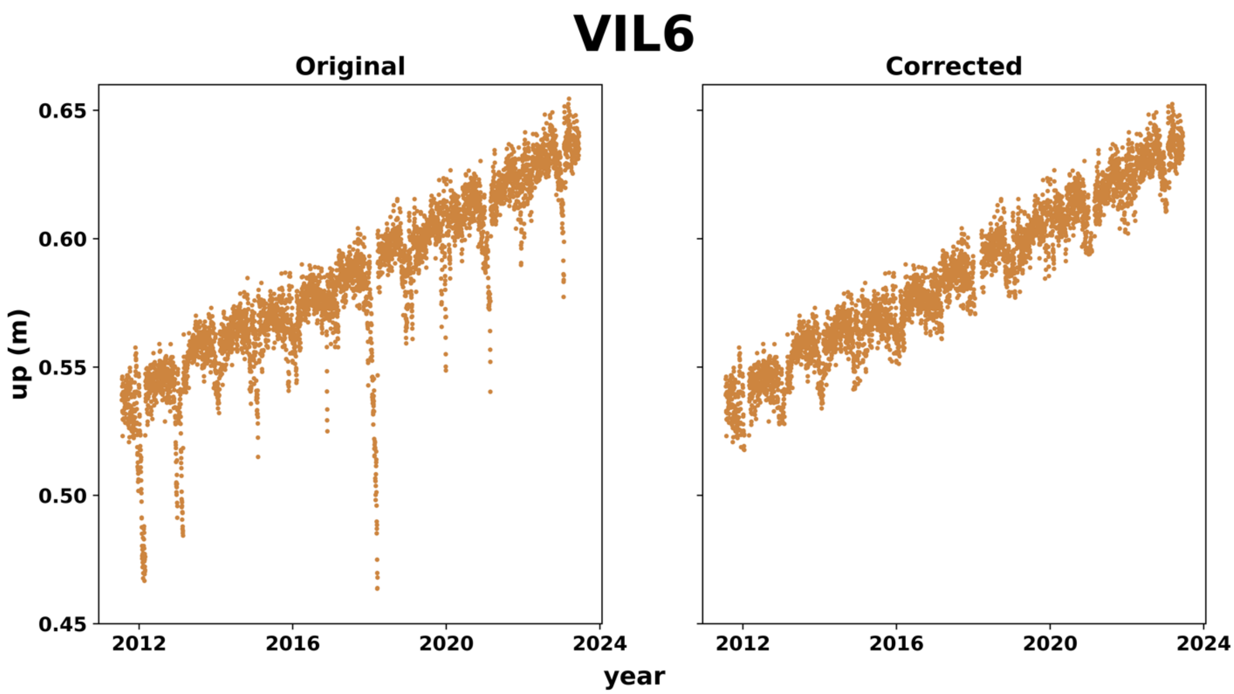

Figure 3.7 Vilhelmina GPS height time series (VIL6), Sweden.

I ran the offset detection filter across every time series, and as part of the quality control, I reviewed visually the linear velocities of each GPS site, and eliminated any outliers that could be affected by regional deformation or local effects. Also, as part of the GPS data preparation, the GPS daily height time series were converted to monthly averages for a consistent comparison between GPS temporal resolution and GRACE monthly solutions. Figure 3.8 shows the final distribution of 846 GPS sites used in the region of interest, the red triangles are the selected GPS stations used in the analysis, the yellow triangles represent the location of the pseudo-land (PSLND) observations, and the blue triangles are the pseudo-ocean (PSOBP) observations.

3.5.1.2. AOD1B – Atmospheric Pressure loading correction

GRACE and GRACE-FO and GPS are affected by non-tidal mass variations in the atmosphere and ocean bottom pressure loading. GRACE and GRACE-FO estimates of mass change have this loading removed as part of the processing (Dahle et al., 2019). For GPS height time series to be compatible with GRACE and GRACE-FO observations, the monthly averaged atmospheric pressure loading must be removed. The atmospheric and ocean mass pressure loading (AOD1B) spherical harmonics products are generated by the GFZ Information System and Data Center and used for the GRACE Level-1B products. The AOD1B GRACE atmospheric de-aliasing product was retrieved and used to correct the GPS heights.

$$\Delta U^{glo}(\theta,\lambda,t) = R\sum_{n=2}^{N}\sum_{m=0}^{n}\frac{h'_n}{1+k'_n}P_{nm}[C^{glo}_{nm}cos(m\lambda)+S^{glo}_{nm}sin(m\lambda)]$$

Equation 3.18

Equation 3.19 converts the de-aliasing atmosphere fields into surface displacement estimates. The *glo* coefficients represent the sum of vertically distributed masses, being the density distribution in the atmosphere and the contributions of the oceanic water column to ocean bottom pressure contributions. This correction was added to the monthly GPS height estimates.

3.5.2. Observation uncertainties

With the GPS sites selected and the pseudo-observations created, I can define the spacing between the pseudo-observations and the GPS sites to invert for the spherical harmonic coefficients representing the viscoelastic signal. I set the pseudo-observations to be 200 km apart across the world, which is appropriate for estimating up to degree 90 solution.

In the regions where there is both GIA and elastic deformation loading, the approach of applying pseudo-observations is no longer viable, as the assumption that the entire GRACE measurement is solely elastic deformation is not correct. In the cases where there is elastic and viscoelastic deformation, the GPS measurements must dominate in the inversion over the pseudo-observations. Otherwise, the pseudo-observations would dominate and the estimated viscoelastic deformation would be incorrect.

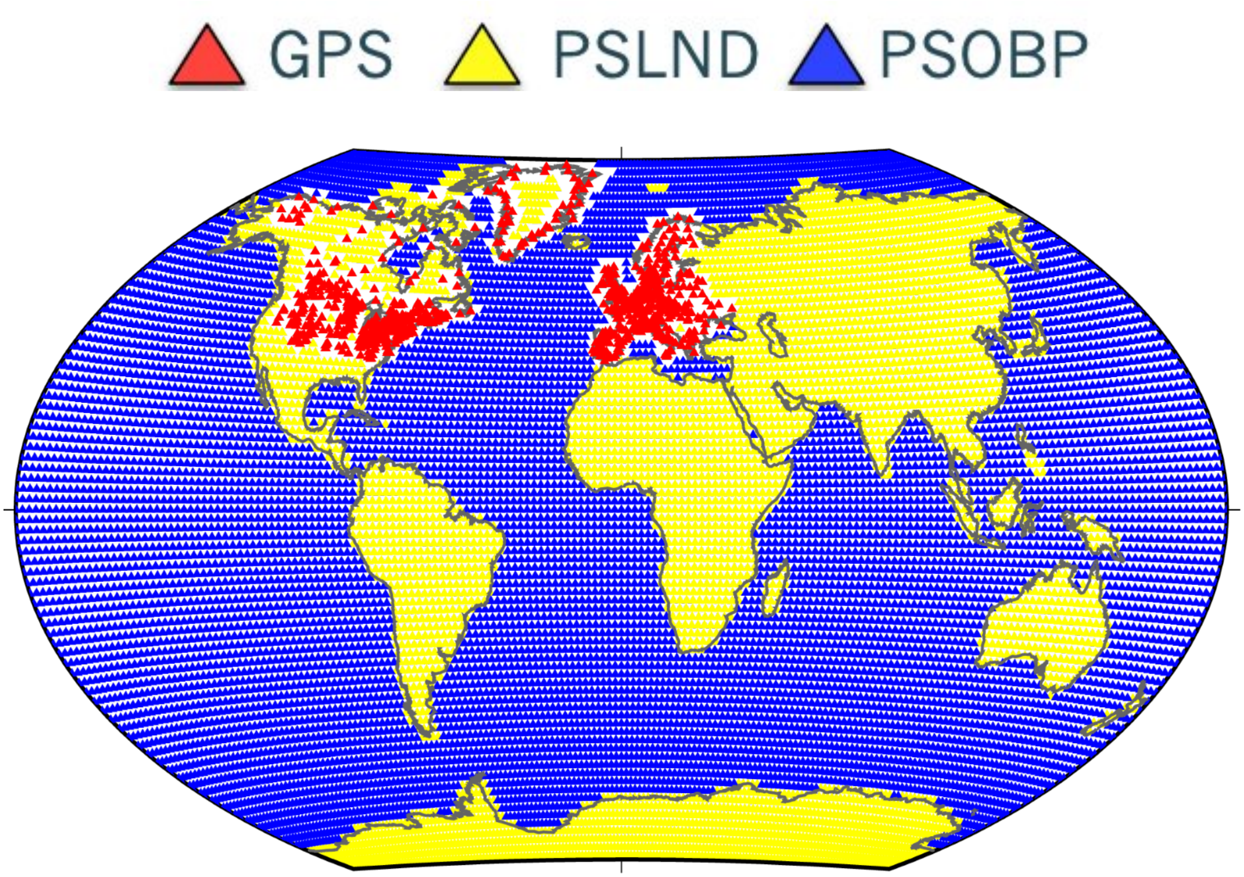

Figure 3.8 Each colour triangle represents the location of the different observation types used in the inversion process.

In the inversion I apply different uncertainties to the observations depending on the type of observation (GPS, PSLND, PSOBP). I characterise GPS observation weights in Fennoscandia, Laurentide and Greenland large enough to include hydrology and GIA signals. Choosing the optimal value for each parameter, so that the model best fits the observation. For PSOBP observations I applied an uncertainty of 10 cm equivalent water height, about ~10 mbar pressure assuming a density of water of ~1000 kg/m^2. The uncertainty assessment is discussed in the results chapter. The weights applied to the pseudo-observations are important and affect the inversion results, this is analysed and discussed in section 4.1.1.

3.5.3. Reconstruction of height time series from GRACE/GRACE-FO data

Given a GIA model, the elastic component of the gravity signal can be identified by subtracting the GIA from GRACE/GRACE-FO. If the GIA model is correct, after removing it from gravity observations, the remaining signal should be the entire elastic component sensed by GRACE/GRACE-FO. Based on equation 3.10, adding the GIA estimated model with the GRACE/GRACE-FO estimated elastic component should create a time series that matches the GPS vertical height changes time series at discrete locations. If the data from the two missions are consistent, the reconstructed time series should reflect the observed GPS height series across both missions. If so, this would validate the GRACE and GRACE-FO data.

A by-product of the method allows for the validation, or otherwise, of any GIA model at discrete points, assessing the quality and accuracy of reconstructed time series against GPS height estimates. That is, if the elastic and viscoelastic signals are separated correctly, it will be possible to reconstruct both a GPS height time series. If the values are not consistent at discrete locations, with both observations, the GIA model is wrong in that area.

4. Results

In the following section, I explain the results of the data preparation and how I assessed the inversion results that provide the separation of the hydrology and the GIA signals. I discuss the height uncertainty assigned to each type of observation, the resulting spatial patterns of the inversion, its accuracy, and the validation of results.

After completing the data preparation, including the assessment of GPS observations and the creation of pseudo-observations, a data file is generated. This file includes GPS height anomalies (comprising both elastic and viscoelastic components), pseudo land observations and pseudo-ocean observations. The spacing of pseudo sites is set to 200 km to permit the inversion to solve for a spherical harmonic model of degree 90. The GRACE/GRACE-FO spherical harmonic solutions height file input data are used in the inversion to solve for the viscoelastic component of GRACE/GRACE-FO spherical harmonics coefficients, using equation 3.10. Figure 3.8 displays the resulting data distribution.

$$\Delta U^{gps}(\theta,\lambda,t) = R\sum_{n=2}^{N}\sum_{m=0}^{n} P_{nm}(cos\theta)\times[\tfrac{h'_n}{1+k'_n}[(\delta C_{nm}^{GRACE}cosm\lambda+\delta S_{nm}^{GRACE}sinm\lambda)$$

$$-\Delta t(C_{nm}^{ve}cosm\lambda+\delta S_{nm}^{ve}sinm\lambda)]+(\tfrac{h_n^{ve}}{k_n^{ve}})\Delta t[C_{nm}^{ve}cosm\lambda+S_{nm}^{ve}sinm\lambda]]$$

Equation 4.1

4.1. Assessment of inversions with simulated data

To test the accuracy and reliability of the inversion process to recover the correct answer, I performed a simulation. To assess the level of accuracy with which the GIA model can be estimated. If the data input into the inversion contains sufficient information, the inversion process will recover the GIA signal from the model used to create the simulated input. This approach allows me to investigate how different noise levels and height uncertainties affect the accuracy of the answer and what geometry of observations is needed to obtain an accurate answer.

Referring to the methods chapter, the total vertical deformation is the combination of elastic and viscoelastic deformation, as given by equation 3.5. For the simulation process, I am starting with a GIA model and with GRACE/GRACE-FO temporal gravity fields expressed in spherical harmonics. Subtracting the GIA signal from the GRACE/GRACE-FO coefficients yields the elastic component in terms of spherical harmonics coefficients. I rearranged equation 3.5 so that, starting with the GRACE/GRACE-FO spherical harmonic fields and any GIA model, I can generate spherical harmonic coefficients of their difference to represent the elastic deformation component. Then, as in equation 3.5, using the calculated elastic component and the viscoelastic model spherical harmonic coefficients, I calculate the elastic and viscoelastic height anomaly. Adding the heights together, yields the simulated height observations. The resulting simulated vertical height anomalies are used as the input observations along with the GRACE/GRACE-FO coefficients in the inversion to solve for the GIA coefficients using equation 3.10. Explained in the simulation side of figure 4.1.

$$\Delta h_{gps} = \Delta h^{e}_{GRACE} + \Delta h^{ve}_{GRACE}$$

Equation 4.2

The results of the simulation are assessed by reconstructing vertical height series and comparing them with GPS observations. As explained in the methods section, with the GIA model estimated using equation 3.10 the elastic signal can be calculated. Based on equation 3.5, the addition of the viscoelastic deformation computed from the estimated GIA model and elastic signals reconstruct the GPS-observed vertical deformations. With the added signals I reconstructed a time series of the vertical heights which are then compared to the simulated heights initially created. Explained in the reconstruction side of figure 4.1.

I show in figure 4.1 how using equation 3.5 I reconstruct a vertical height time series at the location of a GPS receiver, to compare my reconstructed height with the GPS observation, that in this case is simulated to know the true answer. Next, I calculated the velocities of the simulated and reconstructed height time series and calculated the difference in velocities for each site. I use the velocity residual as the metric to assess the quality of the inversions.

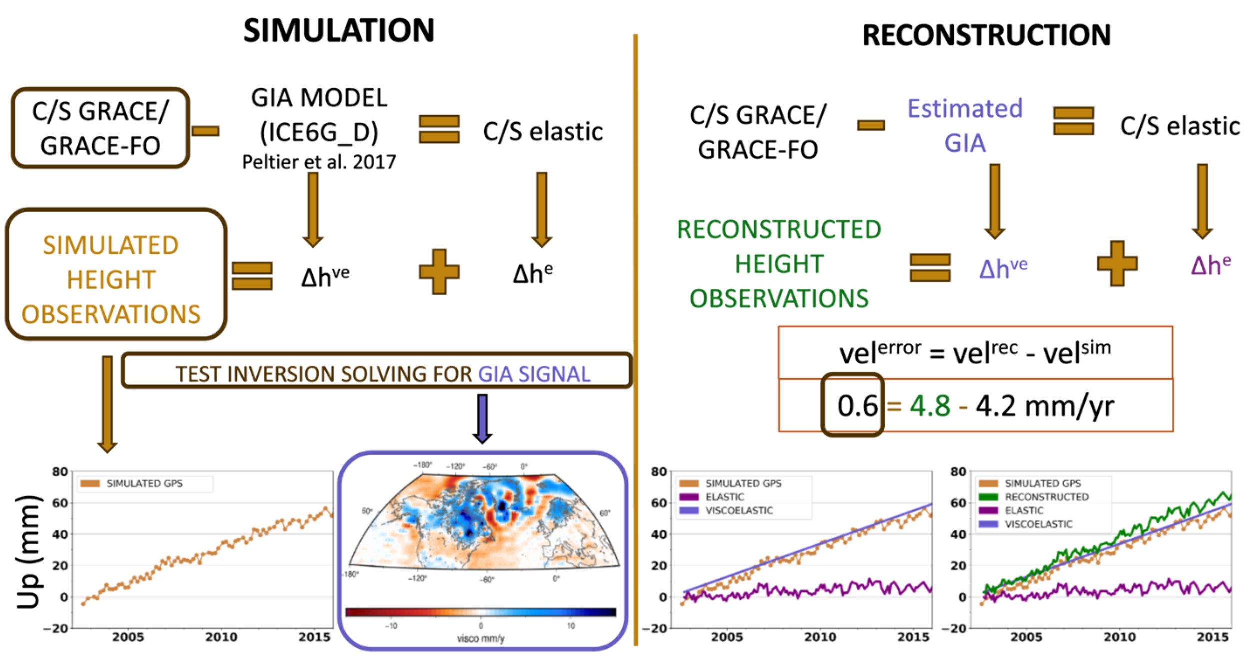

Figure 4.1 Schematic image of simulation and reconstruction process.

4.1.1. Observation uncertainties

To evaluate the influence of different height uncertainties applied to constrain the inversion parameters, I analysed the impact of different height uncertainties for GPS and PSLND observations on the resulting estimates of GIA models. The simulated height observations serve as the control group to determine the ideal uncertainties to apply to the observations and parameters in the inversion of real data.

Given that the project will ultimately use real GPS observations, it is crucial for the simulated data to resemble the real data environment. Therefore, when deciding what observation uncertainty to apply to the GPS simulated height observations, I considered the noise levels of real GPS data, as explained in the GPS background section. With figure 4.2 I assess the impact of using different height uncertainties and various levels of white noise on the GPS observations to decide the preferred values to use for my work.

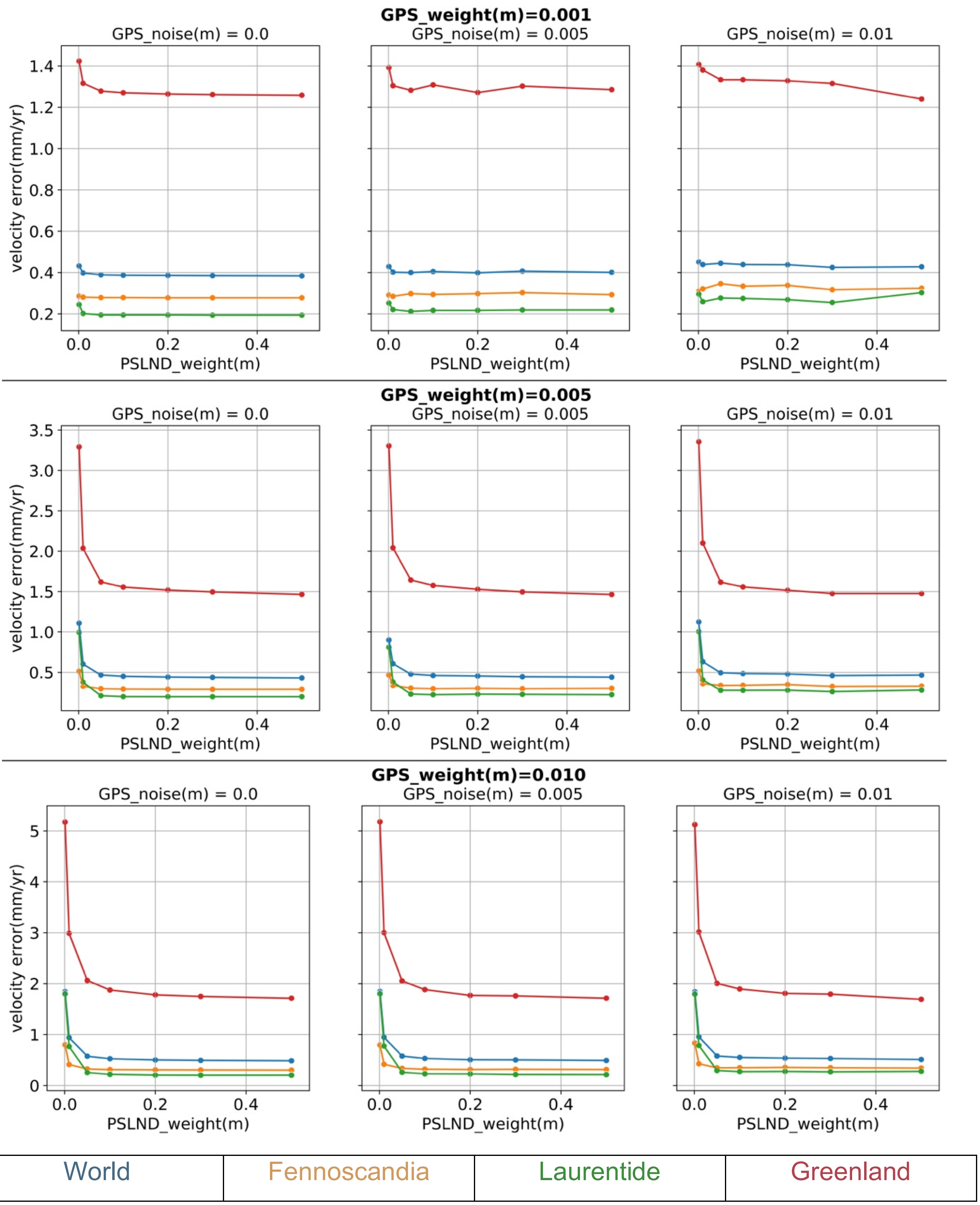

Figure 4.2 The root mean square (rms) of the velocity differences of the simulated and reconstructed time series over each area of interest, as a function of on the different height uncertainties and noise levels assigned in the inversion.

For regional assessments I calculate the root mean square (rms) of the velocity residuals over each area of interest, to evaluate the difference between the velocity residual of the simulated and the reconstructed time series. With these metrics I can see the average velocity error for the reconstructed sites for each area of interest, as shown in figure 4.2.

In figure 4.2 we can see that the highest velocity error tends to be with the higher GPS height uncertainty of 0.01 m and with the smallest PSLND height uncertainty of 0.001 m. This occurs because the pseudo land observations are constructed assuming that all the GRACE/GRACE-FO signal is caused by elastic deformation, which is not true in GIA regions. The more I downweight the GPS height uncertainty, the more it forces the solution towards being just an elastic deformation, which is incorrect. The pseudo sites are overpowering the GPS observation signal and blocking the GIA signal that the GPS observations contain. By downweighting the GPS observations, I lose the ability to estimate the GIA signal.

Accordingly, the velocity error decreases as the GPS height uncertainty decreases to 0.001 m and the PSLND observation uncertainty increases. This is because, as the GPS heights uncertainties are smaller, it restricts the influence of the pseudo-observations at the locations of the GPS sites, making the real observation signals dominate in the inversion.

We can see that, for each different GPS height uncertainty, the velocity error increases with increased noise applied. This is to be expected since the level of noise affects the accuracy of the velocity estimate. In figure 4.2 the error tends to be consistently on par between Laurentide (green line) and Fennoscandia (yellow line). Greenland (red line) has consistently higher error, with the highest error being 5.179 mm/yr. We can see that the velocity error converges as the PSLND height uncertainty increases consistently in the graphs.

The ideal constraints for the inversion would be those that yield the smallest velocity error, which occurs with a GPS height uncertainty of 0.001 m, no GPS noise, and a higher

PSLND height uncertainty of 0.5 m. However, given that I will use real GPS observations, the simulations must be consistent with realistic observation noise.

Since the noise with the largest amplitude/impact on the vertical component is white noise (Wang et al., 2022), I only apply white noise to the simulated data. Several papers found that the realistic level of GPS white noise varies between 2 mm and 9 mm (see discussion of GPS noise in background section). Based on the simulation results and noise assessment of other authors, I chose to use 5 mm of white noise as a realistic representation of GPS height uncertainty for the study. The uncertainty assigned to the GPS height observation should be consistent with the size of the expected noise in the GPS time series of heights. Therefore, since the white noise is 5 mm, I assigned 5 mm uncertainty to the simulated height observations as well. This leads to a convergence of the velocity rms with a PSLND observation uncertainty of 0.3 m, with negligible changes afterwards.

We can see in figure 4.2 that, when applying the appropriate constraints, the velocities can be estimated to better than 1.5 mm/yr; implying that the GIA signal can be estimated with a level of accuracy better than 1.5 mm/yr. Even with the smallest PSLND height uncertainty of 0.001 m the highest velocity error does not exceed 5.18 mm/yr. Overall, the error between the different areas of interest for each solution did not differ by more than 3 mm/yr.

The weights for the pseudo land observations were chosen to be appropriate in the GIA regions. I could have used a tighter value over zero GIA regions, but it would have had no effect on GIA regions, which is the focus of the work.

4.1.2. Simulation model assessment

In figure 4.3 we can see the initial GIA model used to create the simulated height observations (the ICE6G_D model), the estimated model obtained through the inversion, using the simulated GPS height observations, and, at the bottom of figure 4.3 the distribution of the observations.

The spacing between the observations determines the maximum spherical harmonic degree that the inversion can solve for accurately. For a spherical harmonic model to degree 90, there must be a separation of no more than ~200 km between the observations to obtain an accurate answer. If the GPS observations are further apart, I placed pseudo-observations between them to stabilize the inversion.

While it would have been ideal to be able to estimate a global GIA model, the spatial distribution of available GPS data does not make this possible. Therefore, the objective of this work has been to estimate the GIA signal at specific locations monitored by two geodetic techniques: GPS and GRACE/GRACE-FO data.

In figure 4.3 we can see that in the northern hemisphere, particularly in Fennoscandia and Laurentide where there are simulated GPS observations, the inversion successfully retrieves the GIA signal. The inversion recovers the GIA signal best in the areas where I have simulated GPS observations. For example, the signal retrieved across the United States is only present to the extent covered by the simulated GPS data. The inversion fails to capture the remaining GIA signal in the other part of the United States covered by PSLND observations. This shows the impact that the combination of height observations and pseudo-observations have on the estimated GIA model.

This effect can also be seen in the inside of Greenland, where simulated height observations were not included, resulting in the inversion failing to retrieve an accurate GIA signal. This limitation occurs because the method cannot separate the elastic and viscoelastic signals from GRACE/GRACE-FO data alone. The inversion process cannot retrieve any viscoelastic signal in GIA areas when solely relying on PSLND, which are characterised as being elastic deformation alone. Depending solely on pseudo land observations in GIA areas introduces a bias and constraints that limit the signal that can be estimated.

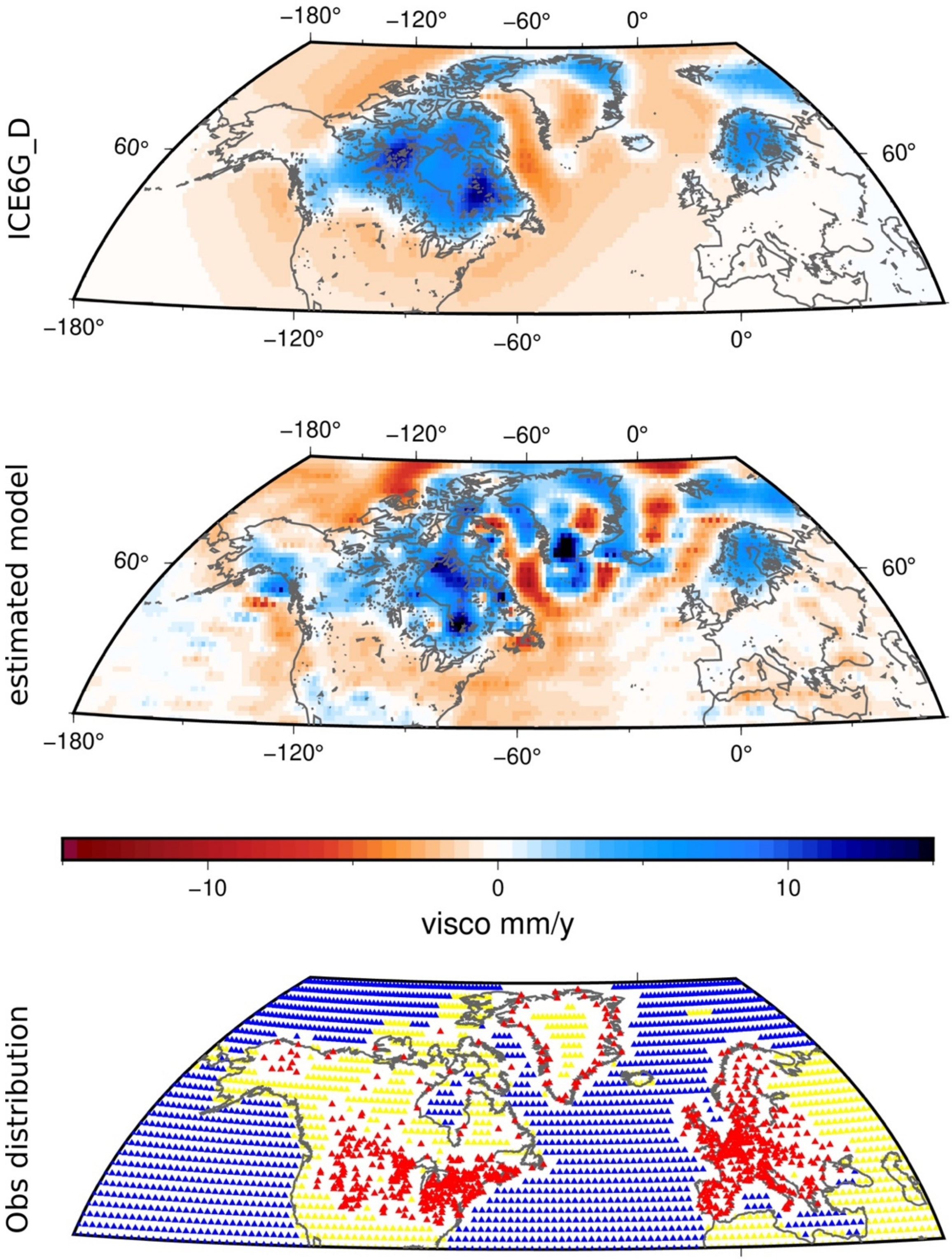

Figure 4.3 The viscoelastic deformation in millimetres per year, for the ICE6G_D model and the estimated model, and the distribution of GPS, PSLND and PSOBP observations.

I examined the velocity residuals between the simulated height estimates and the reconstructed height time series at each GPS location for the areas of interest.

In Fennoscandia, the signal is very well recovered, with an average velocity residual of 0.302 mm/yr computed over all sites in Figure 4.4. Fennoscandia dense GPS coverage did not require PSLND observations to fill in gaps in the observation spacing. The areas with low error correspond to areas with high density GPS coverage. Even though there seems to be a trend in the velocity residuals across Europe, it is minimal with values ranging from –0.64 to 0.71 mm/yr, as seen in figure 4.4.

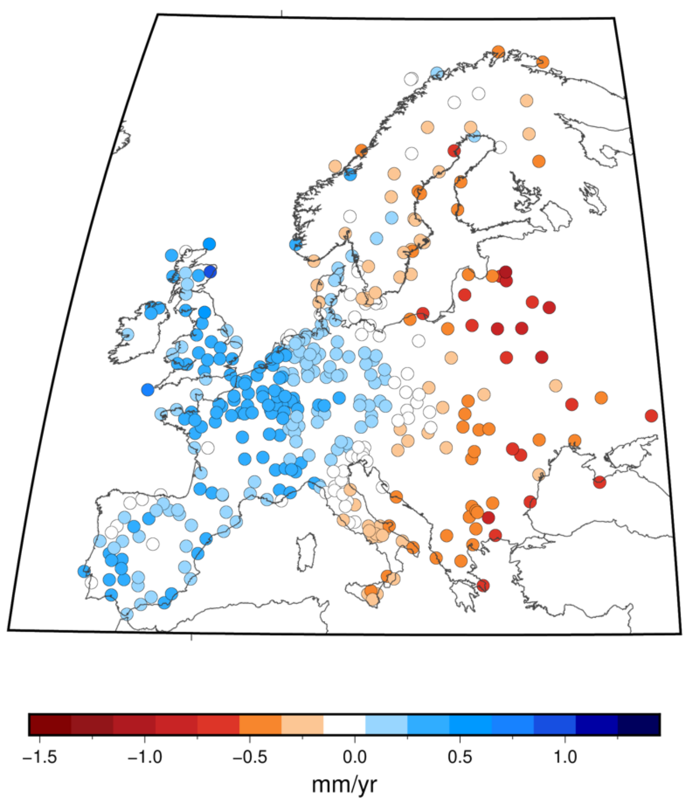

Figure 4.4 GPS velocity residuals in Fennoscandia and Europe.

In the case of Laurentide, in the areas with dense GPS cover across the United States the GIA signal is recovered completely. On the other hand, in Canada where the GPS coverage is not as dense as in the United States or Fennoscandia, the signal is recovered only at the location of the GPS sites, rather than throughout the entire region. This is because the spacing between the observations is greater than the 200 km required to estimate the model. Therefore, this spacing is filled with PSLND observations and in the signal across Laurentide seems patchy, as seen in figure 4.3. Because the spacing is filled with PSLND observations the inversion cannot recover the GIA signal accurately across Laurentide as was possible in Fennoscandia. Despite not being able to recover the spatial signal, figure 4.5 shows that the method can recover the signal at the location of the GPS site. Through simulation, I was able to recover a GIA signal accurate to less than 1 mm/yr, with velocity residuals ranging from –0.95 to 0.86 mm/yr.

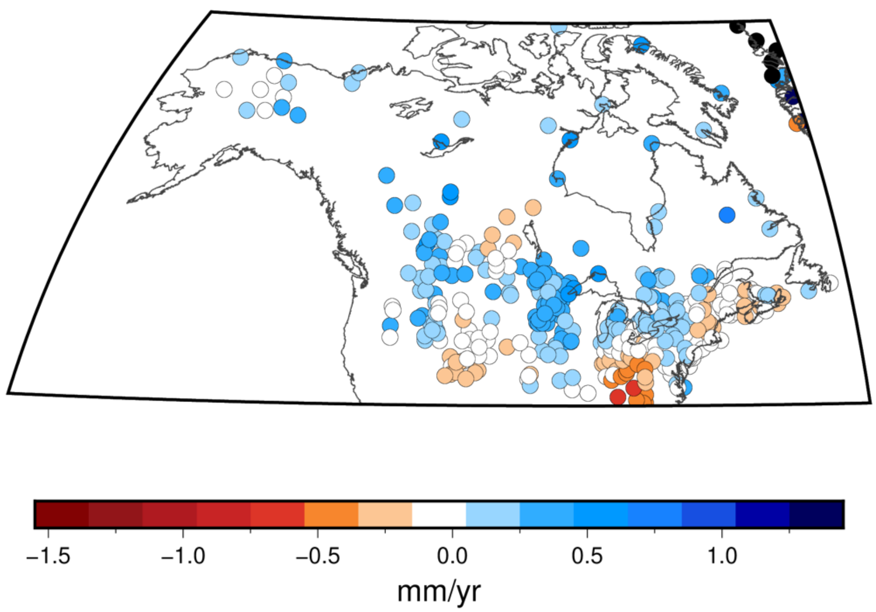

Figure 4.5 GPS velocity residuals in Laurentide.

In Greenland it is also not possible to estimate a GIA signal spatially because of the GPS coverage solely along the coastline, as seen in figure 4.3. However, in Greenland the inversion accurately retrieved the GIA signal where GPS sites are located, with the velocity residual ranging from –0.76 to 3.79 mm/yr, as seen in figure 4.6.

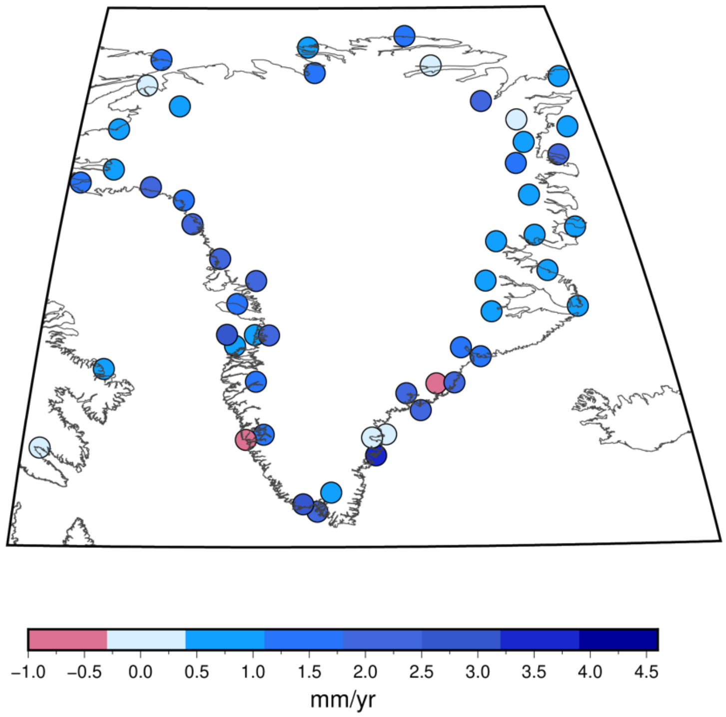

Figure 4.6 GPS velocity residuals in Greenland.

The velocity residuals between the simulated height estimates and the reconstructed time series at each GPS location. The velocity error in rate varies from -0.95 to 3.8 mm/yr. The rms of the velocity residuals in Fennoscandia is 0.3, in Laurentide 0.23 and in Greenland 1.53 mm/yr. This demonstrates that, even though the inversion cannot estimate the GIA across the entire GIA regions, the inversion process can reproduce the simulated height time series at the locations of the GPS observations for the spherical harmonics model to degree 90.

4.2. Inversions assessment with real data

4.2.1. Observation parameters

Based on the results of the simulations, I decided to use uncertainties of the GPS height observations of 0.005 m and 0.30 m PSLND uncertainty. I repeated the analysis of figure

4.2 using real data to ensure that the uncertainty values I am assigning to the observations are appropriate for the real data. The purpose of this is to assess the rms of velocity residuals in the reconstructed height time series with real data using the same range of uncertainties as in the assessment with the simulated data, to see if the simulation has been realistically representative of the real-world scenario. As with the simulation, the rms increases with the level of GPS height uncertainty and the rms decreases as the PSLND uncertainty increases (figure 4.7). However, the difference in the magnitude of rms increases when using real data. This could be because the simulated height data, unlike real data, was created with continuous height measurements throughout 2002 to 2023.

Therefore, it is necessary to re-examine the different outcomes from using simulated observations and real observations. For the real data we can see that, regardless of the GPS height uncertainty used, the velocity error in Fennoscandia and Laurentide seem to converge with a PSLND height uncertainty of 0.30 m, as in the simulation assessment. However, the difference between the GPS velocity and the reconstructed in Greenland converges with a PSLND height uncertainty of 0.50 m, with negligible changes afterwards as seen in figure 4.8. Looking back at the simulation, increasing the PSLND uncertainty does not have a negative impact on the interpretation. Therefore, I modified the uncertainty of the PSLND observations for the assessment of the real data. With the results in figure 4.8, it is appropriate to assign 0.50 m height uncertainty for PSLND observations, as the velocity error in all the areas of interest has already converged with this height uncertainty and will not negatively affect the outcome.

With this assessment I concluded that the ideal uncertainties to apply for the observations are of 0.005 m for GPS and 0.5 m for PSLND.

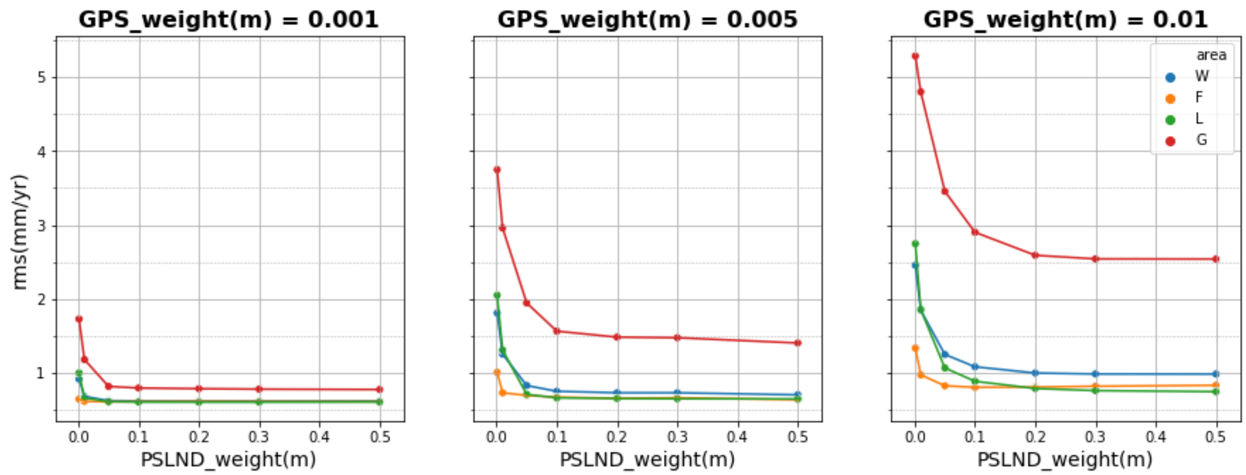

World	Fennoscandia	Laurentide	Greenland

Figure 4.7 shows the different rms mm/yr of the reconstructed heights compared to the observed vertical deformation depending on the different observation uncertainties and noise levels assigned in the inversion.

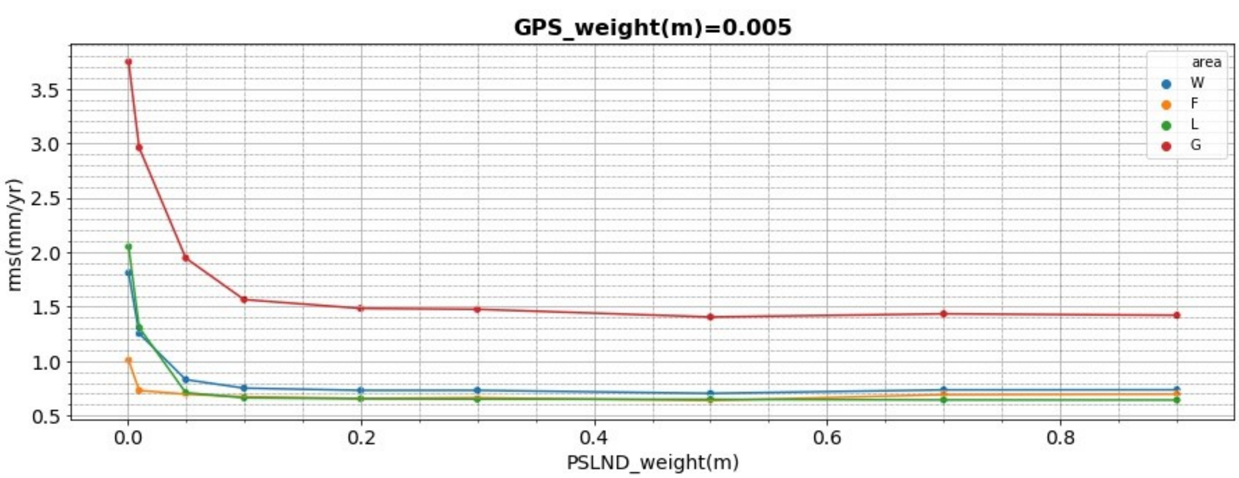

Figure 4.8 Extended plot of uncertainties.

4.2.2. Degree of model

Once observation uncertainties are assigned, the next step is to analyse the influence the maximum degree of the spherical harmonics model estimated on the accuracy of the modelled results. In figure 4.9 I show the spatial patterns obtained in models using a maximum degree of 30, 45, 60, 75 and 90. Next to each model is the histogram of the velocity residual from the difference between the reconstructed and the observed vertical deformation, using the estimated models with different degrees.

We can observe that the spatial patterns of the models deteriorate as the degree increases. As previously explained, the higher the degree used in the inversion, the higher the spatial resolution of the model. For accurate regional GIA models, the presence of GPS throughout the area at a specific distance is imperative. The separation of the GPS must be less than a certain amount (180/n times the kilometre spacing required, *'n'* is the maxim degree of the model) for a spherical harmonics model of a particular degree, otherwise the spatial pattern will not be accurately resolved. The higher the degree the closer together the GPS sites need to be. If they are separated by more than the required distance then the spherical harmonic model will fail to retrieve the GIA signal in between the GPS sites. Examples of this can be seen in figure 4.9.

In Fennoscandia, where there is a dense GPS coverage, the degree 30 model is smooth because the GPS separation is less than 180/degree (600 km), therefore to degree 30 the spherical harmonic model is representing accurately the spatial pattern. Since the GPS distribution is ideal in Fennoscandia, we can see the signal remains well estimated for each model using different degrees, with the velocity residual consistently being less than 1 mm/yr.

In Laurentide there is a wider distribution of GPS, so the signal appears clearer in the lower degrees, and it concentrates at the specific GPS sites in higher degree models, showing pockets of large error in parts where there are no GPS sites. In the northern part of the United States, we can see a consistent band with a clear and correct GIA signal, because of the GPS station density in the area.

We know that in Greenland, due to the limited GPS network only along the coastline, it is not possible to estimate a GIA regional pattern but, with the evidence of Laurentide, it should be possible at the GPS site locations. We can see in figure 4.9 and table 4.1 the significant impact that going to high degree models has. Even though the spatial model seems to deteriorate as the degree increases, the accuracy of the estimated GIA signal is improving. The velocity residual at the location of the GPS site improves from degree 30 with an average velocity residual of 8.7 mm/yr to less than 2 mm/yr with a degree 90 model.

Next to each model I present the histogram of the velocity residuals of the observed and the reconstructed for each model estimated to different degrees. They all show roughly a normal distribution in similar locations, however the variability differs, with low degree models having a broader spread and, as the degree increases, the distribution becomes narrower. We can see the distribution variation between each degree, with the green lines marking one standard deviation about the mean. The vertical land movement calculated from a degree 90 GIA model has a mean velocity residual of –0.02 mm/yr with a standard deviation of 0.83 mm/yr compared to observed GPS vertical land movement in the areas of interest. It is not possible to estimate a model beyond degree 90 due to the 2-degree limit of the GRACE/GRACE-FO solutions used.

Even though the signal in the degree 30 solution appears to be spatially smooth, it does not capture the GIA signal entirely. The reason why I am not getting a spatially accurate GIA signal with a degree 90 solution is because I do not have enough GPS stations in Laurentide and Greenland, since the distance required between GPS for a degree 90 solution (180/degree) is ~200 km. While the degree 90 model is not spatially coherent or accurate, the velocities reconstructed from a higher degree spherical harmonic model match best the observed GPS velocities. This proves that, even though the GIA models cannot not be estimated spatially when I do not have the proper station spacing to be comparable with the degree being estimated, the inversion works very well at the locations of the GPS sites.

I looked at the root mean square error for each area Fennoscandia, Laurentide and Greenland of the reconstructed time series and the observed vertical land movement. The rms consistently decreases as the degree assigned to the GIA model increases. From these results, the 90 degree spherical harmonic model has the smaller rms. In figure 4.9 and table 4.1 show why going to degree 90 is necessary for the model to fir the data more closely, otherwise I do not get the high spatial contribution that allows me to reconstruct the GPS observation. With a degree 90 GIA model I can have high confidence in the GIA that is estimated at the GPS site.

	RMS (mm/yr)			
Degree	**World**	**Fennoscandia**	**Laurentide**	**Greenland**
30	2.534	0.983	1.766	8.730
45	2.048	0.902	1.338	7.088
60	1.481	0.833	1.265	4.345
75	1.034	0.721	0.927	2.668
90	0.806	0.633	0.710	1.946

Table 4.1 Average velocity residuals depending on different degrees used in the inversion.

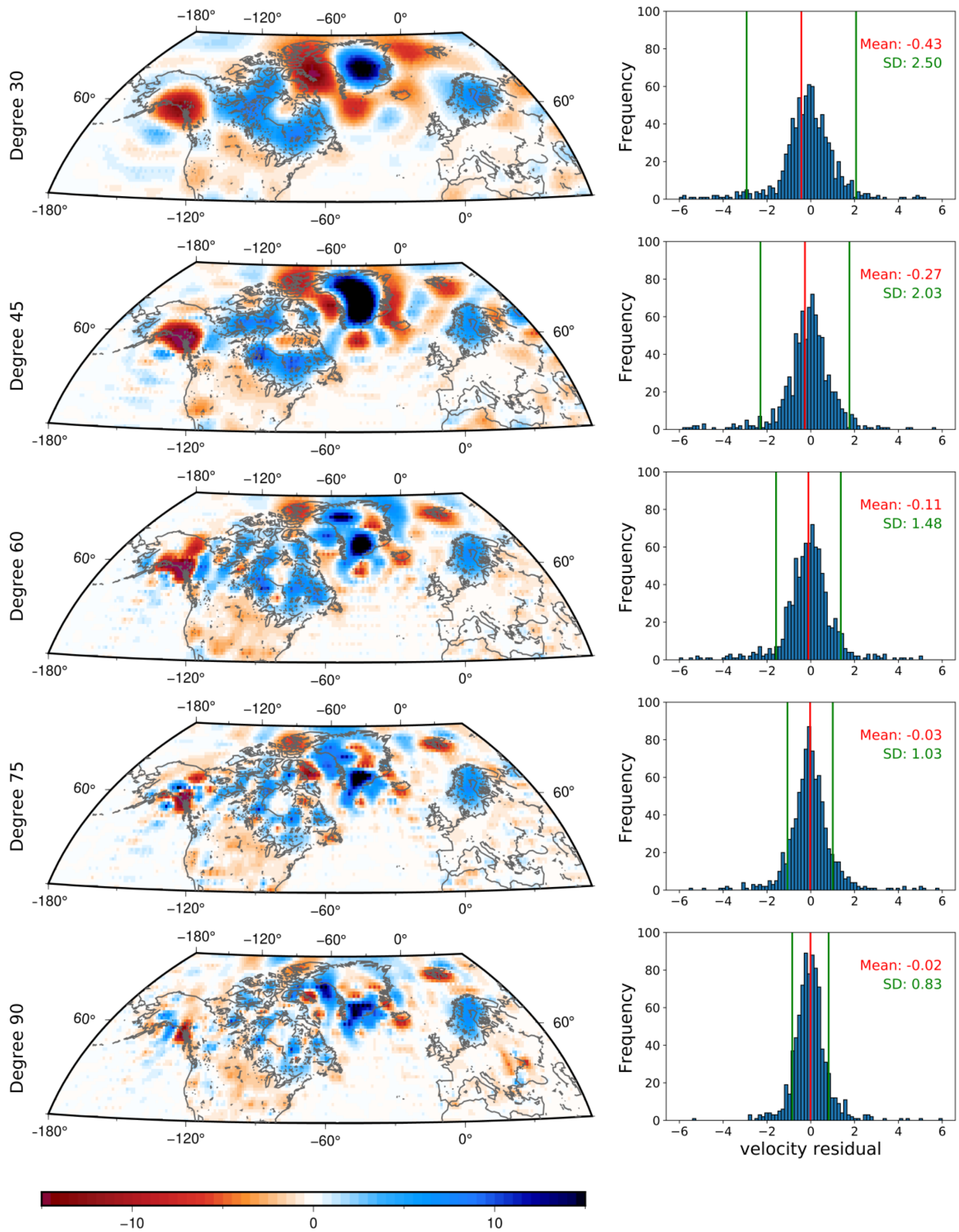

Figure 4.9 Estimated GIA models using degrees 30, 45, 60, 75, and 90. Next to each one is the histogram showing the velocity residuals between the reconstructed and observed height estimates. Red line marks the mean and green line one standard deviation.

I reconstructed the vertical deformation that can be obtained using GIA models estimated at a variety of maximum degrees. I then compared the reconstructed velocities with the observed GPS time series (figure 4.10). I looked at 3 different sites, one for each area of interest, indicated on the map. The legend shows the rate of the GPS and, next to each degree, the velocity residual between the reconstructed and the observed time series.

- In Fennoscandia, the OSLS site shows that the time series can be reconstructed very accurately regardless of the degree used in the GIA model, with a velocity residual of less than 1 mm/yr.

- In Laurentide, at the SCH2 site we can begin to see reconstructions using low degree 30 diverge from the observed heights and higher degree models approximate better the observed time series.

- In Greenland, at the KAGA site we can see the sharper impact the degree used in the model has when comparing to the GPS heights.

It is clear the importance of higher degree models, because models estimated to lower degrees do not reconstruct accurately the observed height time series. Seeing the reconstruction velocity residuals at different degrees, we can see the higher degree models give a better fit to the observations.

These are typical examples of fits between reconstructed and observed, the statistical assessment of the fit of the region is discussed later in detail in Section 4.3.

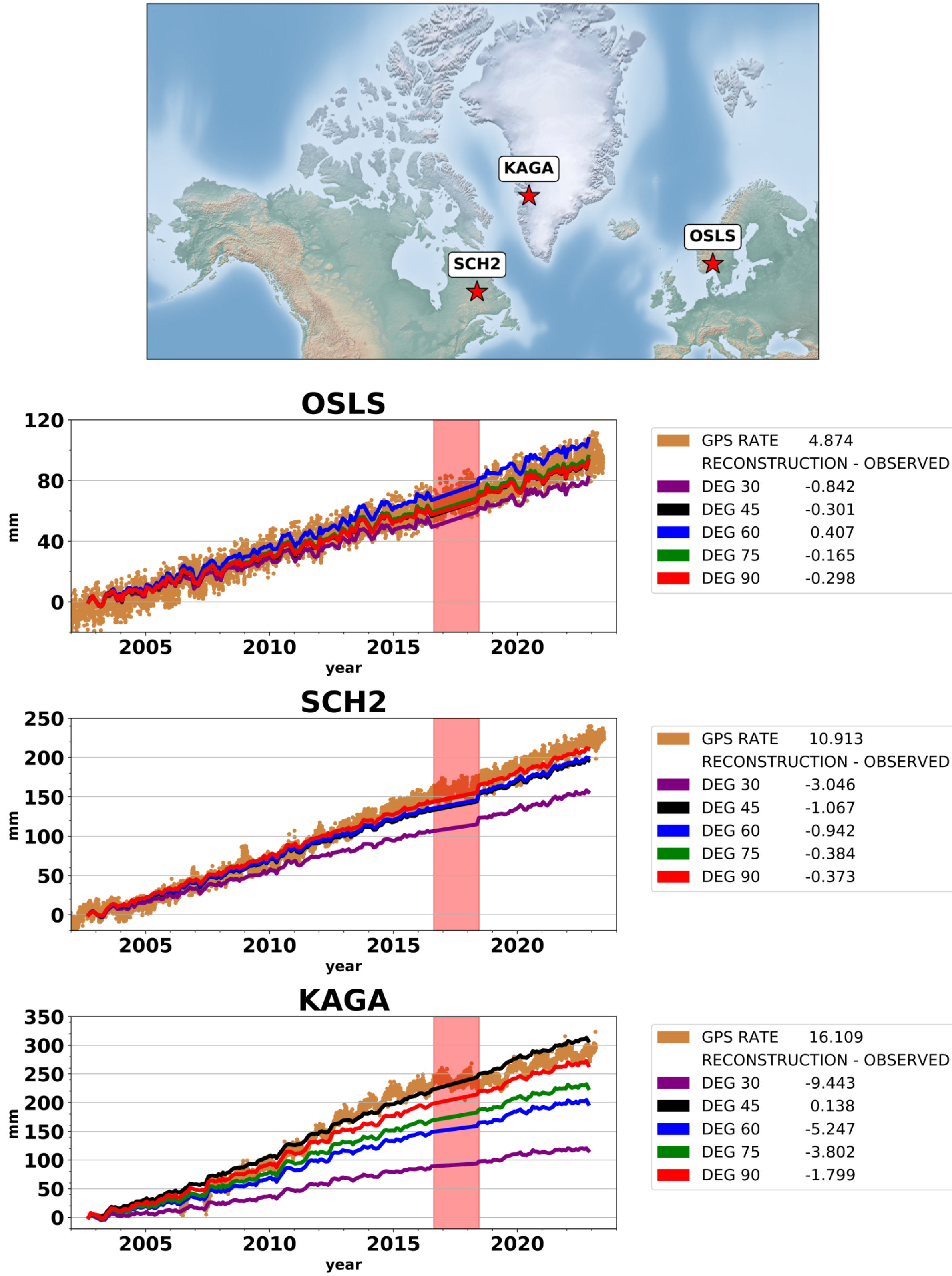

Figure 4.10 Reconstructed height time series using GIA models estimated to different degrees.

The difference from the reconstructed and the observed vertical height velocities for a degree 90 solution are shown spatially for each area of interest in figure 4.11.

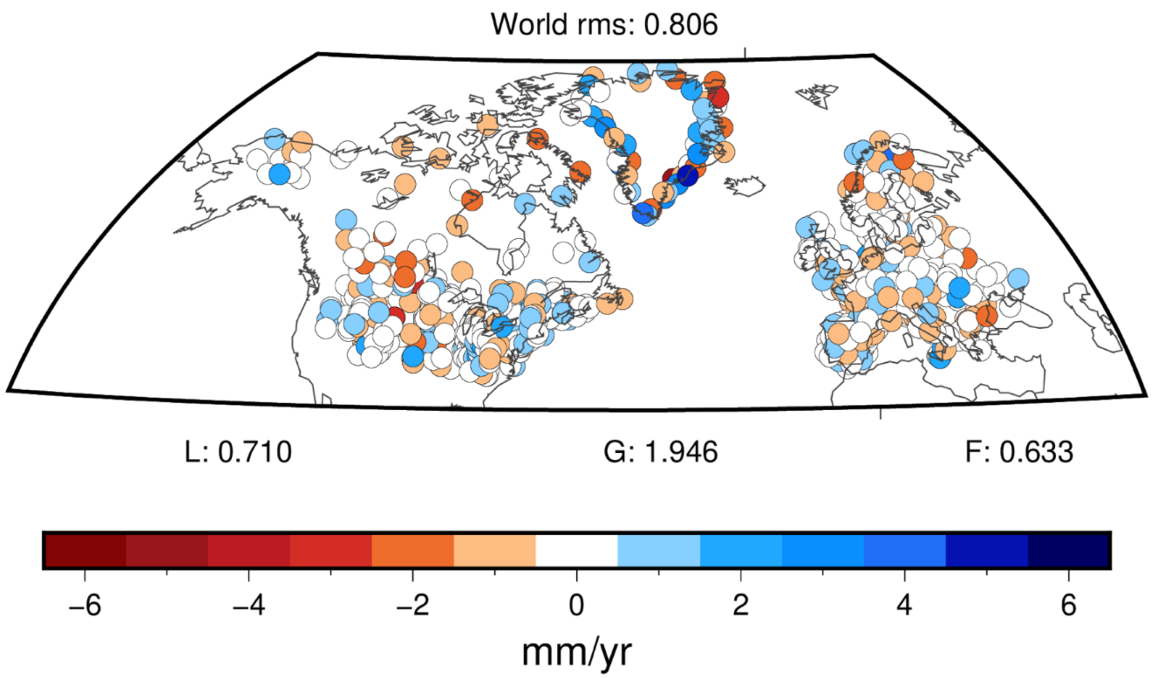

Figure 4.11 Velocity residuals between reconstructed and observed vertical height time series at each GPS site for a degree 90 GIA model.

This assessment is done through the reconstructed time series because the separation of elastic and viscoelastic is different for each spherical harmonic degree model since the GIA model changes.

4.3. Assessment of GIA models

While assessing my results, I realised the method validating my GIA model with reconstructed GPS heights could be applied to evaluate the accuracy of available alternative GIA models. I can substitute my estimated spherical harmonic coefficients of GIA, with the published coefficients of any GIA model to test the accuracy of a published model. If the model is accurate, the reconstructed height time series should match the observed GPS. Differences from the reconstructed heights using other models and the observed GPS heights will quantify the accuracy of other models. In the following section I present how other available models can be evaluated and the insights it provides. I evaluate three different models: the one estimated in my thesis, the G. Alvarez model, the ICE6G_D model (R. W. Peltier et al., 2017), and the ANU model (Lambeck et al., 2017).

4.3.1. Fennoscandia

First, I evaluated the 399 GPS heights observations used across Europe. The maps in figure 4.12 show the residual vertical velocity between the observed height and the reconstructed one according to the GIA model used.

- The G. Alvarez model has a rms of 0.633 with values ranging from -2.29 to 4.12 mm/yr.

- The ICE6G_D model has a rms of 0.801 with values ranging from -2.27 to 3.41 mm/yr.

- The ANU model has a rms of 2.323 with values ranging from –5.11 to 8.91 mm/yr.

The histograms in figure 4.12 present the distribution of the residual rated for each model, with their mean and standard deviation. Both reconstruction rates using G. Alvarez and ICE6G_D models can approximate the observed GPS height observations with a maximum error of ~4 mm/yr, and they roughly have a normal distribution. The ANU model shows a wide spread of residuals with a uniform distribution (note the scale in the velocity error differs for ANU model). This analysis is dependent on the assumption that GPS and GRACE/GRACE-FO are sensing the same signals. The spatial coherence seen on figure 4.12 implies that this assumption is true.

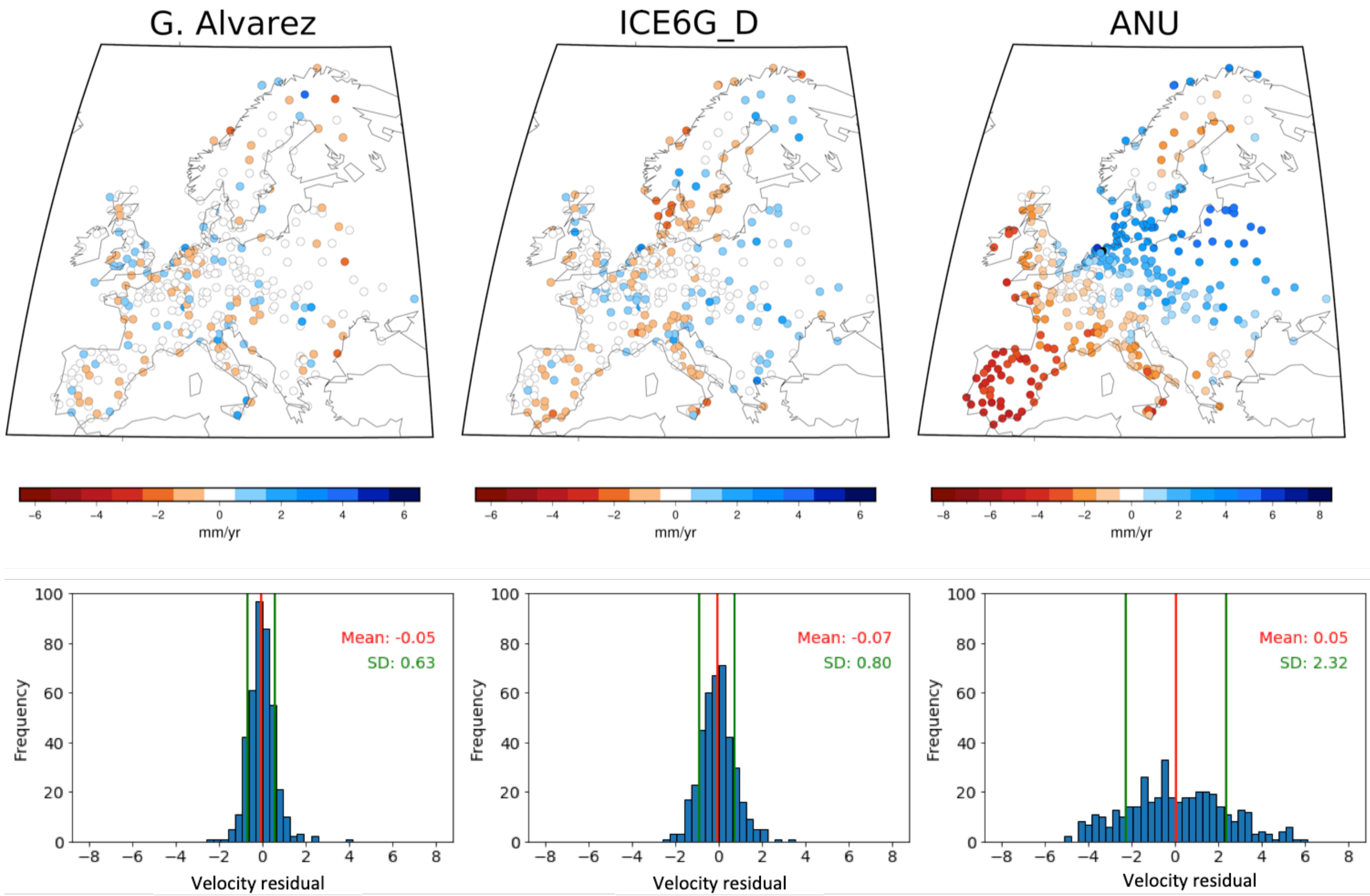

Figure 4.12 Residual vertical velocity in Fennoscandia between the observed height and the reconstructed one according to the GIA model used, with their corresponding histogram of velocity residuals.

These type of maps (figure 4.12) allow us to analyse the quality of each model. The ICE6G_D model show spatially random errors, many close to zero. The ICE6G_D model in Fennoscandia is a very good fit to the data. The ANU model shows systematic spatial errors, specially outside the extent of the ice sheet. The positive (blue) values along the peripheral bulge of Fennoscandia are over-estimating the GIA signal. For comparison, my model spread of residuals is a better fit to the data.

Figure 4.13 shows the rate of the GPS heights of eight sites in Fennoscandia and how much each reconstructed height time series differs depending on the model used. Figure 4.14 shows the corresponding time series of the observed GPS height (yellow), the reconstructed height using my model (black), the reconstructed height using the ICE6G_D model (blue), the reconstructed height using the ANU model (green), and the GRACE/GRACE-FO gap (red).

SITE	GPS RATE	G.ALVAREZ	ICE6G_D	ANU
	mm/yr	RECONSTRUCTED – OBSERVED RATE		
VARS	3.362	0.095	-1.787	3.629
KIRU	6.713	-0.689	1.045	-0.437
SKE0	10.313	-0.299	-0155	-2.07
VAAS	9.156	-0.048	-0.553	-0.478
VIL6	8.489	0.124	0.288	-1.662
SVE6	8.699	-1.075	0.432	-1.695
OSLS	4.874	-0.298	1.037	0.408
TGDE	1.731	0.006	-1.564	2.431

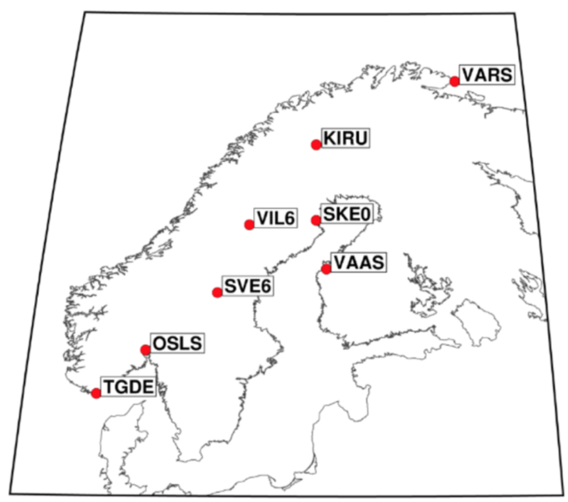

Figure 4.13 Tabulated rates of GPS sites used next to the velocity residual from the reconstructed and observed heights. Sample map of time series presented in figure 4.14.

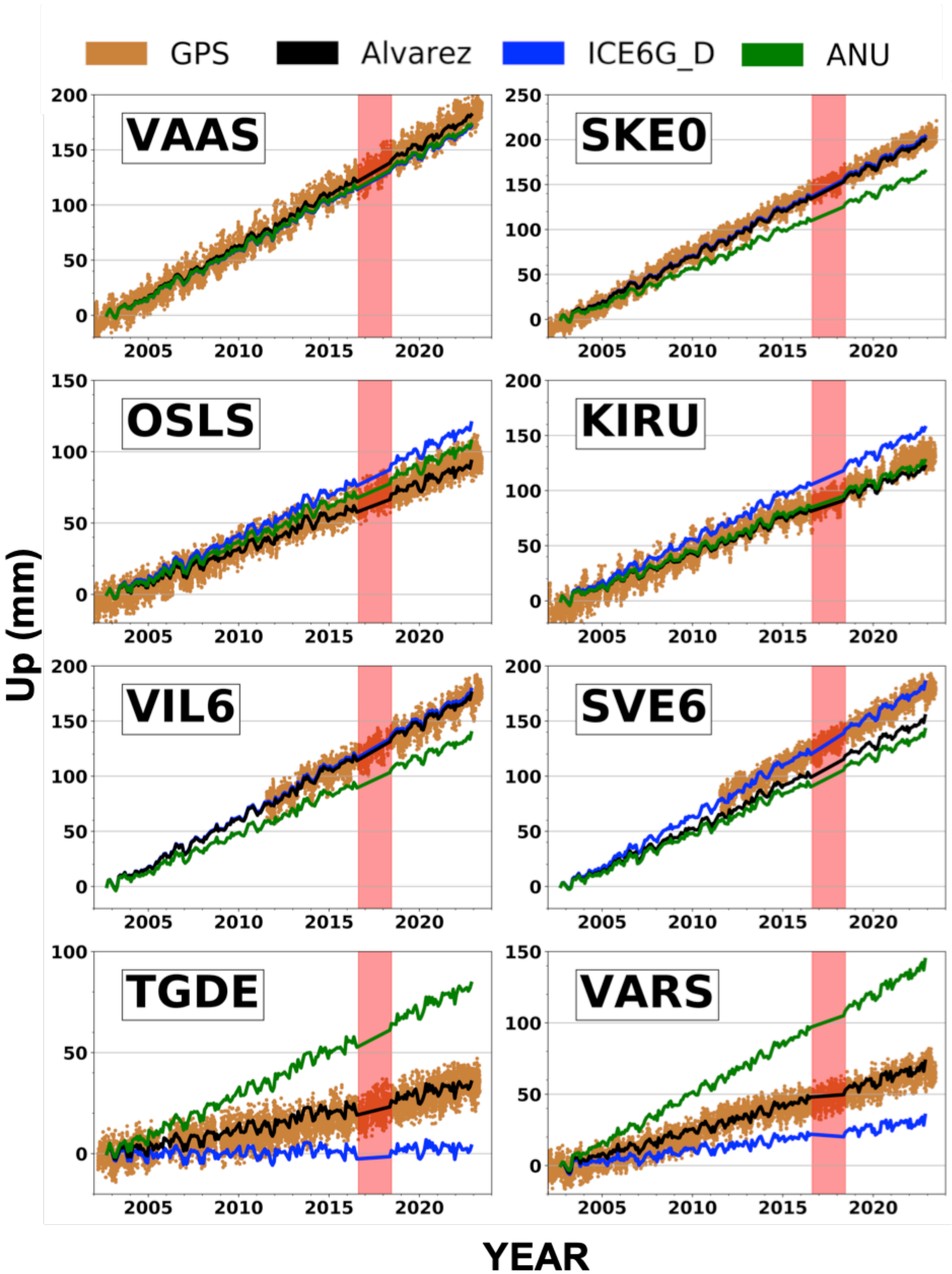

Figure 4.14 Time series of sites reconstructed in Fennoscandia.

There are sites such as SKE0, VIL6 and VAAS where all models can reconstruct the observed time series very accurately, the height is very well estimated, or very closely. When the GIA signal is correct, then the reconstructed timeseries matches the observed timeseries. Sites such as KIRU, SVE6 and OSLS have some variation between the reconstructed heights, but the GPS time series are approximated well, while at sites such as VARS and TGDE my model provides a better reconstructed height estimate than the ICE6G_D and ANU models. This approach can show when the GIA model is right and when it is wrong at a specific location.

With this approach we can see separately the elastic and viscoelastic signal estimated during the inversion process. In figure 4.15, I show the elastic and viscoelastic signal estimated depending on the model used for the TGDE site. Figure 4.15 shows the viscoelastic signal from the ANU model, confirming that indeed the GIA signal is too large, therefore it over-estimates the reconstructed time series, differing from the GPS rate 2.43 mm/yr. With the ICE6G_D model, the elastic coefficients are too large, to compensate for the viscoelastic. Which means there is too much mass gain in that location, which causes a subsidence of elastic deformation. This is why the reconstruction is under-estimated, with the reconstructed rate differing –1.56 mm/yr from the GPS. Meaning that if the GIA model is not accurately representing the GPS vertical deformation. This method is a tool to know in which way models need to be adjusted to improve them. Seeing a positive velocity residual means the viscoelastic component of the GIA model in that location is over-estimating the actual viscoelastic signal. Conversely, when the velocity residual is negative the viscoelastic component of the GIA model in that location is under-estimating the correct viscoelastic signal.

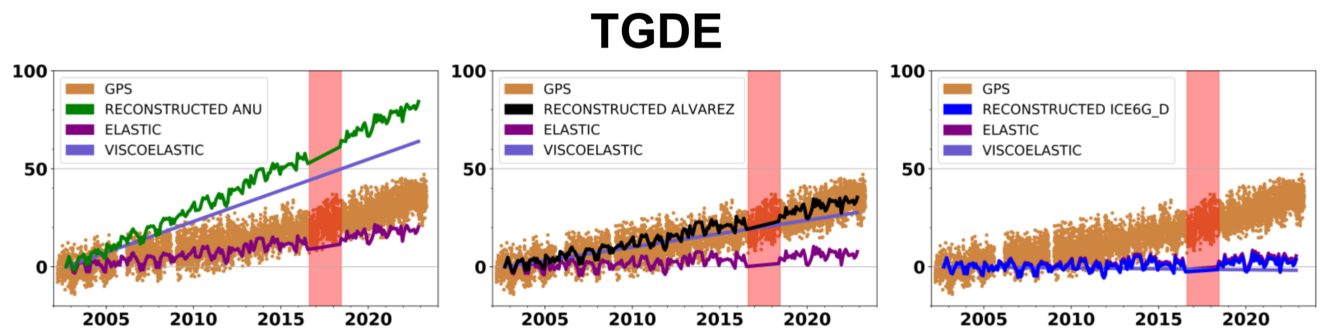

Figure 4.15 TGDE site, showing the GPS heights, the reconstructed one and the elastic and viscoelastic signal from each model.

This analysis can be done with any GIA model in areas with glacial rebound in the northern hemisphere. This approach allows us to test the quality and accuracy of any GIA model. If the slope of the reconstructed time series does not match the slope of the GPS heights, then the GIA model used is incorrect at the location analysed. If the addition of both signals is incorrect, there will be inconsistencies in the reconstructed time series. If the reconstructed time series sits above the GPS observations then it means the viscoelastic signal is too large. When the reconstructed time series sits below the GPS observations then it means the viscoelastic signal is not large enough.

4.3.2. Laurentide

In the case of North America, I used 397 GPS sites. The maps in figure 4.16 show the residual vertical velocity between the observed and reconstructed heights according to the GIA model used.

- The G. Alvarez model has a rms of 0.710 with the values ranging from -2.76 to 2.68 mm/yr.

- The ICE6G_D model has a rms of 1.455 with values ranging from -3.33 to 4.69 mm/yr.

- The ANU model has a rms of 13.84 with values ranging from –1.56 to 39.53 mm/yr.

From the histograms in figure 4.16, we can see the G. Alvarez model has normal distribution. The ICE6G_D model has a similar range as the G. Alvarez model, but with a wider spread and is left skewed, meaning the overall GIA signal is predominantly under-estimated. In the ANU model there is a normal distribution, with a mean of 12.09 mm/yr, meaning the overall signal in Laurentide is over-estimated.

We can observe the spatial distribution of the residual velocities at each location and identify patterns. For instance, for the ICE6G_D model, the signal is over-estimated in sites that were under the icesheet along the southern part of Canada and under-estimated in the sites locates outside the extent of the icesheet, in northern part of the United States. In the case of the ANU model the GIA signal is significantly larger, with systematic over-estimation across all the sites (note the different scale in the map and histogram). In my model the velocity residual distribution is random, and from the histogram my model has a tighter fit, therefore my model at the GPS sites in Laurentide fits the GPS data better.

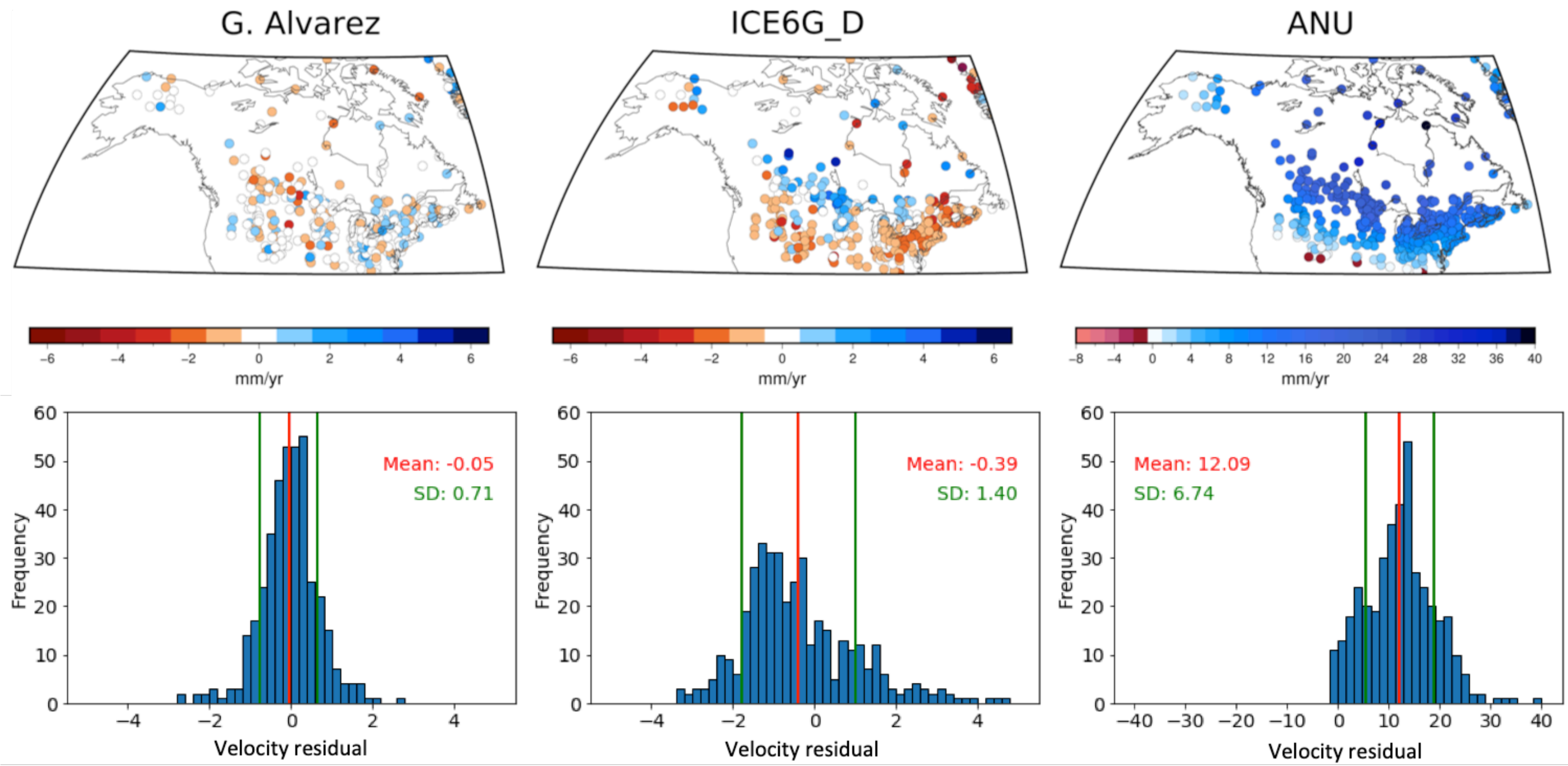

Figure 4.16 Map of residual vertical velocity in Laurentide between the observed height and the reconstructed one according to the GIA model used, with their corresponding histogram below them.

The ANU model is not an accurate representation of the viscoelastic signal observed by GPS in the Laurentide ice sheet. Lambeck et al., (2017) noted in the SCH2 site that, indeed, the present-day rebound is excessively over-estimated. The GIA signal is too large and cannot accurately reconstruct the GPS heights.

Analysing the G. Alvarez and ICE6G_D model there are sites such as BAKE and CHU2 where both models reconstruct the observed time series very accurately. There were sites in this area in which the ICE6G_D model under-estimated the signal (e.g. YFB1, KUUJ, BAIE) or over-estimating it (e.g. REPL, ROSS, and SCHU2).

Even though my approach cannot estimate a regional GIA model across Laurentide, my approach can accurately reconstruct the heights at the GPS location, as shown in figure 4.18, sites around Hudson Bay where the GIA signal is the largest.

SITE	GPS RATE	G.ALVAREZ	ICE6G_D	ANU
	mm/yr	RECONSTRUCTED – OBSERVED RATE		
REPL	9.291	0.101	3.12	28.612
BAKE	12.037	0.226	0.568	26.824
CHU2	10.636	-0.778	-1.496	33.361
ROSS	3.042	0.306	1.573	22.414
YFB1	4.44	0.697	-0.56	26.784
KUUJ	15.002	-0.049	-2.679	24.137
SCH2	10.913	-0.373	3.132	16.322
BAIE	3.729	0.243	-2.568	16.063

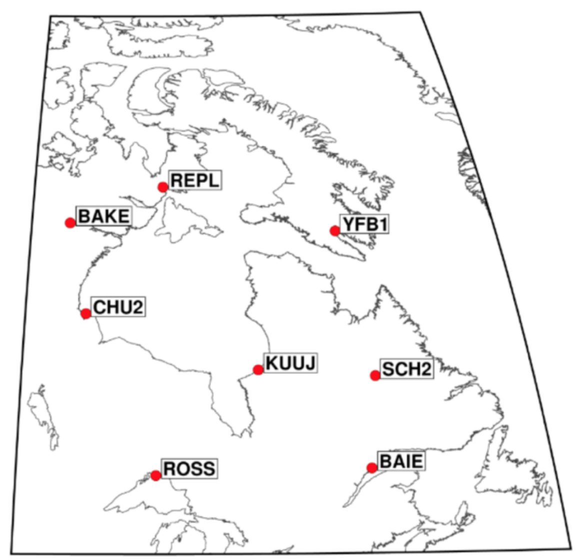

Figure 4.17 Tabulated rates of GPS sites used next to the velocity residual from the reconstructed and observed heights. Sample map of time series presented in figure 4.18.

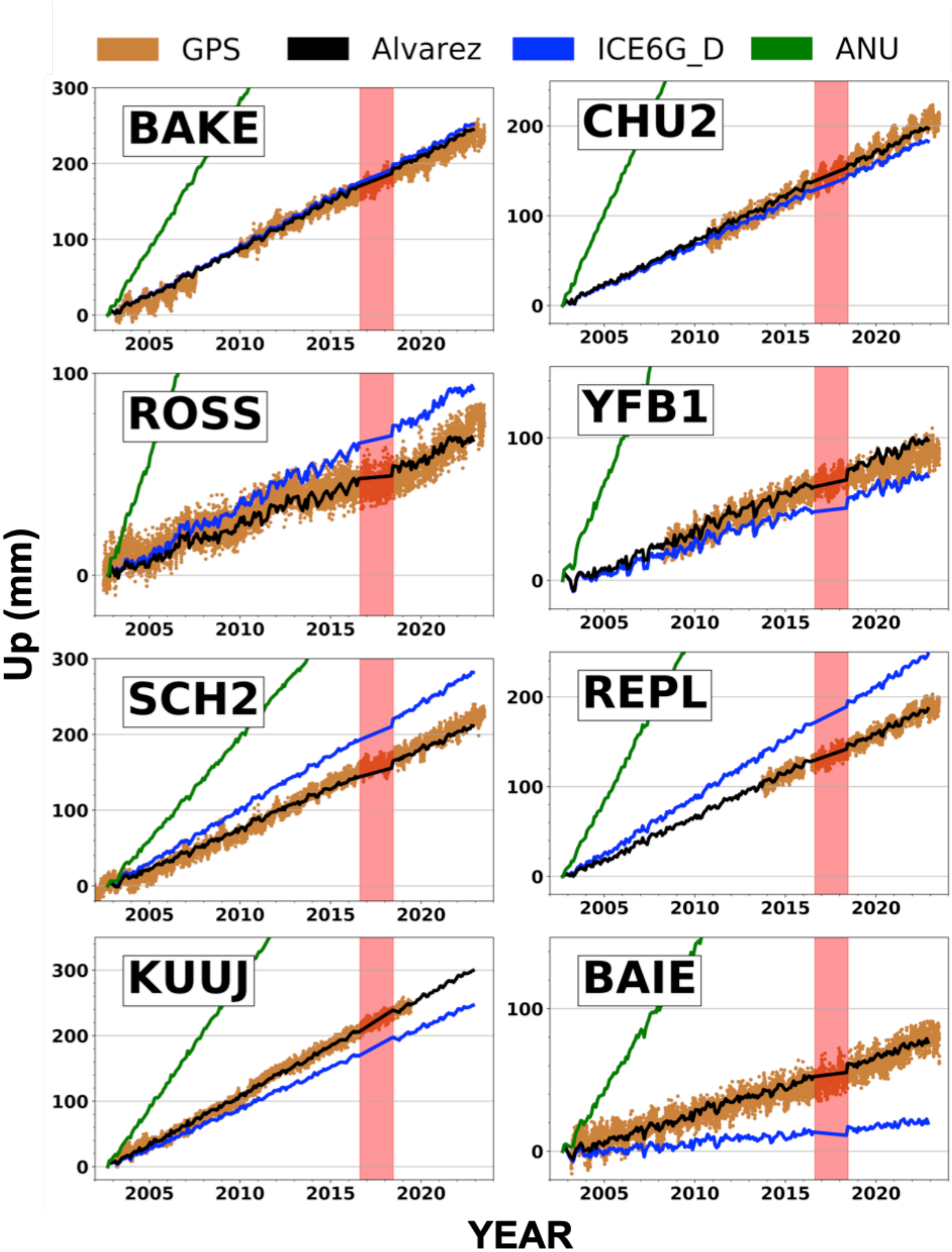

Figure 4.18 Time series of sites reconstructed in Laurentide.

4.3.2.1. Reasons for possible mismatches

There are also unique site scenarios that give insights into specific advantages or challenges to the method. In figure 4.19 and 4.20, I present two cases.

There are instances where doing a site-by-site analysis gives us insights on the misfits in the reconstruction. For GPS site QIKI (Qikiqtarjuaq) at Baffin Island, the model fails to retrieve the signal and the reconstructed heights diverge from the observation. The QIKI site is on the edge of an ice sheet. There may be significant mass loss occurring in localized areas of drainage glaciers. Because of the large spatial resolution of GRACE/GRACE-FO satellites, such localized mass change might not be captured in the GRACE/GRACE-FO data. Thus, the separation of elastic and viscoelastic is breaking down in the inversion. Because Purcell et al. (2011) approximation was shown to be valid over a wide range of Earth models the discrepancy is not likely to be caused in errors in viscosity. Misfits in reconstructions can be assessed case by case, but in general, the reconstructed time series match well the observed GPS time series. This means that the GIA signal is, in general, estimated quite accurately.

There are various things we can interpret from the reconstructed time series for each model, and provide insights into what needs to be adjusted to fit the observed GPS. In the case of the QIKI site, the viscoelastic component is too large in the ANU model. For the G. Alvarez and ICE6G_D model the viscoelastic signal is not large enough; therefore, the elastic signal is introducing a non-linear signal not seen in the actual GPS height estimates. With a higher viscoelastic signal, the slope would increase matching the observed GPS, the elastic component would be smaller and, thus, the reconstructed time series would be more linear.

A strong advantage of the GPS network in Fennoscandia is its extensive spatial density and long observation record, and the lack of such a network to be a potential obstacle in remote areas across Laurentide and Greenland. However, in the case of the site IVKQ, with data from 2008 to 2012, the method was able to accurately retrieve a signal. Even with just four years of data the method works.

SITE	GPS RATE	G.ALVAREZ	ICE6G_D	ANU
	mm/yr	RECONSTRUCTED – OBSERVED RATE		
QIKI	4.24	-2.242	-3.291	20.507
IVKQ	5.967	0.612	2.297	39.521

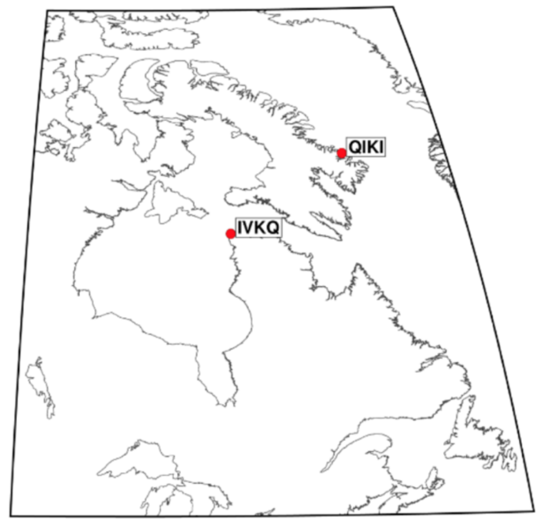

Figure 4.19 Tabulated rates of GPS sites used next to the velocity residual from the reconstructed and observed heights. Sample map of time series presented in figure 4.20.

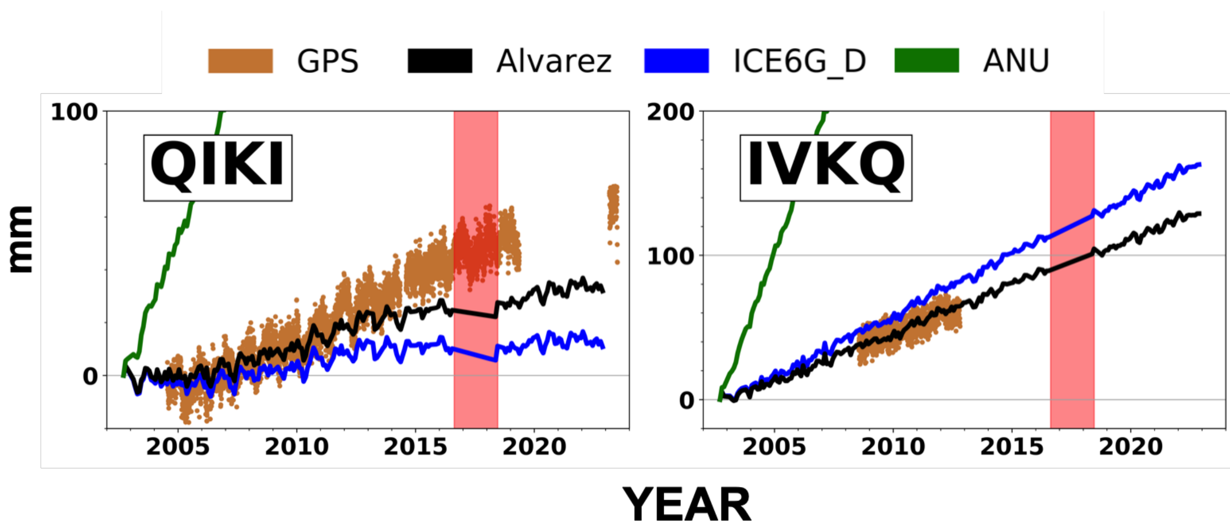

Figure 4.20 Reconstructed time series of QIKI and IVKQ sites in Laurentide.

4.3.3. Greenland

The last area of interest, the most challenging one considering the limited GPS sites and the non-linear height observations present in Greenland. I used 50 GPS sites, located along the coastlines. The maps in figure 4.21 show the residual vertical velocity between the reconstructed and observed heights according to the GIA model used.

- The G. Alvarez model has a rms of 1.946 with values ranging from -5.36 to 5.06 mm/yr.

- The ICE6G_D model has a rms of 4.819 with values ranging from -14.57 to 6.12 mm/yr.

- The ANU model has a rms of 5.439 with values ranging from –12.1 to 13.04 mm/yr.

The ICE6G_D model has spatially coherent negative velocity residuals in the south and western part of Greenland, which is indictive of an under-estimation of the viscoelastic uplift rate. It has positive velocity residuals in the northeast indicative of an over-estimation of the GIA rate. In the ANU model we see the opposite, the large GIA signal along the southwest coast, that could be influenced by the over-estimated GIA signal present in Laurentide, note the scale in the map was adjusted for the ANU model (-14 to 14 mm/yr).

When there are regions where there is a pattern, there might be something in the model that can be adjusted. The way of improving the model where the signal is being under-estimated, would be to increase the ice loss or adjust the timing for more recent ice loss. To improve models where the signal is being over-estimated, it would require less ice loss or earlier ice loss.

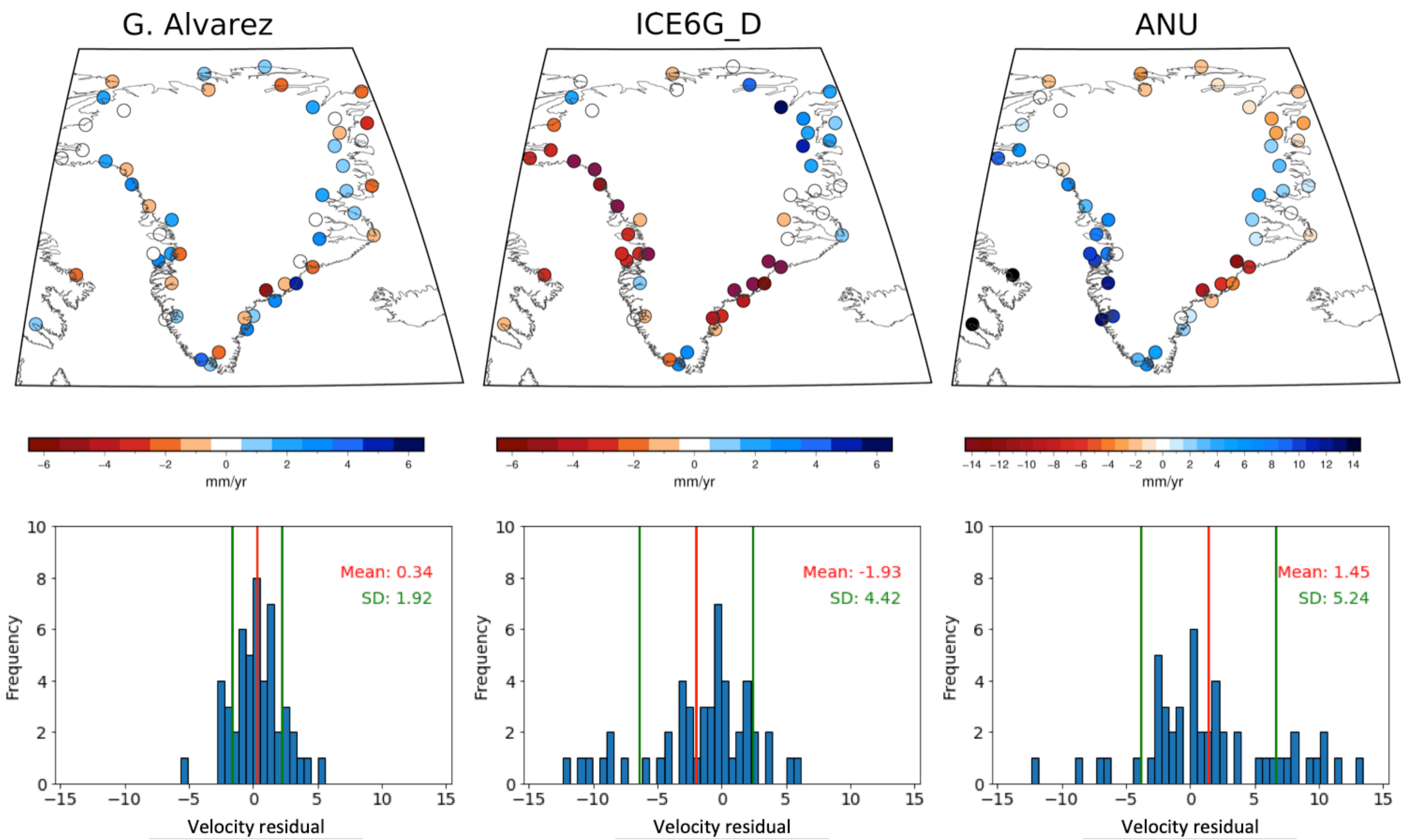

Figure 4.21 Map of residual vertical velocity in Greenland between the observed height and the reconstructed one according to the GIA model used, with their corresponding histogram below them.

No clear spatial patterns in velocity residuals in my model shows there is nothing systematically wrong with the GIA estimated at the sites in Greenland. As previously mentioned it can be investigated site by site, depending on its location it could be impacted by present day mass change in a local way. High velocity residuals may be caused by localised mass loss being captured by GPS but not well captured by GRACE/GRACE-FO. Even so, my velocity residuals are much smaller than the ICE6G_D or ANU.

From the histograms in figure 4.21, we can see the G. Alvarez model has a narrow spread. The ICE6G_D model has a wider spread, right skewed, with a mean of –1.93 mm/yr. The ANU model has a widespread, with a bimodal distribution, with a mean of 1.45 mm/yr.

This study is of particular interest in the area of Greenland because, due to the combination of seasonal hydrological changes along with glacial rebound, height observations are not as linear as they are predominantly in Fennoscandia and Laurentide. In figure 4.22, I present the 18 sites out of the 50 across Greenland with their respective time series in figure 4.23.

In Greenland there are sites where the non-linear trends are very visible (KELY, VFDG, KAGA). There are sites where some models get the reconstruction better than other models (ALRT, TREO, KMJP, YMER, KULU). There are cases where my model gets the reconstruction better than other models (THU3, LEFN, MARG, KUAQ, ASKY, MIK2). And there are cases where no model quite gets the reconstruction accurately (NRSK, NNVN, DANE), but as previously discussed it may be assessed in a case-by-case basis.

My method was able to reconstruct non-linear trends in Greenland, some examples include the sites: KAGA, TREO, KUAQ, MIK2, ASKY, SCBY, KMJP, MARG, YMER, LEFN, THU3 (black line). The results agreed with Berg et al., (2024), the KUAQ site had the largest rates next to the Kangerlussuaq Glacier. This validation approach allows us to see where a GIA signal is not estimated correctly, and the reconstruction diverts from

GPS observations. The ANU model accurately estimates the GIA signal at sites such as SCBY, LEFN, DANE, TREO, KAGA, over-estimate the signal at MARG, NNVN, KELY, THU3 and under-estimate at KUAQ. The ICE6G_D model accurately estimates the GIA signal in sites such as SCBY, ALRT, VFDG, KMJP, DANE, KELY, and under-estimate in KAGA, KUAQ, and ASKY.

It has been pointed out that ICEnG models in Greenland are not tuned to GIA rates observed at GPS stations and that generally the GIA signal is under-estimated (Berg et al., 2024; The IMBIE Team et al., 2019; Wu et al., 2010).

SITE	GPS RATE	G.ALVAREZ	ICE6G_D	ANU
	mm/yr	RECONSTRUCTED – OBSERVED RATE		
SCBY	7.179	0.277	-0.479	0.014
ALRT	6.403	-1.464	-0.305	-1.967
LEFN	5.416	1.635	6.121	-0.691
VFDG	3.785	2.829	0.067	1.336
YMER	1.602	1.253	5.145	2.135
KMJP	3.794	0.95	-0.173	-2.298
DANE	1.639	-2.456	-0.275	0.828
TREO	8.072	-1.11	-4.017	0.16
MARG	8.315	-0.477	-2.51	6.054
NRSK	5.931	-2.709	1.254	-2.738
NNVN	6.201	-2.26	2.615	5.403
KAGA	16.109	-1.799	-10.305	0.03
KUAQ	18.342	0.43	-14.563	-12.099
MIK2	12.505	-2.264	-8.6	-7.263
KELY	3.969	-1.135	0.824	11.721
ASKY	16.028	-0.656	-11.113	-1.366
THU3	7.314	-0.26	-2.744	9.202
KULU	8.122	3.408	-4.355	-1.928

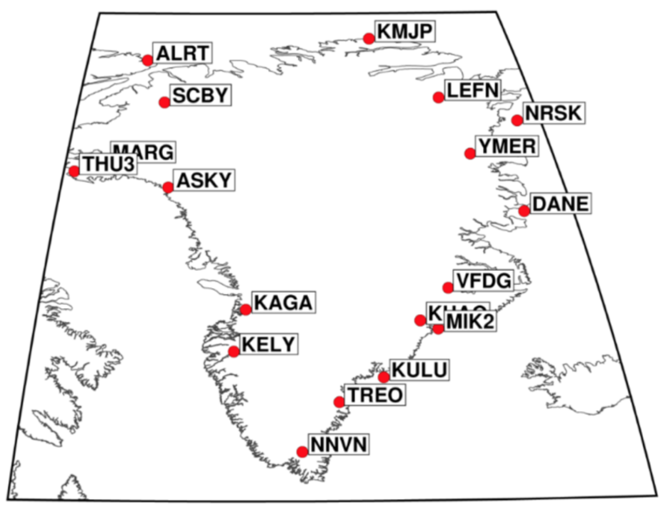

Figure 4.22 Tabulated rates of GPS sites used next to the velocity residual from the reconstructed and observed heights. Sample map of time series presented in figure 4.23.

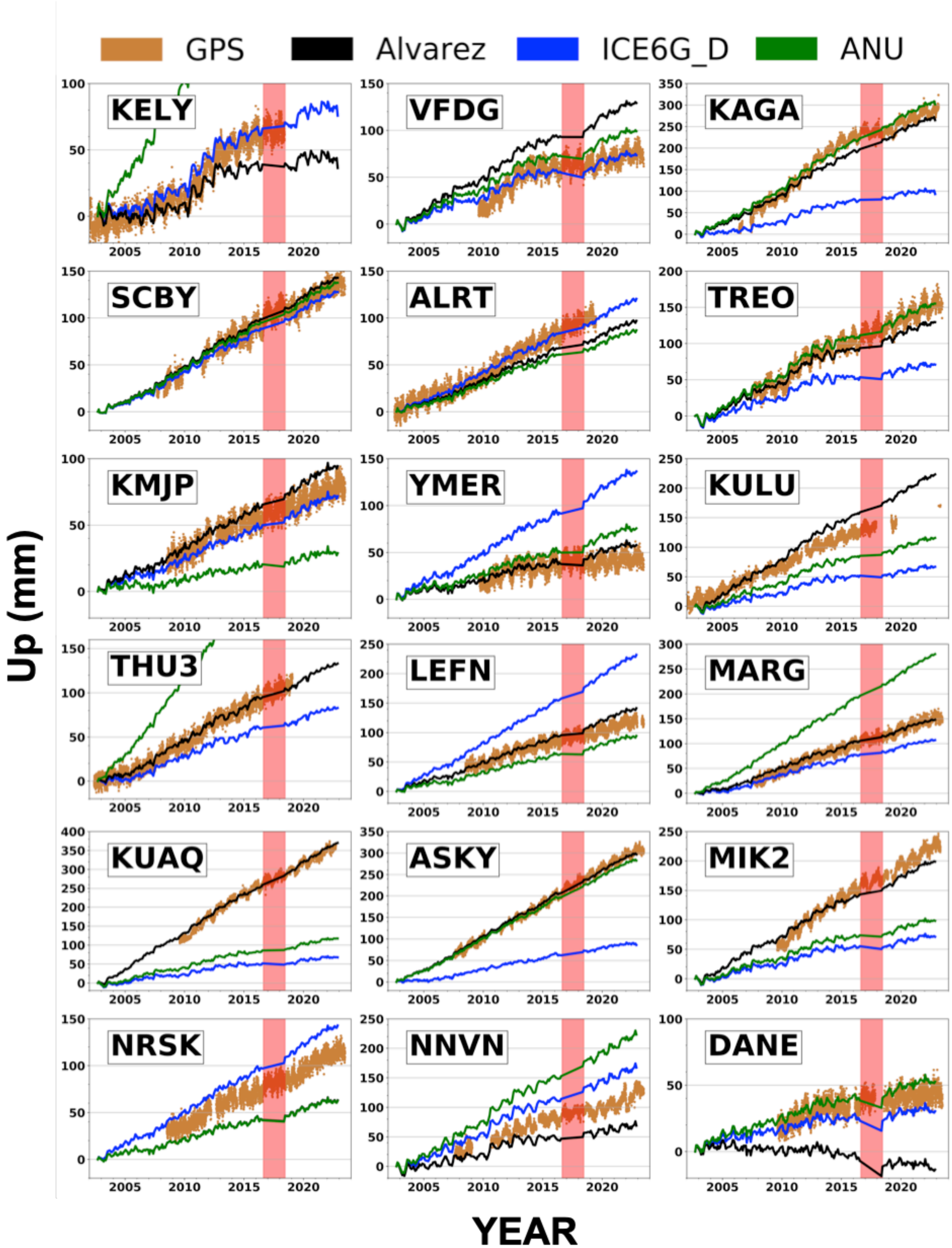

Figure 4.23 Reconstructed time series of sites in Greenland.

4.4. Summary

I developed tool for interpretation, where I can see where GIA model works well and the areas where there might have some shortcomings. I can identify patterns of the velocity residuals and investigate if it is due to potential mismodelling of the mantle or the ice history. Modifications in the GIA would require changing the timing, amount or viscosity either of those or a combination can change the present-day GIA estimate.

My model can reconstruct the GPS observations very well in Fennoscandia. To improve the GIA model in Laurentide and Greenland it would require a larger GPS network covering the areas of interest. This could potentially provide a regional GIA model, rather than at discrete locations as it currently does, this would require GPS stations placed across Laurentide and Greenland every 200 km. Even though the method can be used with larger spacing between observations such as 500 km, it would affect the resolution of the models. My approach works well, seems to have random errors rather than systematic patterns in the misfits.

The ANU model in Fennoscandia is accurate, however it shows systematically spatial errors outside the extent of the icesheet. In Laurentide the GIA signal is too large and the effect of the over-estimated signal extends to the west coast of Greenland. In these areas where the GIA signal is over-estimated, the model would require an adjustment decreasing the amount of ice loss history or adjusting the timing for earlier ice loss.

The ICE6G_D model accurately reconstructs the GPS observations in Fennoscandia, shows systematic spatial errors in Laurentide, under-estimates the GIA signal in the west coast of Greenland and over-estimates the GIA signal in the east coast. This is not an elastic loading issue, it is an error in the modelling of the viscoelastic deformation. To fix the under-estimates the GIA signal in the KAGA site in Greenland, it would need more rebound today than it is currently modelled, meaning there is a need for either more ice loss in that area or more recent ice loss in that area. Whereas in the LEFN site in the northeast it is over-estimating the present-day GIA, so it would need less ice loss or earlier ice loss.

Today the average mass loss estimated in Greenland is of 269 Gt/yr (Nasa and JPL/Caltech), and the GIA correction of the ICE6G_D model (used on ANU solutions) over Greenland is of –5.7 Gt/yr. Even though I cannot do this assessment through the middle of Greenland, since there are no GPS observations. We know the reconstructed heights in the KAGA site is in error by 64%. The ICE6G_D model is spatially under-estimating the GIA signal in the west coast of Greenland. Applying inaccurate GIA corrections to gravity solutions, will lead to inaccurate mass balances estimates of sea level rise happening in Greenland. It is essential to address these issues to improve our understanding of the present-day mass balance estimates.

It is important to address these errors in any GIA model since they contribute to the mass balance estimates of sea level change. Particularly in the case of the ICE6G_D data, where we could identify systematic errors in Greenland (figure 4.21). The ICE6G_D model is currently the one used for the GRACE/GRACE-FO GIA correction. Inaccurate corrections to the GRACE/GRACE-FO data have significant ramifications for mass balance estimates. In the background section I discussed the potential Greenland has to contribute to the global sea level rise, with increasingly accelerated rates.

5. Conclusions

The initial aim of the thesis was to validate the GRACE mission against the GRACE-FO mission; in the process of developing the technique I realised it had the capability to assess the validity and accuracy of any GIA model. The reconstructed time series in Fennoscandia (figure 4.14), that have consistent data across the GRACE/GRACE-FO - gap, the estimated GIA model (G. Alvarez) can obtain the GIA signal and reconstruct the height observation with one standard deviation of 0.63 mm/yr. We can see that the reconstructed time series accurately connects across the gap between the GRACE/GRACE-FO missions. The fact that reconstructed time series are consistent and match across GRACE and GRACE-FO does confirm that the GRACE-FO mission is working properly. The continuity of the reconstructed time series and the GPS observed time series is very good in Fennoscandia where the inversion approach has enough GPS data to permit the estimation of an accurate value of GIA and that validates the GRACE-FO mission. If the GRACE-FO spherical harmonic field were inconsistent the reconstructed time series (black line) would not run through the GPS data. The fact that it does validates the mission.

A significant contribution of the results of my thesis is the testing and validation or invalidation of GIA models in the areas of interest. From this assessment we can conclude that the ANU GIA model highly over-estimates the GIA signal across Laurentide and it extends to the southwest of Greenland. The ICE6G_D model under-estimates the GIA signal across the southwest part of Greenland and over-estimates it on the northeast of Greenland.

From this work it is not possible to derive a better set of spherical harmonic coefficients for existing GIA models. The method shows the areas in error and the magnitude of the inaccuracies. To modify the models requires adjusting the viscosity profiles, or the timing and amount of ice change to rebuild the GIA models. Any new models could then be tested again using the approach outlined in this thesis. Caveats of this approach include:

- I can accurately estimate the GIA signal at the location of the GPS site. The technique cannot yield a spatially accurate independent GIA model.

- The approach can identify shortcomings of GIA models, but it cannot fix them. The GIA model must be rebuild considering the findings using the tool developed in this thesis.

In summary:

- It is possible to separate the elastic and viscoelastic signals accurately, through a least squares inversion using GRACE/GRACE-FO and GPS data.

- This approach can validate the continuity between the GRACE and the GRACE-FO missions, as the estimated vertical deformation estimated from each gravity mission agreed with the vertical land movement at key GPS sites. In this case in Fennoscandia, that had the best conditions for this work.

- I showed through simulations that, in regions with dense GPS site coverage, GIA uplift rates can be estimates with errors smaller than 1 mm/yr. However, I found that unless the true answer is known (simulated GPS) it it not possible to recover an accurate GIA signal, because the inversion will be driven to an elastic only solution because of the pseudo-observations. I found through simulation that it is possible to separate the elastic and viscoelastic components of GRACE to allow me to reconstruct accurately a GPS time series.

- With real data the inversion needs to be done up to degree 90 for an accurate reconstruction.

- The highest possible resolution relied on the GRACE solutions available. Since I used 200 km mascon solutions, the highest degree I could estimate was 90.

- It is possible to estimate the model for lower degrees of spherical harmonics, but it will decrease the resolution of the global model.

- It is possible to estimate a high-resolution spatial GIA model, given a dense distribution of GPS stations.

- If I do not have enough GPS coverage, the technique still works at discrete GPS site.

- The technique provides a GIA assessment tool, where I can identify the accuracy of GIA models at discrete GPS location and I can identify in which way the GIA models are in error. I recommend this technique to quantify the accuracy of current and future GIA models.

References

A, Geruo., Wahr, J., & Zhong, S. (2013). Computations of the viscoelastic response of a 3-D compressible Earth to surface loading: an application to Glacial Isostatic Adjustment in Antarctica and Canada. *Geophysical Journal International*, *192*(2), 557-572.

Allgeyer, S., Tregoning, P., McQueen, H., McClusky, S. C., Potter, E. K., Pfeffer, J., McGirr, R., Purcell, A. P., Herring, T. A., & Montillet, J. P. (2022). ANU GRACE Data Analysis: Orbit Modeling, Regularization and Inter-satellite Range Acceleration Observations. *Journal of Geophysical Research: Solid Earth*, *127*(2), e2021JB022489. https://doi.org/10.1029/2021JB022489

Argo. (n.d.). Retrieved June 1, 2024, from https://argo.ucsd.edu/

Bandikova, T., & Flury, J. (2014). Improvement of the GRACE star camera data based on the revision of the combination method. *Advances in Space Research*, *54*(9), 1818–1827. https://doi.org/10.1016/J.ASR.2014.07.004

Bandikova, T., McCullough, C., Kruizinga, G. L., Save, H., & Christophe, B. (2019). GRACE accelerometer data transplant. *Advances in Space Research*, *64*(3), 623–644. https://doi.org/10.1016/J.ASR.2019.05.021

Bennike, O., & Björck, S. (2002). Chronology of the last recession of the Greenland Ice Sheet. *Journal of Quaternary Science*, *17*(3), 211–219. https://doi.org/10.1002/JQS.670

Berg, D., Barletta, V. R., Hassan, J., Lippert, E. Y. H., Colgan, W., Bevis, M., Steffen, R., & Khan, S. A. (2024). Vertical Land Motion Due To Present-Day Ice Loss From Greenland's and Canada's Peripheral Glaciers. *Geophysical Research Letters*, *51*(2), e2023GL104851. https://doi.org/10.1029/2023GL104851

Bhanja, S. N., Mukherjee, A., Saha, D., Velicogna, I., & Famiglietti, J. S. (2016). Validation of GRACE based groundwater storage anomaly using in-situ groundwater level measurements in India. *Journal of Hydrology*, *543*, 729–738. https://doi.org/10.1016/J.JHYDROL.2016.10.042

Blewitt, G., Hammond, W., & Kreemer, C. (2018). Harnessing the GPS data explosion for interdisciplinary science. *Eos*, *99*(2), e2020943118.

Blewitt, G., Kreemer, C., Hammond, W. C., & Gazeaux, J. (2016). MIDAS robust trend estimator for accurate GPS station velocities without step detection. *Journal of Geophysical Research: Solid Earth*, *121*(3), 2054–2068. https://doi.org/10.1002/2015JB012552

Böning, C., Timmermann, R., Macrander, A., & Schröter, J. (2008). A pattern-filtering method for the determination of ocean bottom pressure anomalies from GRACE solutions. *Geophysical Research Letters*, *35*(18), 18611. https://doi.org/10.1029/2008GL034974

Bruinsma, S., Lemoine, J. M., Biancale, R., & Valès, N. (2010). CNES/GRGS 10-day gravity field models (release 2) and their evaluation. *Advances in Space Research*, *45*(4), 587–601. https://doi.org/10.1016/J.ASR.2009.10.012

Budd, W. F., & Jenssen, D. (1989). The Dynamics of the Antarctic Ice Sheet. *Annals of Glaciology*, *12*, 16–22. https://doi.org/10.3189/S026030550000690X

Caron, L., Ivins, E. R., Larour, E., Adhikari, S., Nilsson, J., & Blewitt, G. (2018). GIA Model Statistics for GRACE Hydrology, Cryosphere, and Ocean Science. *Geophysical Research Letters*, *45*(5), 2203–2212. https://doi.org/10.1002/2017GL076644

Caron, Lambert, & Ivins, E. R. (2020). A baseline Antarctic GIA correction for space gravimetry. *Earth and Planetary Science Letters*, *531*, 115957. https://doi.org/10.1016/J.EPSL.2019.115957

Chen, Q., Shen, Y., Chen, W., Francis, O., Zhang, X., Chen, Q., Li, W., & Chen, T. (2019). An Optimized Short-Arc Approach: Methodology and Application to Develop Refined Time Series of Tongji-Grace2018 GRACE Monthly Solutions. *Journal of Geophysical Research: Solid Earth*, *124*(6), 6010–6038. https://doi.org/10.1029/2018JB016596

Ciufolini, I., Paolozzi, A., Pavlis, E. C., Koenig, R., Ries, J., Gurzadyan, V., Matzner, R., Penrose, R., Sindoni, G., Paris, C., Khachatryan, H., & Mirzoyan, S. (2016). A test of general relativity using the LARES and LAGEOS satellites and a GRACE Earth gravity model. *The European Physical Journal C 2016 76:3*, *76*(3), 1–7. https://doi.org/10.1140/EPJC/S10052-016-3961-8

Clark, P. U., & Mix, A. C. (2002). Ice sheets and sea level of the Last Glacial Maximum.

Quaternary Science Reviews, *21*(1–3), 1–7. https://doi.org/10.1016/S0277-3791(01)00118-4

Croteau, M. J., Sabaka, T. J., & Loomis, B. D. (2021). GRACE Fast Mascons From Spherical Harmonics and a Regularization Design Trade Study. *Journal of Geophysical Research: Solid Earth*, *126*(8). https://doi.org/10.1029/2021JB022113

Dahle, C., Murböck, M., Flechtner, F., Dobslaw, H., Michalak, G., Neumayer, K. H., Abrykosov, O., Reinhold, A., König, R., Sulzbach, R., & Förste, C. (2019). The GFZ GRACE RL06 Monthly Gravity Field Time Series: Processing Details and Quality Assessment. *Remote Sensing 2019, Vol. 11, Page 2116*, *11*(18), 2116. https://doi.org/10.3390/RS11182116

Davis, J. L., Elósegui, P., Mitrovica, J. X., & Tamisiea, M. E. (2004). Climate-driven deformation of the solid Earth from GRACE and GPS. *Geophysical Research Letters*, *31*(24), 1–4. https://doi.org/10.1029/2004GL021435

Denton, G. H., & Hughes, T. J. (2002). Reconstructing the Antarctic Ice Sheet at the Last Glacial Maximum. *Quaternary Science Reviews*, *21*(1–3), 193–202. https://doi.org/10.1016/S0277-3791(01)00090-7

Dmitrieva, K., Segall, P., & DeMets, C. (2015). Network-based estimation of time-dependent noise in GPS position time series. *Journal of Geodesy*, *89*(6), 591–606. https://doi.org/10.1007/S00190-015-0801-9/FIGURES/13

Drinkwater, M. R., Haagmans, R., Muzi, D., Popescu, A., Floberghagen, R., Kern, M., & Fehringer, M. (2007). The GOCE Gravity Mission: ESA's First Core Earth Explorer. *ESA Special Publication*, *2*, 1–8.

Ekman, M. (1996). A consistent map of the postglacial uplift of Fennoscandia. *Terra Nova*, *8*(2), 158–165. https://doi.org/10.1111/J.1365-3121.1996.TB00739.X

Ekman, M., & Mäkinen, J. (1996). Recent postglacial rebound, gravity change and mantle flow in Fennoscandia. *Geophysical Journal International*, *126*(1), 229–234. https://doi.org/10.1111/J.1365-246X.1996.TB05281.X

eXpendable BathyThermographs (XBTs) - Frequently Asked Questions. (n.d.). Retrieved June 1, 2024, from https://www.aoml.noaa.gov/phod/goos/xbtscience/faqs.php

Farrell, W. E. (1972). Deformation of the Earth by surface loads. *Reviews of*

Geophysics, *10*(3), 761–797. https://doi.org/10.1029/RG010I003P00761

Flechtner, F., Reigber, C., Rummel, R., & Balmino, G. (2021). Satellite Gravimetry: A Review of Its Realization. *Surveys in Geophysics 2021 42:5*, *42*(5), 1029–1074. https://doi.org/10.1007/S10712-021-09658-0

Förste, C., Bruinsma, S., Rudenko, S., Abrikosov, O., Lemoine, J. M., Marty, J. C., ... & Biancale, R. (2015, April). EIGEN-6S4: A time-variable satellite-only gravity field model to d/o 300 based on LAGEOS, GRACE and GOCE data from the collaboration of GFZ Potsdam and GRGS Toulouse. In *EGU general assembly conference abstracts* (p. 3608).

Ghobadi-Far, K., Šprlák, M., & Han, S. C. (2019). Determination of ellipsoidal surface mass change from GRACE time-variable gravity data. *Geophysical Journal International*, *219*(1), 248–259. https://doi.org/10.1093/GJI/GGZ292

GRACE-FO Data | Data – GRACE-FO. (n.d.). Retrieved June 3, 2024, from https://gracefo.jpl.nasa.gov/data/grace-fo-data/

Grimes, J. (2007). Global positioning system precise positioning service performance standard. *Department of Defense, United States of America*.

Gunter, B., Urban, · T, Riva, · R, Helsen, · M, Harpold, · R, Poole, · S, Nagel, · P, Schutz, · B, Tapley, · B, Gunter, B., Urban, T., & Helsen, M. (2009). *A comparison of coincident GRACE and ICESat data over Antarctica*. *83*, 1051–1060. https://doi.org/10.1007/s00190-009-0323-4

Han, D., & Wahr, J. (1995). The viscoelastic relaxation of a realistically stratified earth, and a further analysis of postglacial rebound. *Geophysical Journal International*, *120*(2), 287–311. https://doi.org/10.1111/J.1365-246X.1995.TB01819.X

He, X., Bos, M. S., Montillet, J. P., & Fernandes, R. M. S. (2019). Investigation of the noise properties at low frequencies in long GNSS time series. *Journal of Geodesy*, *93*(9), 1271–1282. https://doi.org/10.1007/S00190-019-01244-Y/FIGURES/8

Hofmann-Wellenhof, B., Lichtenegger, H., & Wi en New York, S.-V. (1992). *Global Positioning System Theory and Practice*. https://doi.org/10.1007/978-3-7091-5126-6

Hughes, C. W., Tamisiea, M. E., Bingham, R. J., & Williams, J. (2012). Weighing the ocean: Using a single mooring to measure changes in the mass of the ocean.

Geophysical Research Letters, *39*(17). https://doi.org/10.1029/2012GL052935

Ivins, E. R., & James, T. S. (2005). Antarctic glacial isostatic adjustment: a new assessment. *Antarctic Science*, *17*(4), 541–553. https://doi.org/10.1017/S0954102005002968

Ivins, E. R., James, T. S., Wahr, J., Schrama, E. J. O., Landerer, F. W., Simon, K. M., James, T. R. S., Wahr, J., Schrama, E. J. O., Landerer, F. W., & Simon, K. M. (2013). Antarctic contribution to sea level rise observed by GRACE with improved GIA correction. *Journal of Geophysical Research: Solid Earth*, *118*(6), 3126–3141. https://doi.org/10.1002/JGRB.50208

Jacob, T., Wahr, J., Pfeffer, W. T., & Swenson, S. (2012). Recent contributions of glaciers and ice caps to sea level rise. *Nature 2012 482:7386*, *482*(7386), 514–518. https://doi.org/10.1038/nature10847

James, T. S., & Ivins, E. R. (1995). Present-day Antarctic ice mass changes and crustal motion. *Geophysical Research Letters*, *22*(8), 973–976. https://doi.org/10.1029/94GL02800

Johansson, J. M., Davis, J. L., Scherneck, H.-G., Milne, G. A., Vermeer, M., Mitrovica, J. X., Bennett, R. A., Jonsson, B., Elgered, G., Elósegui, P., Koivula, H., Poutanen, M., Rönnäng, B. O., & Shapiro, I. I. (2002). Continuous GPS measurements of postglacial adjustment in Fennoscandia 1. Geodetic results. *Journal of Geophysical Research: Solid Earth*, *107*(B8), ETG 3-1. https://doi.org/10.1029/2001JB000400

Kaufmann, G., & Wu, P. (2002). Glacial isostatic adjustment in Fennoscandia with a three-dimensional viscosity structure as an inverse problem. *Earth and Planetary Science Letters*, *197*(1–2), 1–10. https://doi.org/10.1016/S0012-821X(02)00477-6

King, M. A., Altamimi, Z., Boehm, J., Bos, M., Dach, R., Elosegui, P., Fund, F., Hernández-Pajares, M., Lavallee, D., Jorge Mendes Cerveira, P., Penna, N., M Riva, R. E., Steigenberger, P., van Dam, T., Vittuari, L., Williams, S., Willis, P., King, M. A., Penna, Á. N., … Williams, S. (2010). Improved Constraints on Models of Glacial Isostatic Adjustment: A Review of the Contribution of Ground-Based Geodetic Observations. *Surveys in Geophysics 2010 31:5*, *31*(5), 465–507. https://doi.org/10.1007/S10712-010-9100-4

Klinger, B., & Mayer-Gürr, T. (2016). The role of accelerometer data calibration within

GRACE gravity field recovery: Results from ITSG-Grace2016. *Advances in Space Research*, *58*(9), 1597–1609. https://doi.org/10.1016/J.ASR.2016.08.007

Kreemer, C., Hammond, W. C., & Blewitt, G. (2018). A Robust Estimation of the 3-D Intraplate Deformation of the North American Plate From GPS. *Journal of Geophysical Research: Solid Earth*, *123*(5), 4388–4412. https://doi.org/10.1029/2017JB015257

Kvas, A., Behzadpour, S., Ellmer, M., Klinger, B., Strasser, S., Zehentner, N., & Mayer-Gürr, T. (2019). ITSG-Grace2018: Overview and Evaluation of a New GRACE-Only Gravity Field Time Series. *Journal of Geophysical Research: Solid Earth*, *124*(8), 9332–9344. https://doi.org/10.1029/2019JB017415

Kvas, A., Brockmann, J. M., Krauss, S., Schubert, T., Gruber, T., Meyer, U., Mayer-Gürr, T., Schuh, W.-D., Jäggi, A., & Pail, R. (2020). *GOCO06s-A satellite-only global gravity field model*. https://doi.org/10.5880/ICGEM.2019.002

Lambeck, K., Purcell, A., Funder, S., Kjær, K., Larsen, E., & Möller, P. (2006). Constraints on the Late Saalian to early Middle Weichselian ice sheet of Eurasia from field data and rebound modelling. *Boreas*, *35*(3), 539–575. https://doi.org/10.1080/03009480600781875

Lambeck, K., Purcell, A., & Zhao, S. (2017). The North American Late Wisconsin ice sheet and mantle viscosity from glacial rebound analyses. *Quaternary Science Reviews*, *158*, 172–210. https://doi.org/10.1016/J.QUASCIREV.2016.11.033

Lambeck, K., Yokoyama, Y., Johnston, P., & Purcell, A. (2000). Global ice volumes at the Last Glacial Maximum and early Lateglacial. *Earth and Planetary Science Letters*, *181*(4), 513–527. https://doi.org/10.1016/S0012-821X(00)00223-5

Landerer, F. W., Flechtner, F. M., Save, H., Webb, F. H., Bandikova, T., Bertiger, W. I., Bettadpur, S. V., Byun, S. H., Dahle, C., Dobslaw, H., Fahnestock, E., Harvey, N., Kang, Z., Kruizinga, G. L. H., Loomis, B. D., McCullough, C., Murböck, M., Nagel, P., Paik, M., … Yuan, D. N. (2020). Extending the Global Mass Change Data Record: GRACE Follow-On Instrument and Science Data Performance. *Geophysical Research Letters*, *47*(12), e2020GL088306. https://doi.org/10.1029/2020GL088306

Lemoine, J. M., Bruinsma, S., Loyer, S., Biancale, R., Marty, J. C., Perosanz, F., &

Balmino, G. (2007). Temporal gravity field models inferred from GRACE data. *Advances in Space Research*, *39*(10), 1620–1629. https://doi.org/10.1016/J.ASR.2007.03.062

Lombard, A., Garcia, D., Ramillien, G., Cazenave, A., Biancale, R., Lemoine, J. M., Flechtner, F., Schmidt, R., & Ishii, M. (2007). Estimation of steric sea level variations from combined GRACE and Jason-1 data. *Earth and Planetary Science Letters*, *254*(1–2), 194–202. https://doi.org/10.1016/J.EPSL.2006.11.035

Loomis, B D, Luthcke, · S B, & Sabaka, · T J. (2019). Regularization and error characterization of GRACE mascons. *Journal of Geodesy*, *93*, 1381–1398. https://doi.org/10.1007/s00190-019-01252-y

Loomis, Bryant D., Felikson, D., Sabaka, T. J., & Medley, B. (2021). High-Spatial-Resolution Mass Rates From GRACE and GRACE-FO: Global and Ice Sheet Analyses. *Journal of Geophysical Research: Solid Earth*, *126*(12), e2021JB023024. https://doi.org/10.1029/2021JB023024

Luthcke, S. B., Rowlands, D. D., Lemoine, F. G., Klosko, S. M., Chinn, D., & McCarthy, J. J. (2006). Monthly spherical harmonic gravity field solutions determined from GRACE inter-satellite range-rate data alone. *Geophysical Research Letters*, *33*(2). https://doi.org/10.1029/2005GL024846

Lyman, J. M., Willis, J. K., & Johnson, G. C. (2006). Recent cooling of the upper ocean. *Geophysical Research Letters*, *33*(18), 18604. https://doi.org/10.1029/2006GL027033

Massotti, L., Siemes, C., March, G., Haagmans, R., & Silvestrin, P. (2021). Next generation gravity mission elements of the mass change and geoscience international constellation: From orbit selection to instrument and mission design. *Remote Sensing*, *13*(19). https://doi.org/10.3390/RS13193935

McClusky, S. (1993). *First epoch determination of crustal motion in the Papua New Guinea region : by comparison of a 1981 Doppler survey and a repeat GPS survey*. (Doctoral dissertation, School of Geomatic Engineering, University of New South Wales (Australia)). https://doi.org/10.26190/UNSWORKS/9362

McGirr, R. (2022). *Estimating earth's temporal gravity field from grace observations: Mitigation of thermal errors and the interplay between orbital characteristics, basis* *functions and spatial resolution* . (Doctoral dissertation, The Australian National University (Australia)). http://hdl.handle.net/1885/262734

McGirr, Rebecca, Tregoning, P., Purcell, A., & McQueen, H. (2024). Significant Local Sea Level Variations Caused by Continental Hydrology Signals. *Geophysical Research Letters*, *51*(10), e2024GL108394. https://doi.org/10.1029/2024GL108394

Meyer, U., Jäggi, A., Jean, Y., & Beutler, G. (2016). AIUB-RL02: an improved time-series of monthly gravity fields from GRACE data. *Geophysical Journal International*, *205*(2), 1196–1207. https://doi.org/10.1093/GJI/GGW081

Milne, G. A., Davis, J. L., Mitrovica, J. X., Scherneck, H. G., Johansson, J. M., Vermeer, M., & Koivula, H. (2001). Space-geodetic constraints on glacial isostatic adjustment in fennoscandia. *Science*, *291*(5512), 2381–2385. https://doi.org/10.1126/SCIENCE.1057022/SUPPL_FILE/1057022S2_THUMB.GIF

Milne, Glenn A., Mitrovica, J. X., Scherneck, H.-G., Davis, J. L., Johansson, J. M., Koivula, H., & Vermeer, M. (2004). Continuous GPS measurements of postglacial adjustment in Fennoscandia: 2. Modeling results. *Journal of Geophysical Research: Solid Earth*, *109*(B2). https://doi.org/10.1029/2003jb002619

Mitrovica, J. X., & Peltier, W. R. (1989). Pleistocene Deglaciation and the Global Gravity Field. *JOURNAL OF GEOPHYSICAL RESEARCH*, *94*(B10), 651–664. https://doi.org/10.1029/JB094iB10p13651

Niu, G. Y., Yang, Z. L., Dickinson, R. E., Gulden, L. E., & Su, H. (2007). Development of a simple groundwater model for use in climate models and evaluation with Gravity Recovery and Climate Experiment data. *Journal of Geophysical Research Atmospheres*, *112*(7). https://doi.org/10.1029/2006JD007522

Otosaka, I. N., Shepherd, A., Ivins, E. R., Schlegel, N. J., Amory, C., Van Den Broeke, M. R., Horwath, M., Joughin, I., King, M. D., Krinner, G., Nowicki, S., Payne, A. J., Rignot, E., Scambos, T., Simon, K. M., Smith, B. E., Sørensen, L. S., Velicogna, I., Whitehouse, P. L., … Wouters, B. (2023). Mass balance of the Greenland and Antarctic ice sheets from 1992 to 2020. *Earth System Science Data*, *15*(4), 1597–1616. https://doi.org/10.5194/ESSD-15-1597-2023

Paolozzi, A., Ciufolini, I., & Vendittozzi, C. (2011). Engineering and scientific aspects of LARES satellite. *Acta Astronautica*, *69*(3–4), 127–134.

https://doi.org/10.1016/J.ACTAASTRO.2011.03.005

Peltier, R. W., Argus, D. F., & Drummond, R. (2017). Comment on "An Assessment of the ICE-6G_C (VM5a) Glacial Isostatic Adjustment Model" by Purcell et al. *Journal of Geophysical Research: Solid Earth*, *123*(2), 2019–2028. https://doi.org/10.1002/2016JB013844

Peltier, W. R. (1974). The impulse response of a Maxwell Earth. *Reviews of Geophysics*, *12*(4), 649–669. https://doi.org/10.1029/RG012I004P00649

Peltier, W. R. (2004). Global glacial isostasy and the surface of the ice-age earth: The ICE-5G (VM2) model and GRACE. *Annual Review of Earth and Planetary Sciences*, *32*(Volume 32, 2004), 111–149. https://doi.org/10.1146/ANNUREV.EARTH.32.082503.144359/CITE/REFWORKS

Peltier, W. R., Argus, D. F., & Drummond, R. (2015). Space geodesy constrains ice age terminal deglaciation: The global ICE-6G-C (VM5a) model. *Journal of Geophysical Research: Solid Earth*, *120*(1), 450–487. https://doi.org/10.1002/2014JB011176

Peltier, W. Richard. (1996). Mantle Viscosity and Ice-Age Ice Sheet Topography. *Science*, *273*(5280), 1359–1364. https://doi.org/10.1126/SCIENCE.273.5280.1359

Purcell, A., Dehecq, A., Tregoning, P., Potter, E. K., McClusky, S. C., & Lambeck, K. (2011). Relationship between glacial isostatic adjustment and gravity perturbations observed by GRACE. *Geophysical Research Letters*, *38*(18). https://doi.org/10.1029/2011GL048624

Reigber, C., Balmino, G., Schwintzer, P., Biancale, R., Bode, A., Lemoine, J.-M., König, R., Loyer, S., Neumayer, H., Marty, J.-C., Barthelmes, F., Perosanz, F., & Zhu, S. Y. (2002). A high-quality global gravity field model from CHAMP GPS tracking data and accelerometry (EIGEN-1S). *Geophysical Research Letters*, *29*(14), 37–1. https://doi.org/10.1029/2002GL015064

Rietbroek, R., LeGrand, P., Wouters, B., Lemoine, J. M., Ramillien, G., & Hughes, C. W. (2006). Comparison of in situ bottom pressure data with GRACE gravimetry in the Crozet-Kerguelen region. *Geophysical Research Letters*, *33*(21). https://doi.org/10.1029/2006GL027452

Roy, K., & Peltier, W. R. (2015). Glacial isostatic adjustment, relative sea level history and mantle viscosity: reconciling relative sea level model predictions for the U.S.

East coast with geological constraints. *Geophysical Journal International*, *201*(2), 1156–1181. https://doi.org/10.1093/GJI/GGV066

Sasgen, I., Klemann, V., & Martinec, Z. (2012). Towards the inversion of GRACE gravity fields for present-day ice-mass changes and glacial-isostatic adjustment in North America and Greenland. *Journal of Geodynamics*, *59–60*, 49–63. https://doi.org/10.1016/J.JOG.2012.03.004

Sasgen, I., Martín-Español, A., Horvath, A., Klemann, V., Petrie, E. J., Wouters, B., Horwath, M., Pail, R., Bamber, J. L., Clarke, P. J., Konrad, H., & Drinkwater, M. R. (2017). Joint inversion estimate of regional glacial isostatic adjustment in Antarctica considering a lateral varying Earth structure (ESA STSE Project REGINA). *Geophysical Journal International*, *211*(3), 1534–1553. https://doi.org/10.1093/GJI/GGX368

Sasgen, I., Wouters, B., Gardner, A. S., King, M. D., Tedesco, M., Landerer, F. W., Dahle, C., Save, H., & Fettweis, X. (2020). Return to rapid ice loss in Greenland and record loss in 2019 detected by the GRACE-FO satellites. *Communications Earth & Environment 2020 1:1*, *1*(1), 1–8. https://doi.org/10.1038/s43247-020-0010-1

Save, H., Bettadpur, S., & Tapley, B. D. (2012). Reducing errors in the GRACE gravity solutions using regularization. *Journal of Geodesy*, *86*(9), 695–711. https://doi.org/10.1007/S00190-012-0548-5/METRICS

Save, H., Bettadpur, S., & Tapley, B. D. (2016). High-resolution CSR GRACE RL05 mascons. *Journal of Geophysical Research: Solid Earth*, *121*(10), 7547–7569. https://doi.org/10.1002/2016JB013007

Schmidt, P., Lund, B., & Näslund, J.-O. (2013). Weichselian ice sheet reconstructions Comparing a thermo-mechanical Weichselian ice sheet reconstruction to GIA driven reconstructions: aspects of earth response and ice configuration Weichselian ice sheet reconstructions Weichselian ice sheet reconstructions. *Solid Earth Discuss*, *5*, 2345–2388. https://doi.org/10.5194/sed-5-2345-2013

Schrama, E. J. O., Wouters, B., & Rietbroek, R. (2014). A mascon approach to assess ice sheet and glacier mass balances and their uncertainties from GRACE data. *Journal of Geophysical Research: Solid Earth*, *119*(7), 6048–6066.

https://doi.org/10.1002/2013JB010923

Segall, P., & Davis, J. L. (1997). GPS applications for geodynamics and earthquake studies. *Annual Review of Earth and Planetary Sciences*, *25*(Volume 25, 1997), 301–336. https://doi.org/10.1146/ANNUREV.EARTH.25.1.301/CITE/REFWORKS

Simon, K. M., James, T. S., & Ivins, E. R. (2010). Ocean loading effects on the prediction of Antarctic glacial isostatic uplift and gravity rates. *Journal of Geodesy*, *84*(5), 305–317. https://doi.org/10.1007/S00190-010-0368-4/METRICS

Simpson, M. J. R., Milne, G. A., Huybrechts, P., & Long, A. J. (2009). Calibrating a glaciological model of the Greenland ice sheet from the Last Glacial Maximum to present-day using field observations of relative sea level and ice extent. *Quaternary Science Reviews*, *28*(17–18), 1631–1657. https://doi.org/10.1016/J.QUASCIREV.2009.03.004

Sinem Ince, E., Barthelmes, F., Reißland, S., Elger, K., Förste, C., Flechtner, F., & Schuh, H. (2019). ICGEM – 15 years of successful collection and distribution of global gravitational models, associated services, and future plans. *Earth System Science Data*, *11*(2), 647–674. https://doi.org/10.5194/ESSD-11-647-2019

Steffen, H., Li, T., Wu, P., Gowan, E. J., Ivins, E., Lecavalier, B., Tarasov, L., & Whitehouse, P. L. (2021). *LM17.3 - a globalvertical land motion model of glacial isostatic adjustment.* https://doi.org/10.1594/PANGAEA.932462

Steffen, H., & Wu, P. (2011). Glacial isostatic adjustment in Fennoscandia—A review of data and modeling. *Journal of Geodynamics*, *52*(3–4), 169–204. https://doi.org/10.1016/J.JOG.2011.03.002

Swenson, S., & Wahr, J. (2006). Post-processing removal of correlated errors in GRACE data. *Geophysical Research Letters*, *33*(8), 8402. https://doi.org/10.1029/2005GL025285

Tapley, B. D., Bettadpur, S., Ries, J. C., Thompson, P. F., & Watkins, M. M. (2004). GRACE measurements of mass variability in the Earth system. *Science*, *305*(5683), 503–505. https://doi.org/10.1126/SCIENCE.1099192/SUPPL_FILE/TAPLEY.SOM.PDF

Tapley, B. D., Watkins, M. M., Flechtner, F., Reigber, C., Bettadpur, S., Rodell, M., Sasgen, I., Famiglietti, J. S., Landerer, F. W., Chambers, D. P., Reager, J. T., Gardner, A. S., Save, H., Ivins, E. R., Swenson, S. C., Boening, C., Dahle, C., Wiese, D. N., Dobslaw, H., … Velicogna, I. (2019). Contributions of GRACE to understanding climate change. *Nature Climate Change 2019 9:5*, *9*(5), 358–369. https://doi.org/10.1038/s41558-019-0456-2

The IMBIE Team, Shepherd, A., Ivins, E., Rignot, E., Smith, B., van den Broeke, M., Velicogna, I., Whitehouse, P., Briggs, K., Joughin, I., Krinner, G., Nowicki, S., Payne, T., Scambos, T., Schlegel, N., A, G., Agosta, C., Ahlstrøm, A., Babonis, G., … Wuite, J. (2019). Mass balance of the Greenland Ice Sheet from 1992 to 2018. *Nature 2019 579:7798*, *579*(7798), 233–239. https://doi.org/10.1038/s41586-019-1855-2

Thomas, I. D., King, M. A., Bentley, M. J., Whitehouse, P. L., Penna, N. T., Williams, S. D. P., Riva, R. E. M., Lavallee, D. A., Clarke, P. J., King, E. C., Hindmarsh, R. C. A., & Koivula, H. (2011). Widespread low rates of Antarctic glacial isostatic adjustment revealed by GPS observations. *Geophysical Research Letters*, *38*(22). https://doi.org/10.1029/2011GL049277

Tregoning, P., McGirr, R., Pfeffer, J., Purcell, A., McQueen, H., Allgeyer, S., & McClusky, S. C. (2022). ANU GRACE Data Analysis: Characteristics and Benefits of Using Irregularly Shaped Mascons. *Journal of Geophysical Research: Solid Earth*, *127*(2), e2021JB022412. https://doi.org/10.1029/2021JB022412

Tregoning, P., Watson, C., Ramillien, G., McQueen, H., & Zhang, J. (2009). Detecting hydrologic deformation using GRACE and GPS. *Geophysical Research Letters*, *36*(15), 15401. https://doi.org/10.1029/2009GL038718

Tregoning, P., and C. Watson (2009), Atmospheric effects and spurious signals in GPS analyses, *J. Geophys. Res.*, 114, B09403, doi:10.1029/2009JB006344.

Tregoning, P. (1996). *GPS Measurements in the Australian and Indonesian Regions, 1989-1993: Studies of the Java Trench Subduction Zone, the Sunda Strait and the Australian Plate* (Vol. 44). (Doctoral dissertation, School of Geomatic Engineering, University of New South Wales (Australia)).

Tucker, E. S., Nerem, R. S., & Loomis, B. D. (2022). Simulation of a Future SLR Satellite to Improve Low-Degree Gravity Estimates. *Journal of Geophysical Research: Solid Earth*, *127*(12), e2022JB025743.

https://doi.org/10.1029/2022JB025743

Tushingham, A. M., & Peltier, W. R. (1991). Ice-3G: a new global model of late Pleistocene deglaciation based upon geophysical predictions of post-glacial relative sea level change. *Journal of Geophysical Research*, *96*(B3), 4497–4523. https://doi.org/10.1029/90JB01583

U.S. East Coast Sea Level | Virginia Institute of Marine Science. (2022). Retrieved June 1, 2024, from https://www.vims.edu/research/products/slrc/compare/east_coast/

Velicogna, I. (2009). Increasing rates of ice mass loss from the Greenland and Antarctic ice sheets revealed by GRACE. *Geophysical Research Letters*, *36*(19). https://doi.org/10.1029/2009GL040222

Velicogna, I., Sutterley, T. C., & Van Den Broeke, M. R. (2014). Regional acceleration in ice mass loss from Greenland and Antarctica using GRACE time-variable gravity data. *Geophysical Research Letters*, *41*(22), 8130–8137. https://doi.org/10.1002/2014GL061052

Velicogna, I., & Wahr, J. (2013). Time-variable gravity observations of ice sheet mass balance: Precision and limitations of the GRACE satellite data. *Geophysical Research Letters*, *40*(12), 3055–3063. https://doi.org/10.1002/GRL.50527

Velicogna, Isabella, & Wahr, J. (2006). Acceleration of Greenland ice mass loss in spring 2004. *Nature 2006 443:7109*, *443*(7109), 329–331. https://doi.org/10.1038/nature05168

Vishwakarma, B. D., Ziegler, Y., Bamber, J. L., & Royston, S. (2022). Separating GIA signal from surface mass change using GPS and GRACE data. *Geophysical Journal International*, *232*(1), 537–547. https://doi.org/10.1093/GJI/GGAC336

Wahr, J., DaZhong, H., & Trupin, A. (1995). Predictions of vertical uplift caused by changing polar ice volumes on a viscoelastic Earth. *Geophysical Research Letters*, *22*(8), 977–980. https://doi.org/10.1029/94GL02840

Wahr, J., Molenaar, M., & Bryan, F. (1998). Time variability of the Earth’s gravity field: Hydrological and oceanic effects and their possible detection using GRACE. *Journal of Geophysical Research: Solid Earth*, *103*(B12), 30205–30229. https://doi.org/10.1029/98JB02844

Wahr, J., Wingham, D., & Bentley, C. (2000). A method of combining ICESat and

GRACE satellite data to constrain Antarctic mass balance. *Journal of Geophysical Research: Solid Earth*, *105*(B7), 16279–16294. https://doi.org/10.1029/2000JB900113

Wang, L., Wu, Q., Wu, F., & He, X. (2022). Noise content assessment in GNSS coordinate time-series with autoregressive and heteroscedastic random errors. *Geophysical Journal International*, *231*(2), 856–876. https://doi.org/10.1093/GJI/GGAC228

Watkins, M. M., Wiese, D. N., Yuan, D. N., Boening, C., & Landerer, F. W. (2015). Improved methods for observing Earth's time variable mass distribution with GRACE using spherical cap mascons. *Journal of Geophysical Research: Solid Earth*, *120*(4), 2648–2671. https://doi.org/10.1002/2014JB011547

Whitehouse, P. L., Bentley, M. J., Milne, G. A., King, M. A., & Thomas, I. D. (2012). A new glacial isostatic adjustment model for Antarctica: Calibrated and tested using observations of relative sea-level change and present-day uplift rates. *Geophysical Journal International*, *190*(3), 1464–1482. https://doi.org/10.1111/J.1365-246X.2012.05557.X/2/190-3-1464-FIG014.GIF

Wiese, D. N., Landerer, F. W., & Watkins, M. M. (2016). Quantifying and reducing leakage errors in the JPL RL05M GRACE mascon solution. *Water Resources Research*, *52*(9), 7490–7502. https://doi.org/10.1002/2016WR019344

Williams, S. D. P., Bock, Y., Fang, P., Jamason, P., Nikolaidis, R. M., Prawirodirdjo, L., Miller, M., & Johnson, D. J. (2004). Error analysis of continuous GPS position time series. *Journal of Geophysical Research: Solid Earth*, *109*(B3). https://doi.org/10.1029/2003JB002741

Willis, J. K., Chambers, D. P., & Nerem, R. S. (2008). Assessing the globally averaged sea level budget on seasonal to interannual timescales. *Journal of Geophysical Research: Oceans*, *113*(C6), 6015. https://doi.org/10.1029/2007JC004517

Wouters, B., & Schrama, E. J. O. (2007). Improved accuracy of GRACE gravity solutions through empirical orthogonal function filtering of spherical harmonics. *Geophysical Research Letters*, *34*(23), 23711. https://doi.org/10.1029/2007GL032098

Wu, X., Heflin, M. B., Schotman, H., Vermeersen, B. L. A., Dong, D., Gross, R. S., Ivins,

E. R., Moore, A. W., & Owen, S. E. (2010). Simultaneous estimation of global present-day water transport and glacial isostatic adjustment. *Nature Geoscience*, *3*(9), 642–646. https://doi.org/10.1038/ngeo938

Young, I. R., Sanina, E., & Babanin, A. V. (2017). Calibration and Cross Validation of a Global Wind and Wave Database of Altimeter, Radiometer, and Scatterometer Measurements. *Journal of Atmospheric and Oceanic Technology*, *34*(6), 1285–1306. https://doi.org/10.1175/JTECH-D-16-0145.1

Ziegler, Y., Dutt Vishwakarma, B., Brady, A., Chuter, S., Royston, S., Westaway, R. M., & Bamber, J. L. (2023). Can GPS and GRACE data be used to separate past and present-day surface loading in a data-driven approach? *Geophys. J. Int*, *232*, 884–901. https://doi.org/10.1093/gji/ggac365